General Disclaimer

One or more of the Following Statements may affect this Document

- This document has been reproduced from the best copy furnished by the organizational source. It is being released in the interest of making available as much information as possible.

- This document may contain data, which exceeds the sheet parameters. It was furnished in this condition by the organizational source and is the best copy available.

- This document may contain tone-on-tone or color graphs, charts and/or pictures, which have been reproduced in black and white.

- This document is paginated as submitted by the original source.

- Portions of this document are not fully legible due to the historical nature of some of the material. However, it is the best reproduction available from the original submission.

FINAL TECHNICAL REPORT

Title of Grant	Seismicity and Active Tectonics of the Andes and the Origin of the Altiplano
Principal Investigator	Peter Molnar
Period Covered	March 1, 1980 through October 31, 1982
Grantee Institution	Massachusetts Institute of Technology 77 Massachusetts Avenue Cambridge, Massachusetts 02139
Grant Number	NAG 5-19

PROJECT SUMMARY

We have not yet completed all of the work that we planned for this project, but we think that we have made considerable progress towards understanding how Andean margins develop. The major study is of large earthquakes and of active deformation on the Andes. A paper "Seismicity, Fault Plane Solutions, Depth of Faulting and Active Tectonics of the Central Andes" by Suárez, Molnar and Burchfiel has been submitted to the Journal of Geophysical Research and is being revised.

We found that earthquakes on the east side of the Andes generally reflect east-west crustal shortening. These earthquakes seem to occur throughout the crust and do not reflect a detachment and low angle thrusting of the sedimentary cover onto the Brazilian shield. Instead they imply deformation of the basement. The rate of shortening is compatible with construction of the Andes by crustal shortening since the late Cretaceous, and we think that the surface geology, at least qualitatively, reflects this process. We do not know why Andean margins form, but we think that their presence is a result of crustal shortening.

The crustal shortening in the sub-Andes occurs concurrently with normal faulting at high elevations in parts of the Andes. We associate the normal faulting with the buoyancy of the thick crust. Crustal shortening thiskens the crust and work is done against gravity. When the crustal thickness and elevation reach limiting values, the range grows laterally by further thrusting on the margins. The normal faulting shows that that limiting thickness has been reached.

Introduction

The west coast of South America is the major active margin where an oceanic plate is being subducted beneath a continental plate. It represents a contemporary example of the tectonic regime that is often presumed to have existed along the western margin of North America before the subduction of oceanic material ceased during the late Cenozoic (e.g. Atwater, 1970; Hamilton, 1969). Thus, understanding the style of deformation and evolution of the Andes, an orogenic belt uncontaminated by a continental collision, may play a crucial role in trying to decipher the complex tectonic history of previously active margins that are now dormant, or where an "Andean" margin has been followed by a continental collision, as in the case of the Alpine-Himalayan belt.

A useful tool to glean the style of deformation and tectonic regime of an active mountain belt is the study of the seismicity ocurring in it. The spatial distribution of seismic activity indicates where deformation is taking place, while the type of faulting inferred from fault-plane solutions allows inferences of the orientation of the stresses responsible for, at least, the brittle deformation. In the Andes, crustal seismic activity is low compared to that of the subduction zone, and the routine hypocentral locations published by the International

Seismological Centre (ISC) and the United States Geological Survey (USGS) are not accurate due both to the poor geographic distribution of stations, and to the sparse coverage of the local stations; this is specially true for focal depth.

To examine the active deformation of the central Andes, we installed a temporary network of portable seismographs in the Altiplano and Eastern Cordillera of the central Andes, east of the city of Lima (Figure 1).

Methods of Analysis

Station Distribution

From May 13 to June 12, 1980, we operated a network of up to sixteen portable seismographs complementing the less dense permanent seismic network operated by the Instituto Geofisico del Peru (Figure 2 and Table 1). Our goal was to monitor the seismic activity in the High Plateaus and the Eastern Cordillera in the vicinity of the city of Huancayo (Figures 1 and 2). Originally, our objective was to monitor the seismic activity in the High Plateaus, the Eastern Cordillera, and the western margin of the sub-Andes. Unfortunately, the poor conditions of the roads after the rainy season and the lack of topographic maps or navigated

aerial photographs required to determine the geographic coordinates of the stations did not permit us to install stations in the sub-Andes, and coverage there and along the Pacific coast was provided by stations of the permanent network. The geographic coordinates and elevation above sea level of the portable stations were determined using topographical maps published by the Instituto Geografico Militar of Peru at a scale of 1:100,000 (Table 1). We estimate the uncertainty of the positions of the stations to be in the order of 250 meters.

Recording Procedure

We used Sprengnether MEQ-800 seismographs with Mark Products L4-C vertical seismometers. The amplifiers were generally set to 84 db, corresponding to a magnification of about 5×10^5 at 10 Hz. Earthquakes were recorded by a fine stylus on smoked paper at a speed of 60 mm/min. Records were changed every 48 hours and the drift of the internal clock of each instrument was checked at this same time interval, by directly recording time pulses transmitted by the WWV station in Colorado, USA. Clock drifts during these 48 hour periods were always less than 0.1 sec.

The arrival times of the phases of interest were digitized on a table-top digitizer. The accuracy of the readings depended on the level of background noise and the sharpness of the onsets. On the average we estimate an

accuracy of about 0.1 seconds for P arrival times. S waves were also picked when they could be confidently identified, and we estimate the error in S wave arrival times to be in the order of 1 second.

Location Procedure

In this study, earthquakes were located using the computer program HYPOINVERSE developed at the USGS by Klein (1978). The problem of locating earthquakes is one of the oldest inverse problems in geophysics and thorough reviews of the problem have been given by various authors (e.g. Aki and Richards, 1980; Buland, 1976; Lee and Stewart, 1981). Here, we shall briefly describe the method of singular value decomposition used by the HYPOINVERSE program and point out some of the distinct advantages of this method to estimate the quality of hypocentral locations.

Through succesive iterations, we seek the solution in the least-squares sense of the system of equations:

$$\underset{m}{R} = \underset{mxn}{A}\ \underset{n}{X} \qquad (1)$$

by minimizing:

$$(R - A\ X)^2 \qquad (2)$$

where R is the vector of travel time residuals (i.e. observed arrival time minus the theoretical arrival time

calculated for the hypocentral location and origin time of the revious step), A is a matrix containing the partial derivatives of the travel times with respect to variations in the earthquake location and origin time, and X is the vector of adjustments to the current hypocenter and origin time that we solve for. Beggining with an initial trial solution, the hypocenter is determined by successively solving for the adjustment vector X and improving the hypocentral parameters obtained in the previous step until a convergence criterion is reached.

Equation 2 is solved in terms of the generalized inverse of A using the singular-value decomposition of A (Lanczos, 1961; Lawson and Hanson, 1974). In this method, the matrix A is decomposed into:

$$A = U \quad S \quad V^T \qquad (3)$$

where U and V represent the eigenvector matrices, and S is the diagonal matrix of the eigenvalues of the matrix A^TA. The generalized inverse of A can be defined as:

$$A^{-1} = V \quad S^{-1} \quad U^T \qquad (4)$$

and substituting in (2) the adjustment vector, X, is solved as:

$$X = A^{-1} \quad R \qquad (5)$$

For the problem of hypocentral determination the generalized inverse is equivalent to the least-squares solution since the system of equations is usually overdetermined. The advantage of the singular value decomposition is that the covariance, resolution, and data importance matrices are readily obtained.

The covariance matrix C is obtained from elements of the decomposition of the matrix A as:

$$\mathbf{C} = \sigma^2 \quad \mathbf{V} \quad \mathbf{S}^{-2} \quad \mathbf{V}^T \qquad (6)$$

where σ^2 is the variance of the arrival times. The covariance matrix, C, gives estimates of the errors in the hypocentral solution due to errors in the data but does not include errors introduced by using an erroneous velocity structure. The four diagonal elements of the covariance matrix represent the variance of the origin time, latitude, longitude, and depth of the final hypocentral solution, respectively.

The data resolution or information density matrix expressed by:

$$\mathbf{B} = \mathbf{U} \quad \mathbf{U}^T \qquad (7)$$

is a parameter that is not computed by most standard location problems. It is a by-product of the singular-value decomposition scheme and it represents the weight of each

of the observations to the final solution. The data importance is useful for examining the effect of the network geometry for individual events and to identify which arrival times contribute the most towards the hypocentral location. This is specially useful to study events falling outside of the network, where the resolution of the hypocentral parameters is low.

Another advantage of the singular-value decomposition scheme is that the eigenvalues of the matrix $\mathbf{A}^T\mathbf{A}$, corresponding to each one of the hypocentral parameters is explicitely obtained. If one or more of the eigenvalues in S becomes very small, the errors in the direction of their associated eigenvectors (parameters) will be large (Equation 6). In general, the largest eigenvalue corresponds to origin time and is of order 5. The eigenvalues corresponding to the spatial coordinates are of order 0.5; where the eigenvalue associated with focal depth is usually the smallest (Klein, 1978). The explicit decomposition of eigenvalues and their associated eigenvectors provides another element with which to judge the quality of a hypocentral location. The application of this technique in other parts of the world empirically shows that when any of the eigenvalues of the matrix $\mathbf{A}^T\mathbf{A}$ becomes less than about 0.02, the hypocentral solution is unstable and very poorly constrained (Klein, 1978).

For the first iteration, P arrival times were assigned a weight of 1 and S arrival times a weight of 0.5. The smaller weights of the S arrival times compensates the larger uncertainty in arrival-time readings of S waves and their inherently greater importance to the solution. The algorithm assigns weights to the observed arrival times as a function of the residual from the previous iteration. This is useful for damping outliers, i.e. arrival times that are grossly in error, as in the case of misidentified phases.

Accuracy of the Locations

Effects of the Velocity Structure Used

The velocity structure in central Peru is poorly known. The refraction studies undertaken to determine the crustal structure of the central Andes have been carried out in southern Peru and northern Bolivia (e.g. Ocola et al, 1971; Ocola and Meyer, 1973; Tatel and Tuve, 1958). Thus, since the velocity models available are based on data from outside the study area, the sensitivity of the hypocentral locations to the assumed velocity model was investigated by testing three alternative velocity models of the crustal structure of the Andes.

One velocity model used was determined by Ocola and Meyer (1973) from a refraction survey across the Andes in southern Peru. Their study spans the region from the trench to the Altiplano, and we have used their results for the eastern Altiplano and Cordillera Oriental. A second model is that of James (1971) who determined the thickness and velocity structure of the crust beneath the Andes studying the dispersion of Rayleigh and Love waves along various paths. Finally, a velocity structure based on the results of a deep crustal refraction experiment carried out in southern Colombia by Meissner et al (1977) serves as a comparison to crustal models proposed for southern Peru and northern Bolivia. The crustal models used have thicknesses of between 55 and 65 km and are listed in Table 2.

A ratio of $/V_s$ of 1.75 corresponding to a Poisson ratio of 0.25 was used in all cases and a station time correction (station delay) was applied to all arrival times at a given station to compensate for differences in elevation. Station elevation varied from a few tens of meters to 4900 meters above sea level (Table 1). The station corrections were applied assuming a reference datum of 3500 meters (the average elevation at the center of the array) and assuming a mean P-wave velocity of 5.0 km/sec for the top crustal layer. Other studies have shown that varying the ratio of V_p/V_s by about 0.3 produces changes in the hypocentral

locations usually not larger than 2 km (e.g. Prevot et al, 1980; Trehu, 1982).

A random selection of 29 earthquakes ocurring at various depths were located using these three seismic velocity structures (Table 3). The epicentral coordinates and focal depths of events located with the crustal model of Ocola and Meyer (1973) were substracted from the hypocentral coordinates obtained using the velocity structure proposed by James (1971) and Meissner et al (1977) and are shown independently in Figures 3 and 4 in histogram form. In general, epicentral locations do not seem to depend strongly on the choice of the velocity structure; changes in epicentral coordinates are usually less than four to six kilometers. Focal depths are more sensitive to changes in the velocity structure and may change by as much as 8 to 14 km depending upon the location of the event relative to the network, and the velocity model used. In both cases, however, those earthquakes that exhibited changes in epicentral coordinates larger than about 10 km are events that are poorly constrained because they lie outside or on the periphery of the network.

The velocity model obtained by Ocola and Meyer (1973) generally produced the smallest root mean square (rms) values of travel time residuals and was adopted to locate all the events recorded.

Selection Criteria

During the four weeks of recording a total of 344 earthquakes were located (Figure 5). The located events span an area of about 400 by 400 km. Most of these earthquakes occurred within the crust in the sub-Andes, east of the Andean Cordillera. The high Andes appear to be seismically relatively inactive with the exception of the region near the Huaytapallana fault in the Eastern Cordillera, (near 12°S, 75°N). This activity defines a clear linear northwest-southeast trend (Figure 5). Intermediate-depth events were also located beneath the high Andes and the sub-Andes. Very few events, however, were recorded along the main thrust contact between the Nazca and the South American plate probably because this area is far from our network.

As can be observed in Figure 5, many of the events lie outside the network and the maximum azimuthal gap is sometimes quite large. Using synthetic data, Lilwall and Francis (1978) showed that this does not necesarily imply poor resolution of the hypocentral coordinates if the distance from the epicenter to the nearest station is not large. A useful rule of thumb for judging the accuracy of hypocentral depth determination is that the distance from the event to the closest station should be less than or roughly equal to the focal depth. For most of the crustal earthquakes in the sub-Andes this is clearly not the case,

focal depths for these crustal events appear to be less than 40 km and the distance to the closest station is often a few tens of kilometers. This lack of resolution in focal depth is evident when one examines the eigenvalues for these shallow events in the sub-Andes. For most of these events, the eigenvalue associated with depth is usually very small (less than 0.015), and the calculated error in focal depth is accordingly very large (see equation 7). Ellsworth and Roecker (1981) conclude that the critical geometric factor controlling the location of the earthquake is the spread of ray take-off angles from the source to the stations. Clearly, refracted rays deflected at the same layer leave the source with the same ray take-off angle, and focal depth and origin time cannot be resolved.

Many of the events located have large errors in the epicentral coordinates (ERH) and the focal depth (ERZ). Therefore, it is necessary to establish screening criteria to separate well located earthquakes from poor and unreliable locations. We consider as reliable locations those events for which at least five arrivals, including at least one S phase were used, and the condition number of the matrix (the ratio of the largest to the smallest eigenvalue) was less than 200. This implies a cutoff value for the smallest eigenvalues of about 0.02, which Klein (1978) empirically determined to be the minimum value required for a stable and well constrained solution. We

also required that the values of calculated errors in the horizontal (ERH) and vertical (ERZ) directions be less than 10 km and the rms of the travel time residuals to be less than 0.5 sec. Admittedly, an rms value of 0.5 for the travel time residuals is large. However, large residuals may be a function of local lateral variations of the assumed velocity structure rather than indicative of poor locations. The screened events are shown projected onto cross section A-B (Figure 6) in Figure 7.

Seismicity of the High Andes

Seismicity in the Altiplano

It is clear that crustal seismicity in the Altiplano is relatively low (Figures 5, 6, and 7). Although the majority of our portable stations were deployed in the western part of the Altiplano, only about fifteen earthquakes in the crust were located beneath the network; the overwhelming majority of the crustal earthquakes occured in the eastern margin of the Cordillera and the sub-Andes (Figures 5 and 6). This pattern of seismicity is consistent with studies of teleseismic events showing that most large, shallow events occur in the western part of the sub-Andes (e.g. Stauder, 1975; Suarez et

al, 1983). Thus, insofar as both the microearthquakes reported here and the historic seismicity reflect the degree of active tectonics, the Altiplano appears to be more stable and at present is not subjected to orogenic deformation as intense as that affecting parts of the Eastern Cordillera and the whole of the western sub-Andes. Unless the deformation is absorbed by creep or viscoelastic behavior.

Those few events registered in the Altiplano are all very small, and unfortunatley none of them yielded a well constrained fault-plane solution. Thus,we could not address one of our original objectives: whether or not normal faulting occurs in the Altiplano of the central Andes, as it does in the Cordillera Blanca of the high Andes in northern Peru (Dalmayrac, 1974; Yonekura et al, 1979) and in the Bolivian Altiplano (Lavenu, 1978, 1979; Mercier, 1981).

The Huaytapallana Fault

The Huaytapallana fault is located in the Eastern Cordillera of central Peru, a few kilometers east of the city of Huancayo (Figure 1). Two fault-plane solutions of two large earthquakes that occurred on this fault in July 24, 1969 and October 1, 1969 show reverse faulting (Stauder, 1975). This latter event caused great damage in the nearby villages killing 130 people (ISC Bulletin). The

October 1, 1969 earthquake produced a steep fault scarp dipping east, with a vertical displacement reaching 1.6 meters (Deza, 1971; Philip and Megard, 1977) (see Figure 8). Philip and Megard interpret the fault as one of a group of reactivated parallel faults trending NNW-SSE. Two of these faults mark the contact between three different formations: from east to west the Precambrian gneiss of the Huaytapallana Range, an intermediate block of Triassic metamorphosed limestones, and a block of Late Paleozoic sandstones and limestones (Paredes, 1972) (Figure 9).

The existence of a large number of small microearthquakes shows that the Huaytapallana fault (or system of faults) is still active (Figures 6 and 9). Station HYT, installed at the southeastern end of the mapped surface rupture, registered an average of about 30 events per day with S-P time differences of less than 4 seconds. The epicenters of earthquakes located in the vicinity of the Huaytapallana area follow a trend in a NNW-SSE direction, parallel to the the mapped surface faults and to the strike of the east-dipping nodal plane of the fault-plane solutions of the two largest Huaytapallana earthquakes (Stauder, 1975, Suarez et al, 1983) (Figure 9). It is not clear, however, whether the seismicity is due to activity along a single fault or a series of faults.

Both the fault-plane solution of one of the largest events and a composite fault-plane solution for four events

show reverse faulting with some left-lateral strike-slip motion ocurring on a fault plane dipping east with a strike of about 30° east of north (Figures 11 and 13). This agrees with the sense of motion observed at the fault (Philip and Megard, 1977) and with the fault plane-solutions of the two large 1969 earthquakes.

In the basins just west of the Huaytapallana fault, Dollfus and Megard (1968) reported folding of Quaternary glacial terraces. The strike of these folds, in a direction N30°W, and the orientation of the P axes of the fault-plane solutions of earthquakes in the Huaytapalllana fault (Figure 11) suggest this region is being deformed by a horizontal compressive stress oriented roughly east-west, in the direction of plate motion.

Based on a study of the fault scarp, Philip and Megard (1977) suggest that the overall length of the fault is approximately 3.5 km. The length of the fault of the October 1, 1969 earthquake can be estimated by considering the average displacement u on the fault to be 1.6 m, the rigidity μ equal to 3.3×10^{11}, a fault width of between 10 to 15 km, and a seismic moment of 1.0×10^{26} dyne cm (Suarez et al, 1983). From the formula $M_0 = u\mu S$ (Aki, 1966), where S is the area of the fault, the October 1 earthquake requires a fault about 12 to 20 km long. Thus, it is likely that the 1969 earthquakes ruptured a fault that extends north of the surface break, to where the microseismicity occurs today.

The epicenters of most of the earthquakes recorded in this area lie about 10 km east of the projected location of the fault (Figure 9).

A cross section across the fault shows that the earthquakes are deeper towards the east (Figure 10), consistent with an east-dipping fault plane (Figure 11). The deepest events occur at a depth of about 18 km. The locations are not accurate enough to determine, however, whether the earthquakes take place on a single fault plane or a on a series of imbricate faults.

Although focal depths and epicentral locations are poorly constrained, epicenters of a group of crustal earthquakes are aligned in the same general direction of the Huaytapallana fault east of the station PAM, to the southeast of Huaytapallana (see Figure 5). Only one of these events passed our filtering criteria and appears to be well constrained. The fault-plane solution for this event (Figure 12) is not well constrained and could be interpreted as a pure strike-slip or a pure dip-slip event, or a combination of both. The first motions, however, suggest that the P axes lie in a general east-west direction, as for the events in the Huaytapallana. Another large historical event occurred in this part of the Eastern Cordillera. On November 1, 1947 an earthquake of magnitude 7.3 occured about 50 kilometers northwest of the Huaytapallana fault.

The Huaytapallana fault is one of only two reverse faults in the high Andes known to have broken by an earthquake that has been instrumentally recorded. The other is associated with the 1944 and 1979 San Juan earthquakes in central Argentina. It is interesting that both faults occur where an aseismic ridge is being subducted: the Nazca Ridge in Peru and the Juan Fernandez Ridge in central Argentina, and that normal faulting and crustal extension occurs in much of the rest of the high Andes. Suarez et al (1983) associate this apparently greater horizontal compressive stress with the added resistance of these high and buoyant ridges to subduction of the Nazca plate.

Seismicity of the sub-Andes

Description of the Seismicity

The sub-Andes of central Peru are seismically more active than the high Andes and appear to be the physiographic province in the central Andes currently undergoing the most intense brittle deformation. The vast majority of earthquakes in the overiding continental plate are concentrated in the western margin of the sub-Andean region, over an area roughly 100 km wide. These events lie east of the main Andean Cordillera and occur beneath areas

of low topographic elevation (Figures 5 and 6). Most of these events occurred at large distances from the eastern margin of the network, and therefore the focal depths of these events are very poorly resolved. Station POC operated by the Instituto Geofisico del Peru is the only station located in the sub-Andes, but due to its low gain it could not be used to locate most of the microearthquakes that occurred in the area.

Despite the errors in focal depths, there are enough well located events to show that the seismicity in the sub-Andes affects most of the crust at least to depths of about 40 to 50 kilometers, in agreement with the depths of two nearby larger events (Suarez et al, 1983). Although most of the microearthquakes seem to occur at midcrustal depths between 15 and 25 km, one event clearly takes place at a depth of about 50 km. This earthquake occurred beneath the network and was located by 15 stations; the horizontal distance to the nearest station was about 30 km. Although the travel-time residuals are relatively large (about 0.4 sec), the estimated focal depth changes by less than 5 km for the different velocity models used (Table 3), and the errors in the vertical direction are always less than four kilometers. Below a depth of about 50 km no earthquakes occur within the South American plate. An aseismic zone extends to a depth of about 90 km where

intermediate depth earthquakes associated with the subducted slab occur (Figure 7).

Fault Plane Solutions and Tectonic Interpretation

A composite fault-plane solution from six events located just east of the network at depths of between 15 and 26 km shows thrust faulting with a component of strike-slip motion (Figure 14). This solution is very similar to that of a larger event that occurred about 25 km east of this group of events at a depth of 20 km (Suarez et al, 1983) (Figures 13 and 14). A fault-plane solution obtained for a single event in the in the sub-Andes suggests nearly pure reverse faulting (Figure 15). Both of these fault mechanisms have P axes oriented northwest-southeast, in the same general direction as the subduction of the Nazca plate beneath South America, and similar to those of the larger events (Suarez et al, 1983) in the sub-Andes.

The existence of earthquakes in the sub-Andes at middle and lower crustal depths of between 20 and 50 km is unusual. Chen and Molnar (1981) and Meissner and Strelhau (1982) compiled catalogs of earthquakes ocurring in intracontinental areas of the world and show that, in general, brittle behavior of the crust is confined to roughly the top 15 km of the upper crust. This is inferred to be due to the sharp decrease in strength of the typical crustal

minerals at that depth, under normal geothermal gradients (e.g. Brace and Kohlstedt, 1980; Caristan, 1980). To explain both the concentration of intense deformation along the western margin of the sub-Andes and the unusually deep brittle deformation up to 40 or 50 km, Suarez et al (1983) suggested that the seismicity results from an underthrusting of the cold Brazilian shield beneath the eastern margin of the Cordillera Oriental. Crustal shortening thickens the crust and uplifts the topography of the eastern Cordillera causing the Andean mountain range to grow eastward, with progressively younger deformation to the east (e.g. Megard, 1978; Dalmayrac et al, 1980).

Intermediate Depth Microearthquakes

Shape of the Subducion Zone Beneath the Central Andes

Based on the study of a carefully selected catalog of teleseismically located events, Barazangi and Isacks (1976, 1979) inferred that the seismic zone beneath Peru dips at about 10°. As James (1978) pointed out, most of the events used by Barazangi and Isacks to infer this dip are shallow events along the coast or from a cluster of intermediate-depth earthquakes in northern Peru (section B in Figure 16).

Using earthquakes recorded by a network of nine stations in souther Peru, Hasegawa and Sacks (1981) inferred the seismic zone beneath the northern part of their network dips at about 30° down to a depth of 100 km and then flattens. Because of the locations of their stations, Hasegawa and Sacks (1981) could not confidently locate events more than 150 km from the coast to determine how far the seismic zone remains horizontal.

During our field investigation we recorded about twenty well located intermediate-depth earthquakes ranging in depth from 85 to 110. They too seem to define a flat seismic zone about 25 km thick beneath the Andes (Figure 7). Therefore our data supports Hasegawa and Sacks contention and suggests the seismic zone remains flat at a depth of about 100 km for at least a distance of 450 km from the trench (Figure 7). Hence, the zone does not seem to dip at a constant slope of 15° as inferred by Barazangi and Isacks (1976, 1979)

Very few events were located on the main thrust contact between the Nazca and South American plates and we were unable to document the dip of the initial portion of the subduction zone.

Fault Plane Solutions and the Continuity of the Slab

The fault-plane solutions determined for four of

these intermediate-depth microearthquakes show normal faulting with almost horizontal T axes and parallel to the direction of relative plate motion (Figures 18 and 19). The orientation of the T axes in the direction of of the dip of the seismic zone at intermediate depths in other subduction zones of the world has usually been interpreted as a result of the gravitational body force acting on the downgoing slab (Isacks and Molnar, 1969). If the intermediate part of the slab lies flat, however, and it is decoupled from its deepest segment as suggested by the absence of earthquakes at depths of between 200 and 550 km in Peru, it becomes rather difficult to explain the nature of these normal faults. Hasegawa and Sacks (1981) suggest that the normal faults could be explained by a continous slab descending to a depth of 600 km with an aseismic portion between 200 and 550 km. Their results and our microearthquake study suggest the slab remains horizontal to a distance of about 650 km from the trench, where it bends again and continues to greater depth with a relatively steep angle. This interpretation is supported by the presence of a cluster of intermediate-depth events ocurring at depths of about 150 km beneath eastern Peru (see section B in Figure 16). In this scenario, these earthquakes would represent the kneecap of a second bend in the slab (Figure 20). One could speculate that a large number of earthquakes occur here because of the stresses produced by the forces

bending the slab, in a situation analogous to that of a plate bent at a trench.

It is unclear what causes these contortions of the downgoing slab: a sudden unbending of the plate to underplate the Andes over a distance of about 300 km, and a second sharp change in dip thereafter. A possible culprit for this behavior may be the buoyant nature of the Nazca ridge that resists subduction due to its lighter composition. Based on reconstructions of past plate motions, Pilger and Handshumacher (1981) suggest the Nazca and Tuamotu Ridges represent mirror images of hot-spot traces formed at the Pacific-Farallon plate boundary, the former resting now on the Nazca plate, the latter on the Pacific plate. Being a mirror image of the Tuamotu Islands, the subducted eastern continuation of the Nazca Ridge bends to the northeast and lies now beneath Peru (Pilger, 1981) (Figure 21). The buoyancy added to the slab by the ridge induces the very shallow dip of the subduction zone in this area. South of the Nazca Ridge, in southern Peru and northern Chile, the subducted slab does not possess this positive buoyancy and the subduction process reverts to a steeper and more normal dip of about 30°. The steep-dipping slab lying to the east of the flat seismic zone (Figure 20) may be interpreted as a remnant of a normal episode of plate subduction prior to the arrival of the easternmost extension of the Nazca Ridge to the trench.

Summary

During the summer of 1980 we operated a network of portable seismographs to monitor the seismicity in the Central Andes of Peru east of the city of Lima. Although most of our stations were located in the High Plateau only about 15 earthquakes were located in the crust beneath the network. The majority of the microearthquakes in the crust occurred along the eastern margin of the Cordillera Oriental in the sub-Andes. The western part of the sub-Andes appears to be the physiographic province subjected to the most intense brittle deformation. Focal depths for these crustal earthquakes are as deep as 50 km. The Huaytapallana fault in the Cordillera Oriental also shows relatively high seismicity along a northeast-southwest trend that agrees with the fault scarp and the east-dipping nodal plane of two large earthquakes that occurred on this fault on July 24 and October 1, 1969. The fault-plane solutions of events in the sub-Andes and near the Huaytapallana fault show P axes oriented east-west, in the general direction of relative plate motion between the Nazca and the South American plate. Microearthquakes of intermediate depth recorded during the experiment show a flat seismic zone about 25 km thick at a depth of 100 km. This agrees with the contention of Hasegawa and Sacks (1981) who suggest that beneath Peru the slab first dips at

an angle of 30° to a depth of 100 km and then flattens. The fault-plane solutions of intermediate-depth microearthquakes have horizontal T axis oriented in an east-west direction

TABLE 1

STATION COORDINATES

NAME	LAT	LONG	DELAY (sec)	LOCATION	ELEV (m)
ACO	-11.981	-75.095	0.08	ACOPALCA	3900
SAC	-11.778	-75.191	0.16	SACSACANCHA	4250
MAR	-11.604	-75.653	0.11	MARCAJASHA	4050
UNC	-11.235	-75.374	-0.36	UNCUSH	1925
COS	-12.140	-75.562	0.23	COSMOS	4600
CUL	-12.203	-75.211	0.06	CULHUAS	3800
LAI	-12.308	-75.359	0.07	LAIVE	3850
PAC	-11.778	-75.727	0.03	PACHACAYO II	3700
HYT	-11.960	-75.039	0.23	HUAYTAPALLANA	4600
PAM	-12.435	-74.870	0.04	PAMPAS	3750
PAG	-12.003	-74.917	0.01	PAGUA	3600
ATO	-12.341	-75.087	0.08	ATOMPAMPA	3900
MOL	-11.726	-75.409	0.02	MOLINOS	3650
PAR	-11.666	-75.085	0.12	PARCO II	3000
COC	-11.890	-75.305	-0.01	CONCEPCION	3500
COM	-11.699	-75.082	-0.12	COMAS	3000
YAU	-11.714	-75.469	-0.02	YAULI	3450
PA1	-11.782	-75.721	-0.03	PACHACAYO I	3700
PR1	-11.672	-75.083	-0.12	PARCO I	3000
VIS	-12.592	-74.961	0.12	VISCAPATA	4100
CHA	-12.011	-75.374	0.00	CHAMBARA	3350
GUA	-13.993	-75.789	-0.64	GUADALUPE	678
CAL	-12.627	-75.978	-0.42	CALACOCHA	1655
QUI	-12.943	-76.437	-0.68	QUILMANA	510
SJU	-15.356	-75.189	-0.77	SAN JUAN	75
NNA	-11.998	-76.843	-0.67	NANA	555
LM2	-12.068	-77.033	-0.67	LIMA2	127
HUA	-12.038	-75.323	-0.05	HUANCAYO	3313
VES	-12.213	-76.937	-0.77	V.EL SALVADOR	110
ANC	-11.775	-77.150	-0.78	ANCON	56
AYA	-13.080	-74.250	-0.17	AYACUCHO	2800
POC	-11.250	-74.600	-0.63	PTO OCOPA	750

TABLE 2

VELOCITY MODELS

Ocola and Meyer (1975)

Vp (km/sec)	Depth to layer (km)
5.0	0.0
5.6	10.0
6.0	22.0
7.9	65.0
8.0	100.0

Meissner et al (1977)

Vp (km/sec)	Depth to layer (km)
5.9	0.0
6.2	10.0
6.7	30.0
8.1	50.0

James (1970)

Vp (km/sec)	Depth to layer (km)
5.0	0.0
6.0	8.0
6.6	25.0
7.9	60.0
8.0	100.0

TABLE 3

COMPARISON OF HYPOCENTRAL LOCATIONS USING DIFFERENT VELOCITY MODELS

DATE	TIME	LAT	LON	H	RMS	ERX	ERZ	DIST	NUMBER PHASES
800513	16:35:22.5	11.05	74.67	106.4	0.35	5.20	4.00	23.1	14
800513	16:35:23.3	11.02	74.67	107.6	0.31	5.50	4.50	26.4	
800513	16:35:23.0	10.93	74.64	112.4	0.28	4.30	2.80	35.8	
800515	7:57: 3.8	11.68	74.77	23.4	0.06	6.50	5.10	47.40	8
800515	7:57: 5.1	11.69	74.79	14.3	0.07	3.90	11.10	44.90	
800515	7:57: 5.4	11.68	74.77	12.4	0.06	4.60	2.10	46.80	
800519	13:23:49.4	12.22	76.22	37.9	0.23	5.10	14.00	52.30	10
800519	13:23:50.6	12.21	76.23	24.4	0.27	49.60	51.50	53.40	
800519	13:23:51.4	12.21	76.21	22.4	0.24	5.30	21.30	52.60	
800520	1: 3:36.6	10.98	74.86	24.4	0.05	9.50	93.60	80.80	12
800520	1: 3:37.8	10.97	74.86	24.1	0.13	14.20	31.50	81.50	
800520	1: 3:37.8	10.96	74.85	24.9	0.12	3.10	2.20	83.50	
800523	1:39:27.2	11.97	74.90	9.4	0.13	1.50	0.60	3.90	9
800523	1:39:27.7	11.97	74.91	6.2	0.12	1.40	0.70	3.80	
800523	1:39:28.1	11.97	74.88	2.8	0.11	2.80	5.10	5.90	
800523	9:32:30.1	11.53	75.31	27.1	0.04	3.10	5.60	26.90	5
800523	9:32:30.1	11.52	75.31	30.3	0.04	3.80	5.80	27.30	
800523	9:32:30.1	11.52	75.31	32.7	0.04	4.60	5.40	27.80	
800523	13:34:31.2	11.87	77.33	54.8	0.42	6.00	2.90	22.0	8
800523	13:34:31.3	11.87	77.39	56.6	0.48	7.60	4.40	27.6	
800523	13:34:31.2	11.85	77.45	57.9	0.52	8.70	6.70	33.4	
800529	3:45:38.7	11.88	75.06	12.9	0.01	1.50	3.50	9.30	6
800529	3:45:39.1	11.88	75.06	9.8	0.05	1.50	4.70	9.50	
800529	3:45:39.8	11.88	75.06	6.1	0.06	1.20	5.10	9.60	
800530	4:57:16.3	11.20	75.02	40.8	0.08	3.60	4.50	52.40	7
800530	4:57:20.2	11.35	75.08	29.2	0.05	13.40	5.10	35.80	
800530	4:57:20.2	11.33	75.07	29.3	0.05	14.10	3.10	38.10	

800530	10:41:57.5	12.70	76.48	46.3	0.47	2.80	6.60	27.0	14
800530	10:41:57.7	12.77	76.53	53.1	0.37	2.10	1.20	21.9	
800530	10:41:59.6	12.73	76.49	38.9	0.31	1.40	1.20	24.6	
800530	10:45:16.2	11.13	73.88	11.9	0.20	21.60	57.60	143.90	13
800530	10:45:19.9	11.18	73.99	8.1	0.20	22.20	4.70	131.40	
800530	10:45:20.1	11.17	73.95	16.4	0.19	17.90	5.80	136.10	
800531	1:57:21.1	11.91	75.89	104.3	0.12	5.10	5.70	55.90	9
800531	1:57:22.7	11.91	75.89	98.4	0.12	6.40	10.60	55.80	
800531	1:57:22.7	11.94	76.02	92.0	0.09	3.80	7.10	71.20	
800531	3: 3: 6.8	12.11	75.60	110.3	0.13	6.40	15.20	43.90	11
800531	3: 3: 8.4	12.10	75.59	105.7	0.10	4.30	6.90	42.60	
800531	3: 3: 8.9	12.10	75.60	108.0	0.11	5.10	8.40	44.10	
800602	16: 3:18.8	11.11	74.79	50.7	0.38	3.30	6.10	25.8	12
800602	16: 3:22.8	11.22	74.86	17.4	0.38	2.40	2.00	28.5	
800602	16: 3:21.7	11.12	74.81	33.7	0.45	13.30	19.80	27.3	
800602	20:58:44.4	12.26	75.35	9.8	0.10	2.00	1.60	5.30	7
800602	20:58:44.6	12.29	75.33	9.3	0.09	2.00	3.30	3.60	
800602	20:58:44.0	12.34	75.32	14.1	0.07	1.20	2.30	5.70	
800603	3:44:59.4	11.05	74.72	21.3	0.14	7.70	22.90	74.30	12
800603	3:44:59.7	11.03	74.68	17.9	0.13	2.60	3.50	78.90	
800603	3:44:59.6	10.99	74.65	16.6	0.17	2.40	46.80	83.50	
800603	11:14:55.4	11.87	76.23	108.9	0.09	2.40	7.80	68.40	9
800603	11:14:57.6	11.88	76.22	97.2	0.11	1.90	4.30	68.90	
800603	11:14:58.5	11.87	76.23	96.6	0.07	2.10	6.40	68.50	
800603	16:31:13.1	11.24	74.59	88.8	0.14	2.20	2.80	71.30	23
800603	16:31:13.4	11.18	74.52	88.2	0.15	2.60	3.80	81.70	
800603	16:31:13.6	11.12	74.45	84.7	0.19	3.00	5.00	91.90	
800604	3: 8: 5.8	11.78	75.10	13.5	0.08	1.40	3.40	10.00	6
800604	3: 8: 6.3	11.78	75.10	10.2	0.11	1.50	4.40	10.40	
800604	3: 8: 7.0	11.78	75.10	6.2	0.12	1.10	3.60	10.00	
800604	4: 7:28.1	11.12	75.13	54.5	0.42	2.80	4.30	29.5	15
800604	4: 7:28.6	11.06	75.11	53.6	0.34	2.50	4.00	34.2	
800604	4: 7:29.4	11.05	75.10	45.3	0.40	3.30	2.10	36.8	
800604	6:22: 7.3	11.73	74.76	25.6	0.10	2.50	3.60	36.50	9
800604	6:22: 7.9	11.73	74.75	23.2	0.10	2.20	4.50	36.80	
800604	6:22: 7.9	11.72	74.71	20.5	0.12	2.50	5.40	40.90	
800604	12:37:30.2	11.86	75.05	15.7	0.10	0.50	0.90	11.5	12
800604	12:37:31.0	11.86	75.06	8.7	0.15	0.60	2.30	11.5	
800604	12:37:31.7	11.86	75.06	4.4	0.12	0.50	2.30	11.5	

800605	20:42:25.7	13.13	76.42	48.4	0.45	3.30	1.20	20.80	15
800605	20:42:25.0	13.33	76.45	41.8	0.48	4.70	1.70	42.90	
800605	20:42:24.9	13.39	76.64	35.6	0.50	5.00	1.80	54.30	
800606	3:26: 0.7	12.93	76.31	91.0	0.25	4.40	5.90	13.5	9
800606	3:26: 3.0	12.94	76.26	77.4	0.28	3.50	4.10	18.6	
800606	3:26: 3.9	12.93	76.31	78.2	0.23	3.00	3.30	13.8	
800606	6: 3:36.6	12.19	76.17	79.3	0.19	1.70	9.60	76.50	10
800606	6: 3:37.0	12.18	76.19	91.8	0.17	2.10	8.80	73.90	
800606	6: 3:37.3	12.16	76.21	99.5	0.16	2.50	9.40	71.60	
800609	0: 5: 8.5	12.12	75.23	98.8	0.18	2.20	3.40	9.60	15
800609	0: 5: 9.6	12.13	75.23	98.0	0.19	2.60	4.30	8.60	
800609	0: 5: 9.7	12.14	75.23	102.4	0.20	2.90	4.50	6.60	
800610	7:42:18.9	11.87	75.59	97.6	0.14	1.80	6.10	17.9	12
800610	7:42:20.6	11.87	75.59	92.3	0.14	1.80	6.20	17.9	
800610	7:42:21.8	11.87	75.59	87.2	0.14	1.80	6.10	18.0	
800610	23:17:34.0	11.82	75.16	12.7	0.02	0.60	2.40	18.5	5
800610	23:17:34.4	11.82	75.16	7.3	0.02	0.50	0.50	18.6	
800610	23:17:35.2	11.82	75.16	1.1	0.05	0.50	25.60	18.6	
800611	14:25:41.0	12.75	75.10	116.0	0.33	37.90	44.20	45.30	10
800611	14:25:44.9	12.65	75.12	95.5	0.37	6.10	7.20	34.80	
800611	14:25:45.0	12.72	75.11	96.2	0.30	6.10	6.70	42.30	

°Latitudes and longitudes in degrees, south and west, respectively; H is the focal depth in km; rms root mean square travel time residual; ERX and ERZ are the projections of the error ellipse onto the horizontal and vertical planes, respectively; DIST is the distance of the epicenter to the closest station. The three epicenters and origin times for each microearthquake correspond to locations using the velocity models of Ocola and Meyer (1973), James (1971), and Meissner (1977).

TABLE 4

HYPOCENTRAL PARAMETERS OF SCREENED EVENTS

DATE	TIME	LAT	LON	H	RMS	ERX	ERZ	DIST	NUMBER PHASES
800513	5:31:14.6	10.94	74.67	18.9	0.01	3.20	2.70	35.1	5
800513	13:49:53.9	11.56	73.80	20.9	0.24	2.50	3.90	148.4	12
800513	16:35:22.5	11.05	74.67	106.4	0.35	5.20	4.00	23.1	14
800514	3:46:49.6	12.12	74.71	95.4	0.09	4.50	8.60	39.1	5
800514	8:53:52.1	11.76	75.05	13.5	0.07	1.10	1.20	15.8	8
800514	9: 0:30.0	11.77	75.05	12.6	0.09	1.40	1.60	15.4	10
800515	3:52:32.7	12.36	74.75	17.0	0.11	2.40	1.50	15.3	7
800515	7:57: 5.3	11.72	74.85	23.6	0.08	2.40	1.60	38.0	8
800515	22:26:49.6	13.79	73.59	34.5	0.43	9.90	3.40	204.4	10
800516	4: 1:53.8	11.45	77.51	30.5	0.29	3.60	1.70	95.1	8
800517	3: 6:16.7	11.83	75.07	11.3	0.16	1.00	3.50	14.1	6
800517	11:12:50.4	11.24	75.56	111.4	0.16	2.30	3.80	20.4	11
800518	7: 3: 7.1	12.51	75.23	101.8	0.07	2.40	5.70	30.2	6
800518	23: 2:49.2	11.82	75.08	17.1	0.19	1.00	2.40	13.6	8
800519	6:21: 4.8	11.78	75.08	12.3	0.08	0.90	1.40	12.0	8
800519	8:48:15.6	11.91	75.03	13.6	0.02	0.90	2.70	16.0	6
800519	19:38:53.8	11.24	75.44	19.7	0.01	4.30	0.90	47.0	5
800520	1: 3:37.6	10.97	74.86	24.2	0.17	2.70	1.80	80.8	12
800520	2:48:48.1	11.91	74.74	18.3	0.08	9.80	7.50	21.9	5
800520	22:18:44.7	11.91	75.05	12.8	0.26	1.10	2.90	9.3	7
800521	4:25:47.0	11.25	77.71	15.9	0.14	2.80	2.30	234.1	6
800521	6: 8:22.8	13.79	74.72	108.2	0.16	4.40	5.30	93.3	11
800522	17:35:12.1	11.55	75.19	23.4	0.19	8.10	3.90	18.4	5
800522	21:13:14.1	11.26	74.64	92.4	0.12	3.10	2.40	66.6	8
800522	23:33:21.4	12.88	75.00	95.6	0.43	5.30	2.50	32.8	14
800523	1:39:27.1	11.97	74.90	9.5	0.12	0.80	0.30	4.3	9
800523	9:32:30.2	11.53	75.31	27.1	0.05	1.40	2.40	26.9	5
800523	13:34:31.2	11.87	77.33	54.8	0.42	6.00	2.90	22.0	8
800524	7:36:39.5	11.97	74.90	15.3	0.21	2.30	2.20	4.0	6
800524	8:39:20.8	11.42	74.69	32.1	0.06	1.90	2.50	51.0	6
800525	10:35: 7.4	11.75	75.20	92.6	0.06	2.90	8.10	15.9	5
800525	23:20:31.0	11.82	75.07	18.3	0.07	0.80	1.90	14.4	5
800526	10:25:59.0	12.23	77.04	52.6	0.07	1.40	0.60	10.9	7
800527	1:16:18.4	11.10	74.95	35.2	0.05	6.70	4.60	48.7	6
800528	12: 4:47.7	11.33	75.31	103.9	0.12	1.70	4.20	12.2	8
800528	12:28:31.9	11.90	75.92	105.0	0.49	3.00	5.30	25.6	15
800528	18:31:13.2	11.88	74.48	31.0	0.07	1.60	3.40	49.7	8
800528	21: 5:34.9	11.84	75.07	9.3	0.02	0.50	0.60	15.1	5
800529	0: 3: 9.5	11.06	74.96	38.5	0.13	5.20	3.40	49.4	11

800529	3:45:38.7	11.88	75.06	13.0	0.02	0.60	1.40	9.3	6
800529	9:29:58.8	12.50	75.13	85.9	0.17	2.50	2.50	18.5	12
800529	18:16:49.6	12.56	75.36	90.8	0.22	3.30	2.40	38.6	9
800529	18:29:44.9	12.34	75.09	10.7	0.03	2.20	2.20	0.8	5
800529	19: 6:16.8	11.42	74.71	25.9	0.11	1.90	3.20	49.5	12
800530	4:57:18.4	11.32	75.07	38.0	0.05	2.60	2.10	39.5	7
800530	7:25:51.7	11.27	75.47	19.2	0.13	1.10	0.80	11.3	12
800530	10:41:57.5	12.70	76.48	46.3	0.47	2.80	6.60	27.0	14
800530	13: 0:24.0	11.73	74.69	27.1	0.05	2.80	1.90	39.6	8
800530	13:57:28.7	11.90	75.05	82.2	0.18	1.80	1.00	6.5	13
800530	14:15:14.0	11.84	75.06	9.7	0.02	1.00	0.70	13.9	5
800531	3: 3: 8.9	12.13	75.56	93.2	0.18	3.10	4.20	38.6	11
800531	21:56:31.3	11.03	74.89	38.3	0.04	1.60	3.20	57.0	6
800531	22:46:24.7	11.93	75.00	13.2	0.30	1.00	1.60	5.3	12
800601	4:45:22.3	11.02	74.99	34.7	0.15	1.00	2.30	48.3	18
800601	15:53: 8.1	12.29	74.66	80.7	0.13	3.00	1.30	27.3	8
800601	17:32:41.3	11.20	75.28	21.2	0.24	2.40	1.00	11.5	11
800602	6:52: 0.9	12.29	75.35	14.2	0.06	0.60	0.90	2.5	8
800602	11:12:48.0	12.12	75.09	87.9	0.14	2.20	1.20	15.9	10
800602	20:58:42.2	12.37	75.35	22.1	0.11	2.00	1.30	7.0	7
800602	21:14:59.6	11.87	74.96	17.3	0.12	3.50	1.40	13.3	5
800603	8: 8:41.6	11.08	74.74	20.6	0.15	1.40	1.90	71.0	15
800603	10:10:27.8	11.13	74.78	20.9	0.13	2.50	1.10	65.4	11
800603	10:43:29.8	11.31	75.22	28.9	0.27	1.20	1.80	18.8	19
800603	11:14:55.4	11.87	76.23	108.7	0.09	1.20	3.80	68.5	9
800604	0:55:56.4	11.19	74.86	21.6	0.11	5.10	1.10	56.3	7
800604	2: 9:35.8	11.23	74.86	21.5	0.05	7.50	1.00	53.9	6
800604	3: 8: 5.8	11.78	75.10	13.6	0.08	0.70	1.60	10.0	6
800604	4: 7:28.1	11.12	75.13	54.5	0.42	2.80	4.30	29.5	15
800604	6:22: 7.9	11.74	74.79	26.2	0.09	1.20	1.50	32.7	9
800604	12:37:30.2	11.86	75.05	15.7	0.10	0.50	0.90	11.5	12
800604	23:19:57.9	10.98	74.28	10.1	0.41	5.60	3.10	45.9	14
800605	4:48: 4.6	11.14	74.75	19.8	0.13	2.90	1.40	68.5	6
800605	5: 0:21.7	11.29	75.04	23.6	0.07	1.20	2.90	42.0	5
800605	7: 9:27.9	10.67	74.88	19.5	0.48	5.80	3.60	82.9	16
800605	10:13:33.7	11.21	74.85	33.1	0.22	1.40	2.80	27.7	16
800605	15:42:59.4	10.97	74.60	18.9	0.16	2.50	2.80	89.8	8
800605	23:11: 0.8	11.09	74.74	20.9	0.14	1.90	2.50	70.6	8
800606	0:39:17.6	11.21	74.60	82.3	0.13	1.20	2.30	73.5	10
800606	1:10: 3.6	11.66	74.62	21.5	0.06	1.00	0.50	50.3	11
800606	3:26: 0.7	12.93	76.31	91.0	0.25	4.40	5.90	13.5	9
800606	5:37: 8.2	12.45	76.66	50.3	0.18	1.40	3.50	53.7	10
800606	14: 8: 5.8	12.31	74.26	18.1	0.24	3.30	1.60	89.3	7
800607	5: 7:34.4	11.93	75.00	14.1	0.33	1.10	1.70	5.0	16
800607	5:50:21.7	11.93	74.95	15.6	0.01	0.70	1.00	9.8	7
800607	6:29:52.7	12.39	74.37	18.7	0.20	3.50	2.80	78.3	6
800607	13:46:28.5	11.22	74.72	19.9	0.12	1.40	0.70	63.6	10
800608	2:54:42.5	11.35	75.14	16.8	0.16	1.40	3.00	28.4	9
800608	6:32:42.4	10.89	75.11	43.2	0.08	1.10	1.50	47.5	10
800608	9:52:31.4	11.42	74.84	72.2	0.11	6.10	5.80	38.0	7
800608	10:51:10.0	11.04	74.80	20.3	0.13	1.20	0.90	66.3	10
800608	13: 9:45.2	11.83	75.06	9.8	0.02	0.70	4.90	14.1	5
800608	15:23:32.8	11.83	75.03	9.9	0.08	3.80	4.20	14.8	6

800608	15:48:24.5	11.36	74.81	32.3	0.07	1.10	2.20	46.0	7
800608	16:40:31.3	11.22	74.92	18.9	0.37	5.60	1.80	52.1	14
800608	20:17: 2.6	11.26	74.66	20.4	0.12	1.10	0.90	64.6	9
800609	0: 5: 9.2	12.11	75.25	92.3	0.15	1.20	2.20	11.1	15
800609	6: 8:14.9	11.81	75.15	20.4	0.13	0.50	1.30	5.6	11
800609	7:10:39.6	11.83	75.15	15.0	0.08	0.40	1.00	6.7	10
800609	9:35:28.2	14.22	76.45	36.4	0.43	2.80	0.90	75.6	15
800609	18:58:23.9	11.37	74.82	31.5	0.13	1.00	2.30	44.1	10
800610	1:37:43.0	12.08	75.22	87.3	0.10	1.00	2.50	13.3	13
800610	1:41: 0.0	11.38	74.93	84.2	0.10	3.00	3.60	35.4	7
800610	7:42:18.9	11.87	75.59	97.6	0.14	1.80	6.10	17.9	12
800610	7:55:26.9	11.10	74.85	28.7	0.12	2.00	7.60	67.8	6
800610	8: 1:58.8	11.42	75.67	19.7	0.15	1.90	1.00	20.6	8
800610	8:47:38.6	11.43	75.31	96.3	0.10	2.00	3.90	34.6	10
800610	9: 4: 0.9	11.34	75.12	21.9	0.10	1.70	0.60	36.4	6
800610	11:17:26.2	11.83	75.04	13.1	0.10	0.80	2.10	14.4	7
800610	23:17:34.0	11.82	75.16	12.7	0.02	0.60	2.40	18.5	5
800611	5: 5:11.9	11.84	75.05	11.0	0.02	0.60	1.60	13.5	5
800611	6:53:26.3	11.81	75.09	14.0	0.20	1.20	3.40	15.6	8
800611	8:55: 6.9	11.74	74.48	19.9	0.01	1.80	1.20	56.1	6
800611	11:38:23.1	11.39	75.18	23.2	0.23	1.90	2.60	32.4	7
800612	10:36:22.1	11.91	74.94	7.0	0.05	0.50	2.00	11.0	6

°See note on Table 3 for abbreviations.

Figure Captions

Figure 1. Main physiographic units of the central Andes of Peru (after Megard, 1978). Dotted area is the coastal batholith and hatchured area indicates location of Andean volcanic rocks.

Figure 2. Location of the seismographic stations used in the study. Open symbols show the portable stations; filled symbols are the stations of the permanent Peruvian Network.

Figure 3. Histograms showing distances between calculated epicenters and focal depths for 29 events using the velocity structures proposed by Ocola and Meyer (1973) and James (1971) for the central Andes.

Figure 4. Histograms showing distances between calculated epicenters and focal depths for 29 events using the velocity structures proposed by Ocola and Meyer (1973) for southern Peru and by Meissner et al (1977) for southern Colombia.

Figure 5. Epicenters of all 344 earthquakes recorded during field experiment. Crosses indicate calculated depths

shallower than 50 km and the triangles events deeper than 50 km. Closed symbols show locations of stations used to locate the earthquakes. Dashed lines show the 1000 and 3000 meter topographic contours of the central Andes.

Figure 6. Epicenters of screened catalog of well located microearthquakes. Symbols as in Figure 5.

Figure 7. Hypocenters of screened microearthquakes shown in Figure 6 projected on the cross section A-B. Vertical lines show the projected positions of the stations.

Figure 8. Fault scarp of the Huaytapallana fault produced by the October 1, 1969 earthquake (after Philip and Megard, 1977).

Figure 9. Epicenters of shallow events in the vicinity of the Huaytapallana fault plotted on a gelogical sketch-map of the Eastern Cordillera (after Philip and Megard, 1977). Closed circles show epicenters and filled symbols the seismic stations. Stars are the epicentral locations of the July 24 and October 1, 1969 earthquakes given by the ISC. Their uncertainties are at least 10 km and perhaps 20 km.

Figure 10. Hypocenters of the events shown in Figure 9 projected onto cross section A-B (Figure 9). Arrows indi-

cate position of the stations and dashed line is the assumed dip of the Huaytapallana fault from the fault-plane solution of the 1969 events (Stauder, 1975).

Figure 11. a) Composite fault-plane solution of four earthquakes b) Solution for single event located near the Huaytapallana fault, and c) Fault-plane solution for the July 24, 1969 earthquake (Suarez et al, 1983). Lower-hemisphere equal-area projection. Open symbols indicate dilatation and closed symbols compression.

Figure 12. Two alternative fault-plane solutions for an earthquake occuring in the high Andes at a depth of 17 km, southeast of the Huaytapallana fault. Symbols as in Figure 11.

Figure 13. Map of the central Andes summarizing lower hemispheric projections of fault-plane solutions of shallow crustal events obtained in this study. Dark areas represent quadrants of compressional first motion. Also shown are the fault-plane solutions of two large events (stars) studied by Suarez et al (1982) in this area.

Figure 14. Comparison of the composite fault-plane solution for six events in the sub-Andes and the fault-plane

solucion of the May 15, 1976 earthquake (Suarez et al, 1982) that was located about 20 km east of the events used in the composite solution. Symbols as in Figure 11.

Figure 15. Fault-plane solution of an earthquake located in the western sub-Andes. Symbols as in Figure 11.

Figure 16. Seismicity map of Peru showing the events selected by Barazangi and Isacks (1979).

Figure 17. Vertical cross sections of earthquakes relocated by Hasegawa and Sacks (1981) inside rectangles shown in the inserted map. Solid line is the assumed shape of the seismic zone inferred from the seismicity below a depth of 50 km.

Figure 18. Fault-plane solutions for four intermediate-depth events recorded in this study. Note T axes are nearly horizontal and oriented roughly east-west in all cases.

Figure 19. Map of central Peru summarizing lower hemisphere projections of the fault plane-solutions of intermediate-depth earthquakes obtained in this study. Shown as stars are the locations and fault-plane solutions of the

intermediate-depth events studied by Stauder (1975). Dark areas indicate quadrants of compressional first motions.

Figure 20. Cross section showing the inferred geometry of the subducted slab beneath Peru. To the earthquakes located in this study (shown as circles) we have added the intermediate-depth events selected by Barazangi and Isacks (1976) in Peru (shown as squares). T axes of intermediate-depth events in this area are shown as arrows.

Figure 21. Position of the Nazca and Juan Fernandez Ridges on the Nazca plate relative to South America as a function of time (after Pilger, 1981).

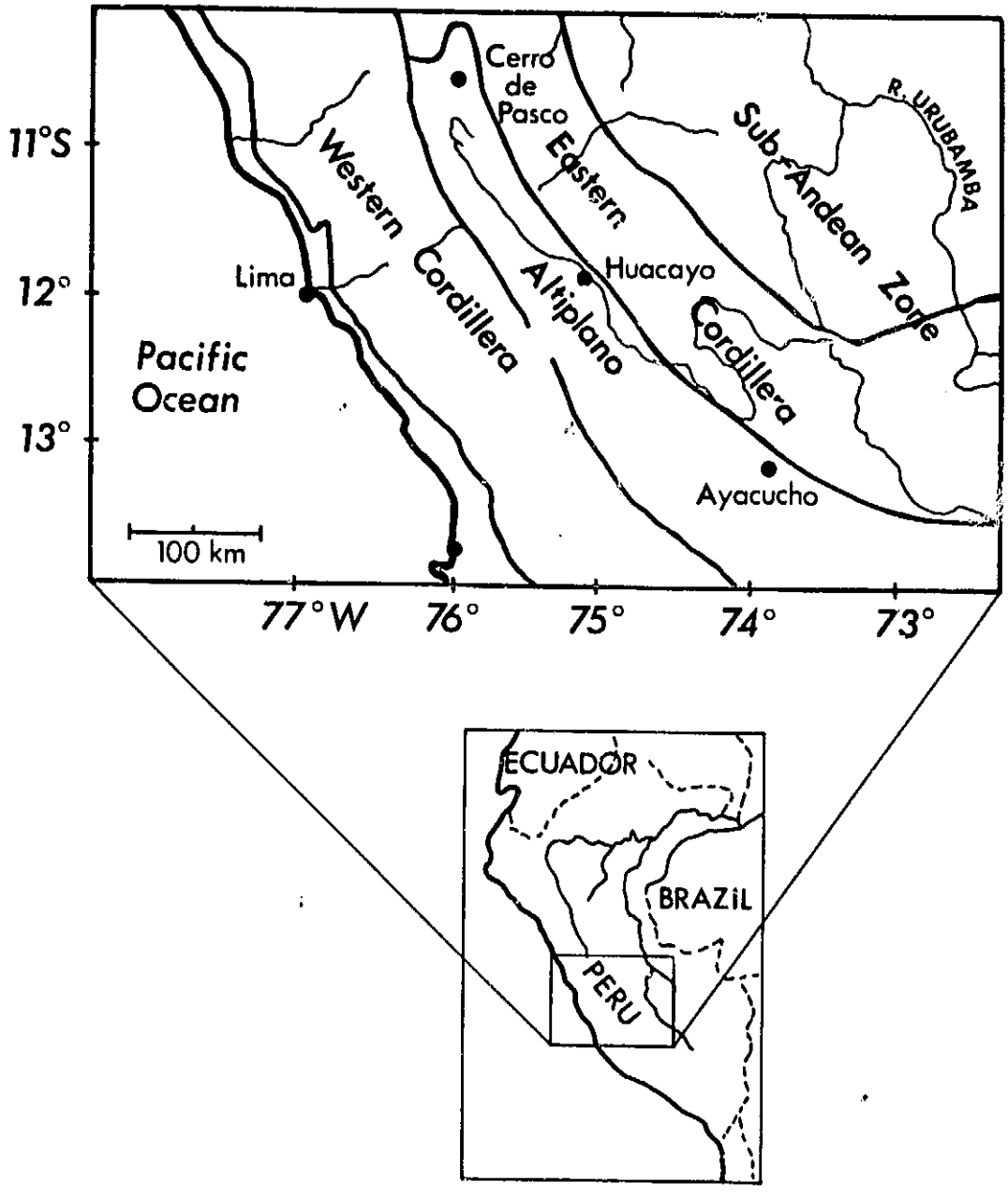

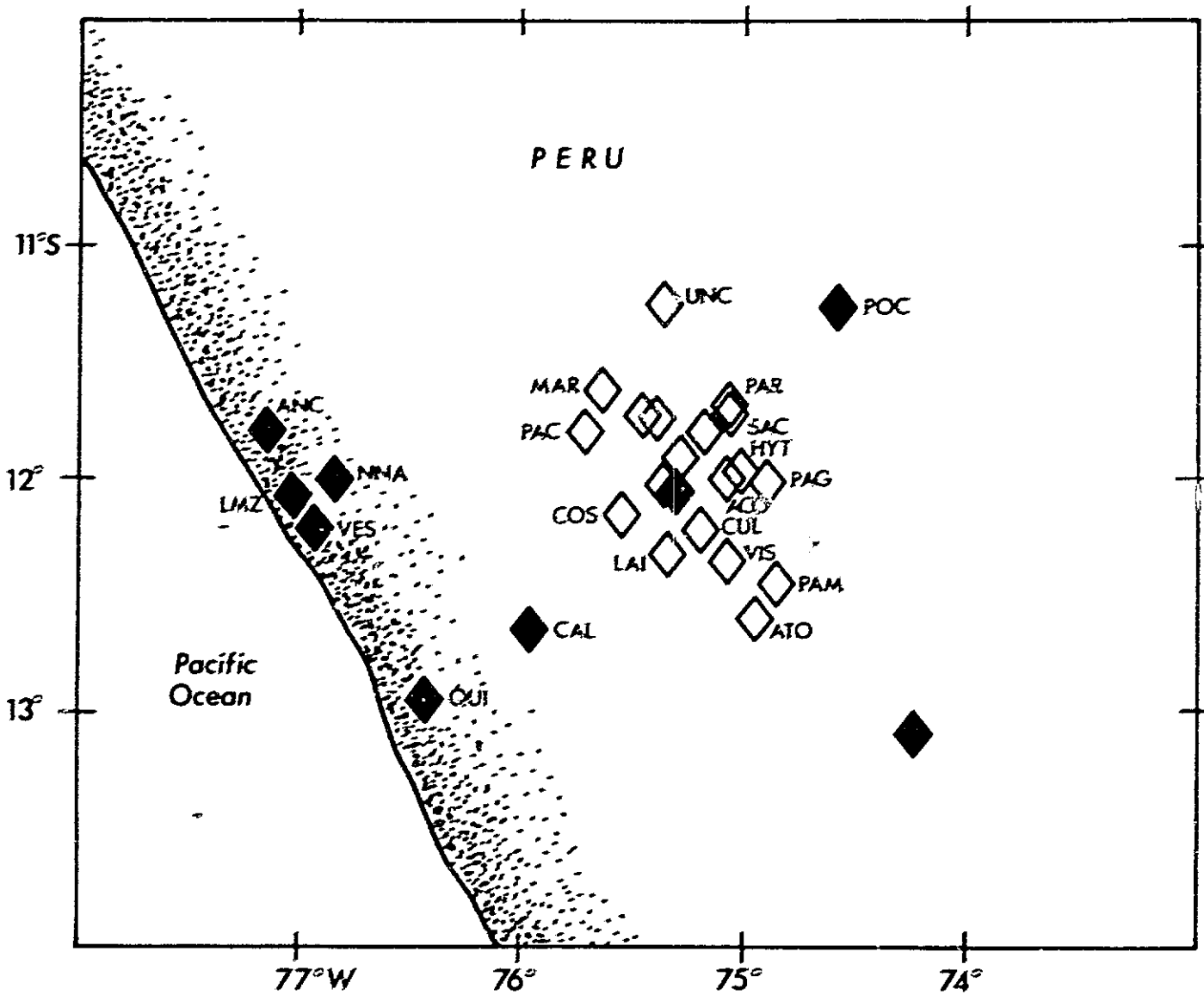

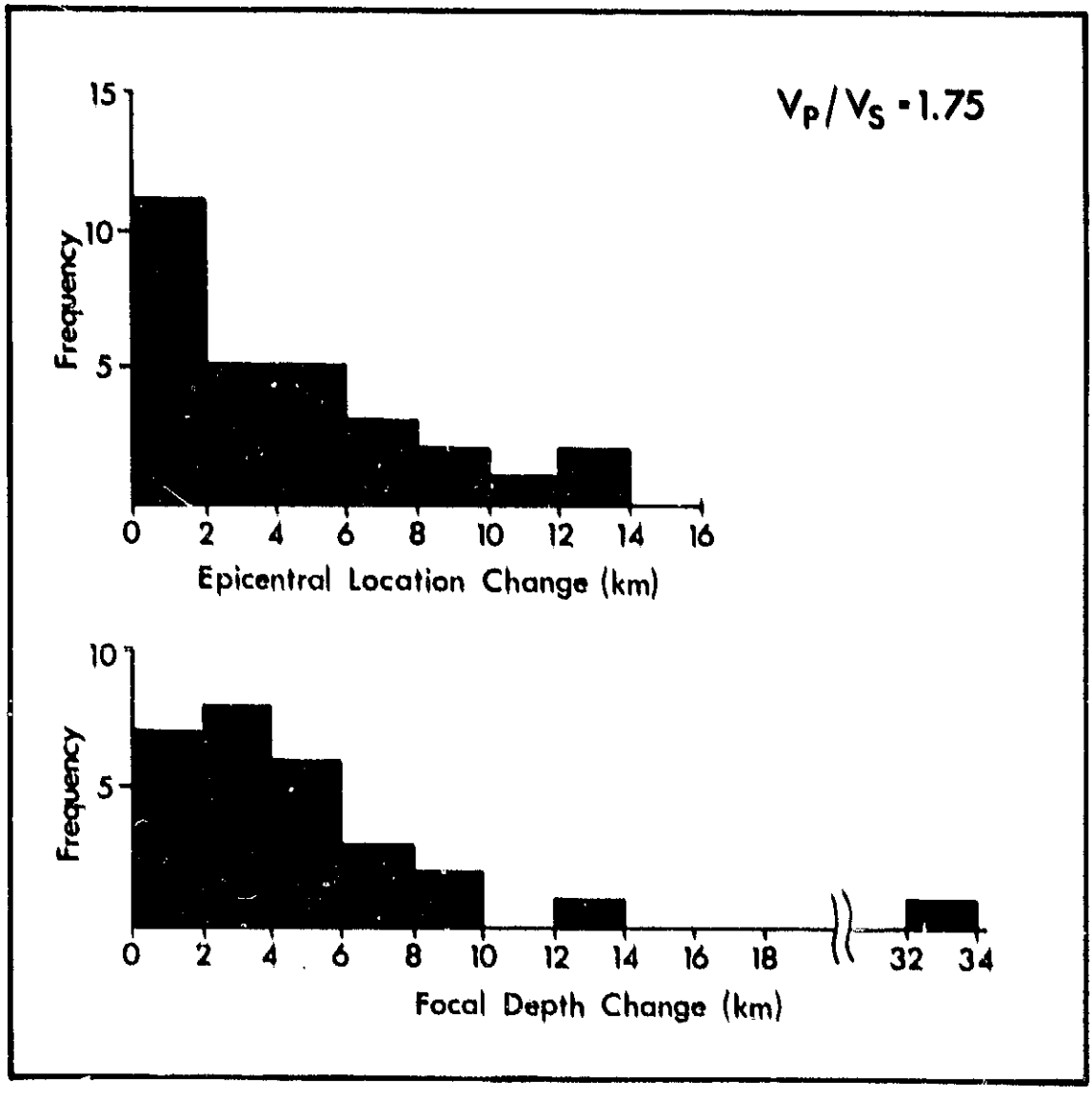

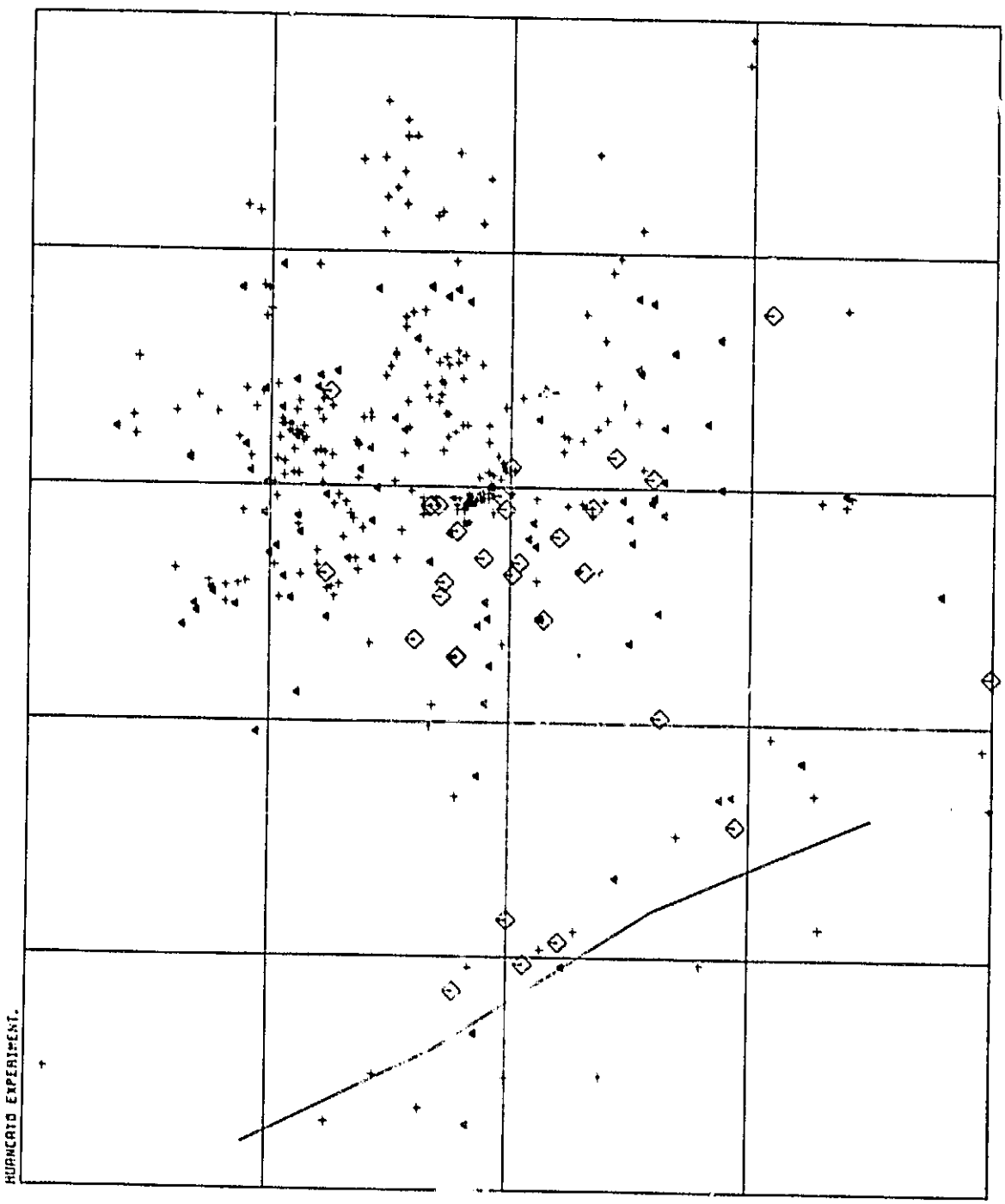

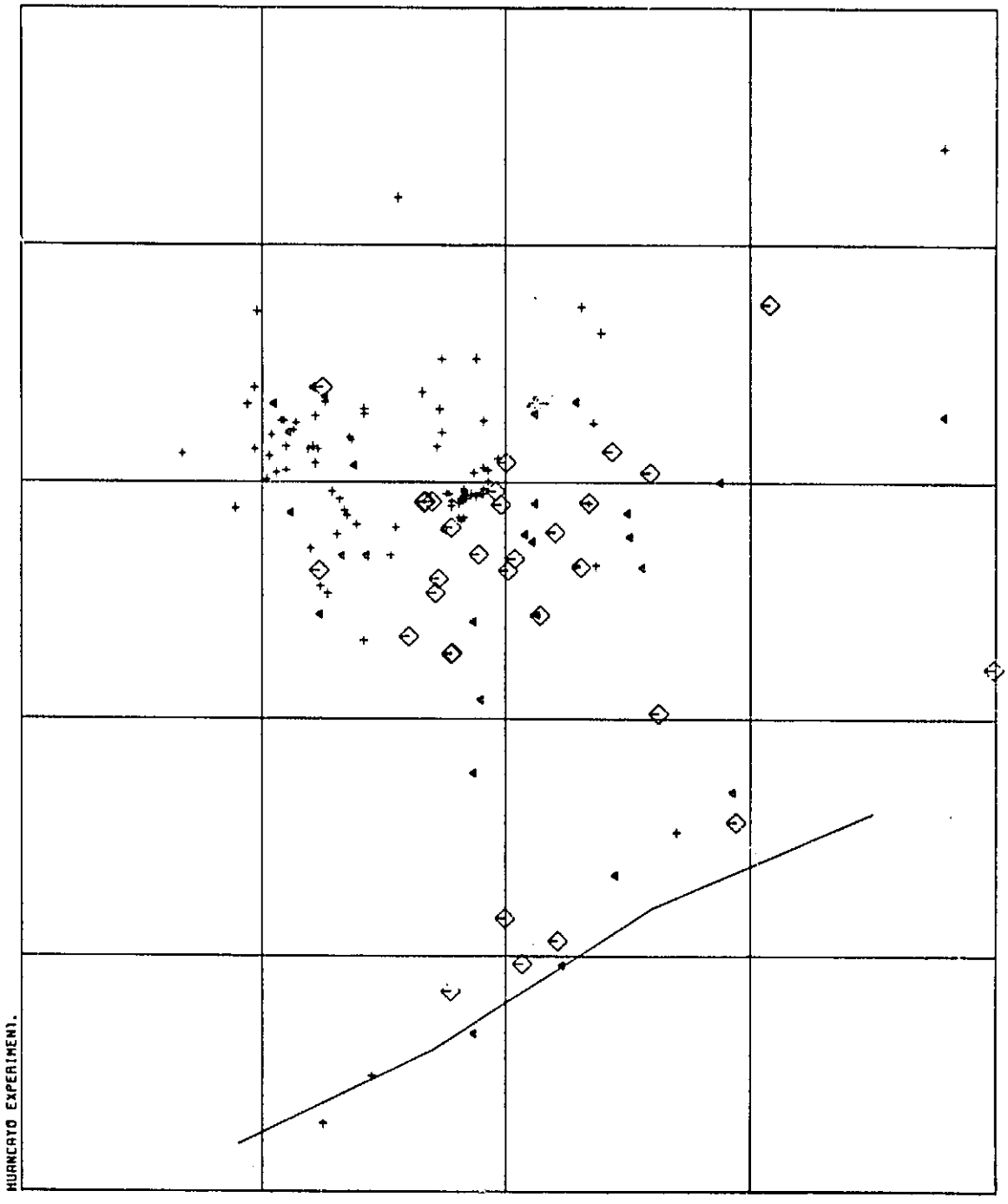

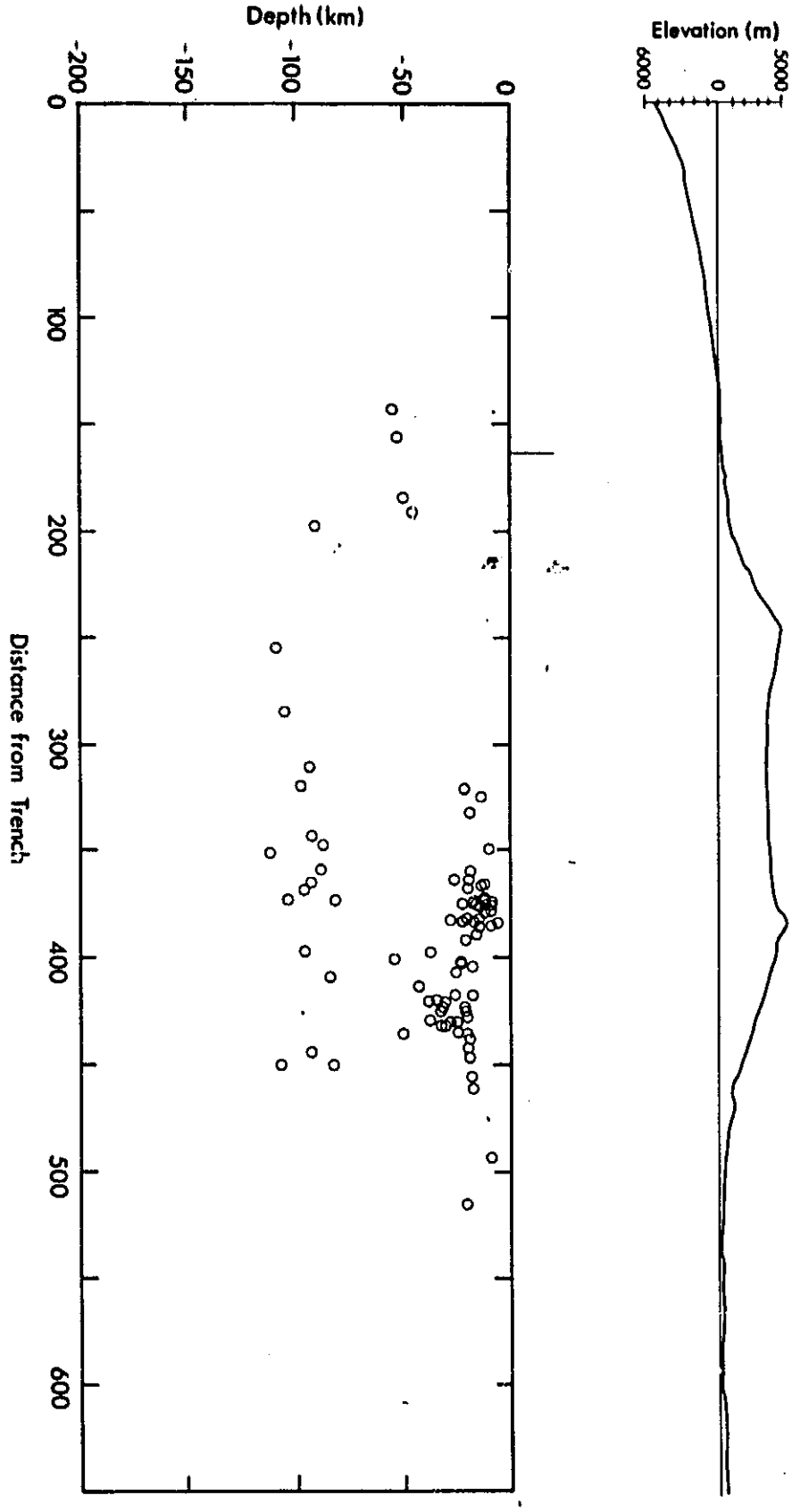

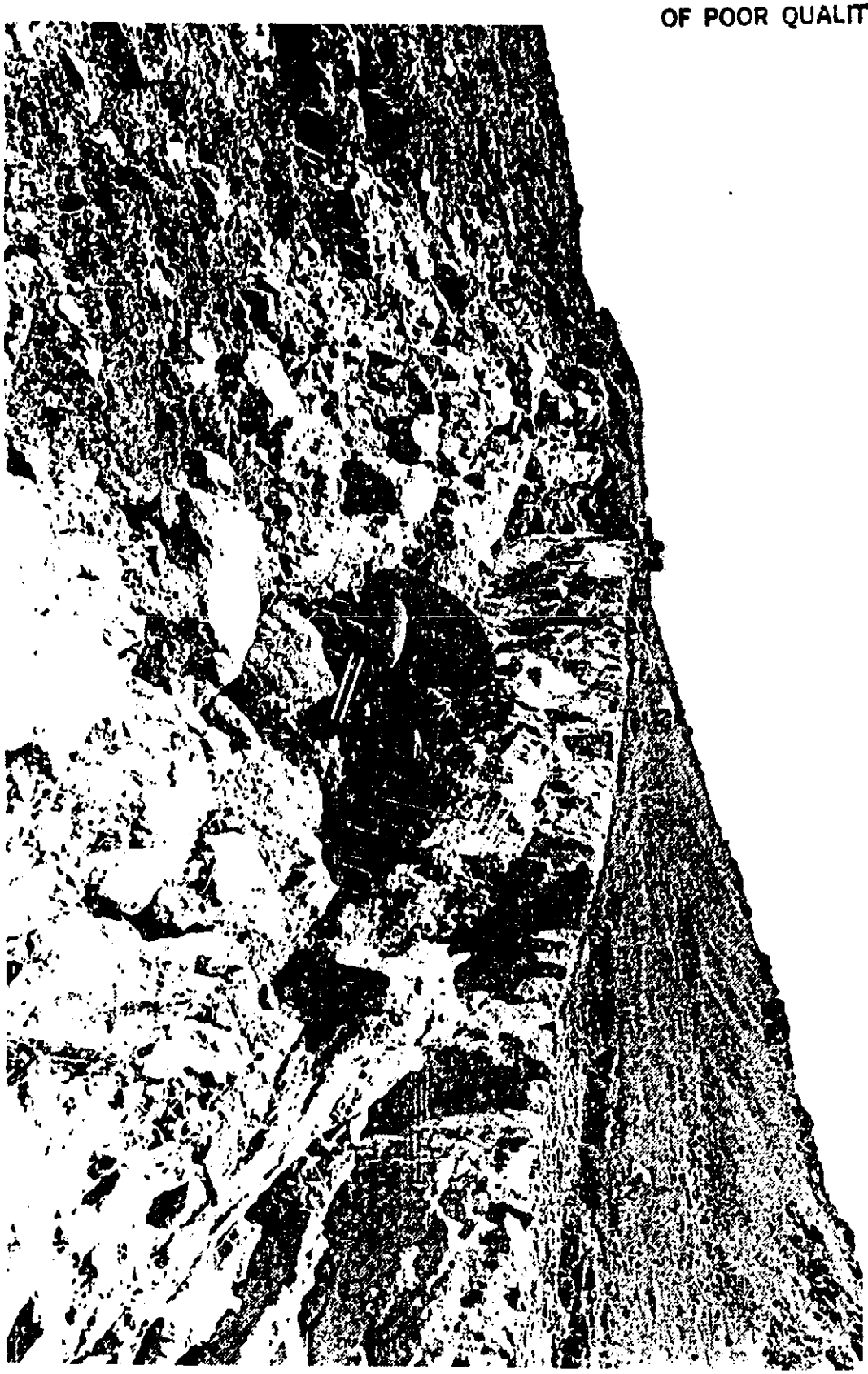

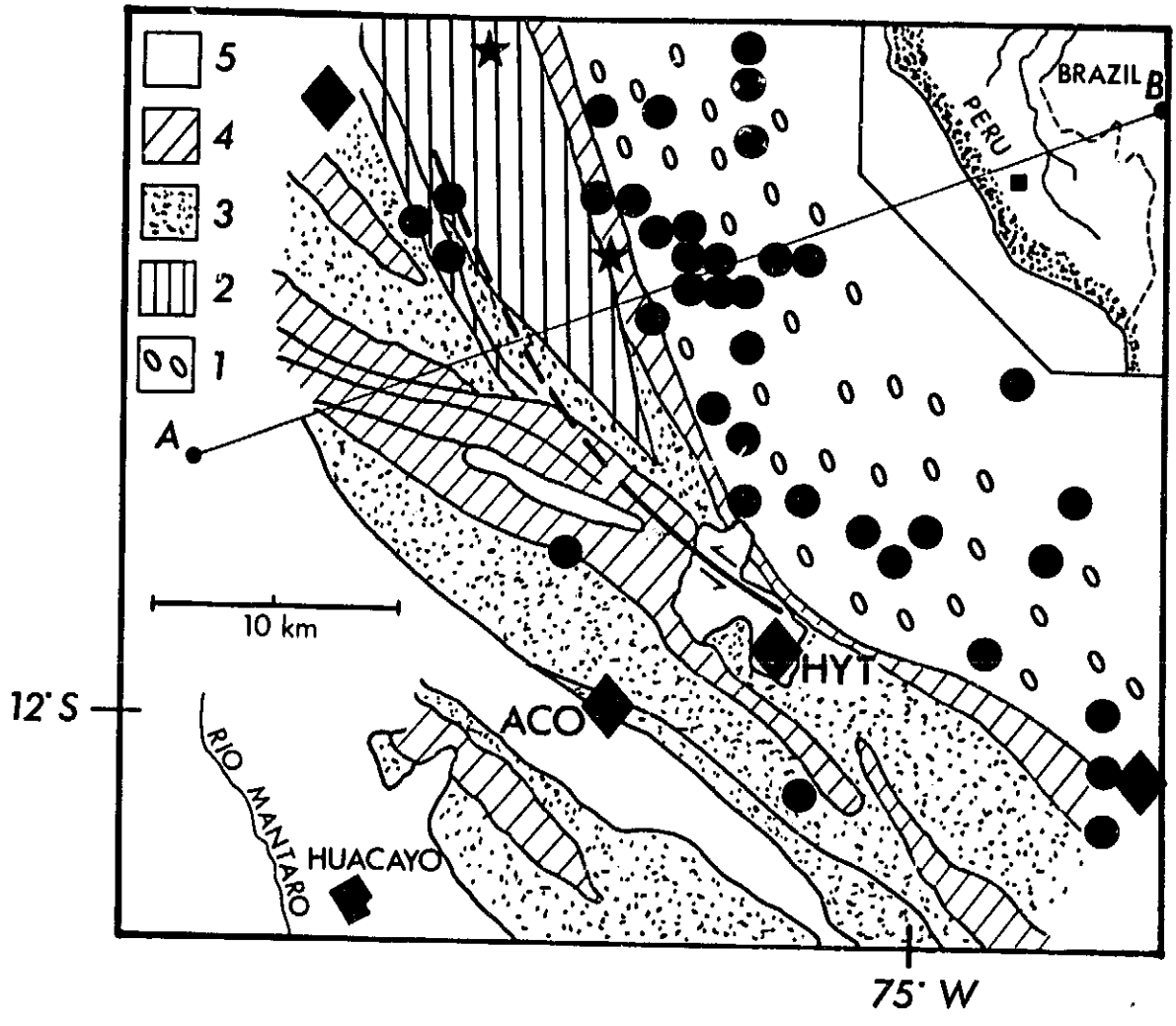

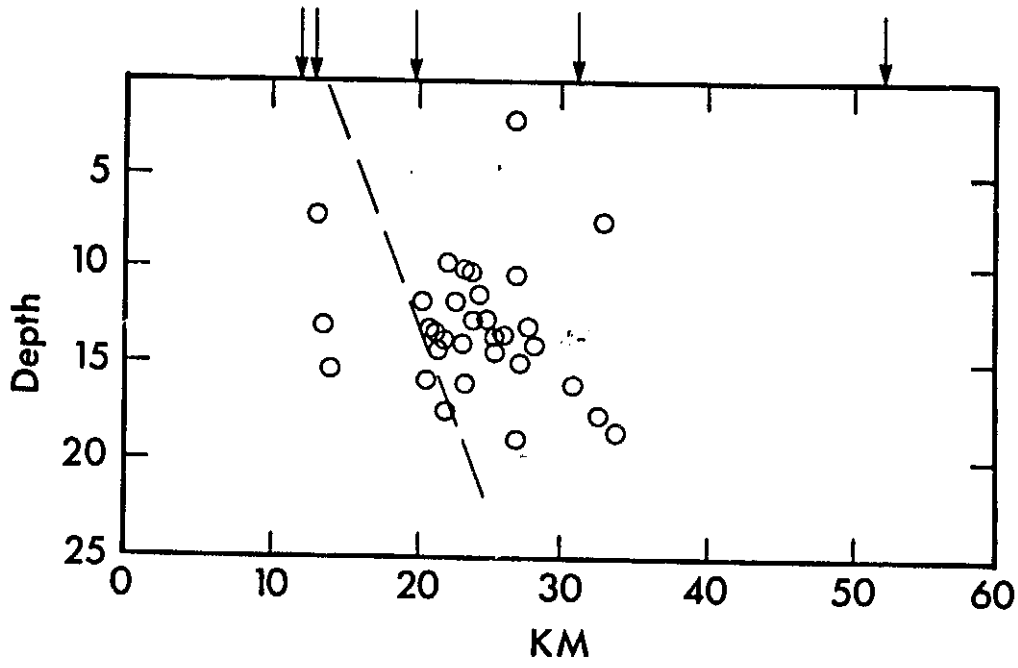

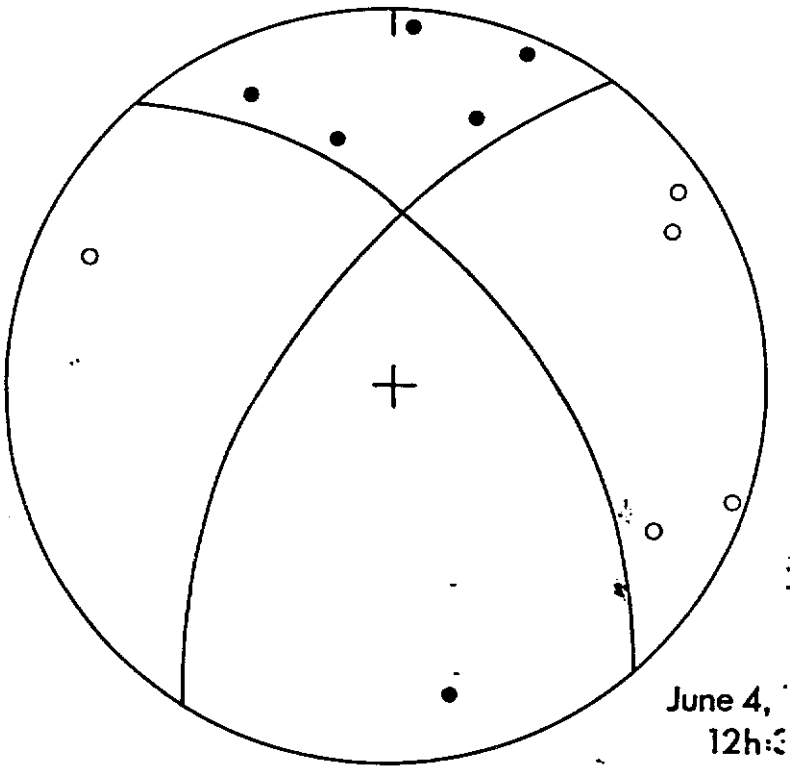

June 4,
12h:3

Huaytapallana Event

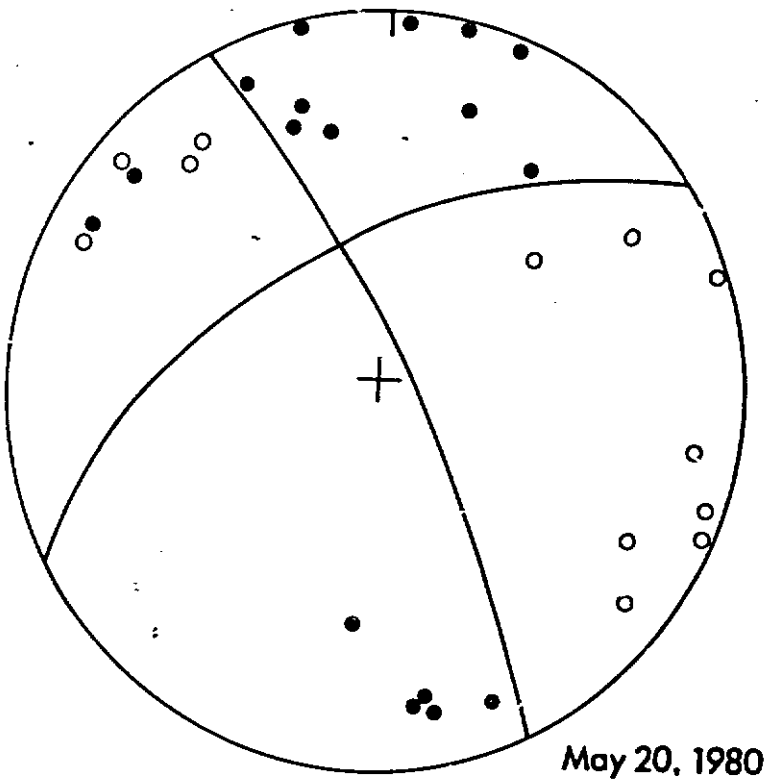

Huaytapallana Composite
Fault-Plane Solution

May 20, 1980
May 31, 1980
June 4, 1980
June 9, 1980

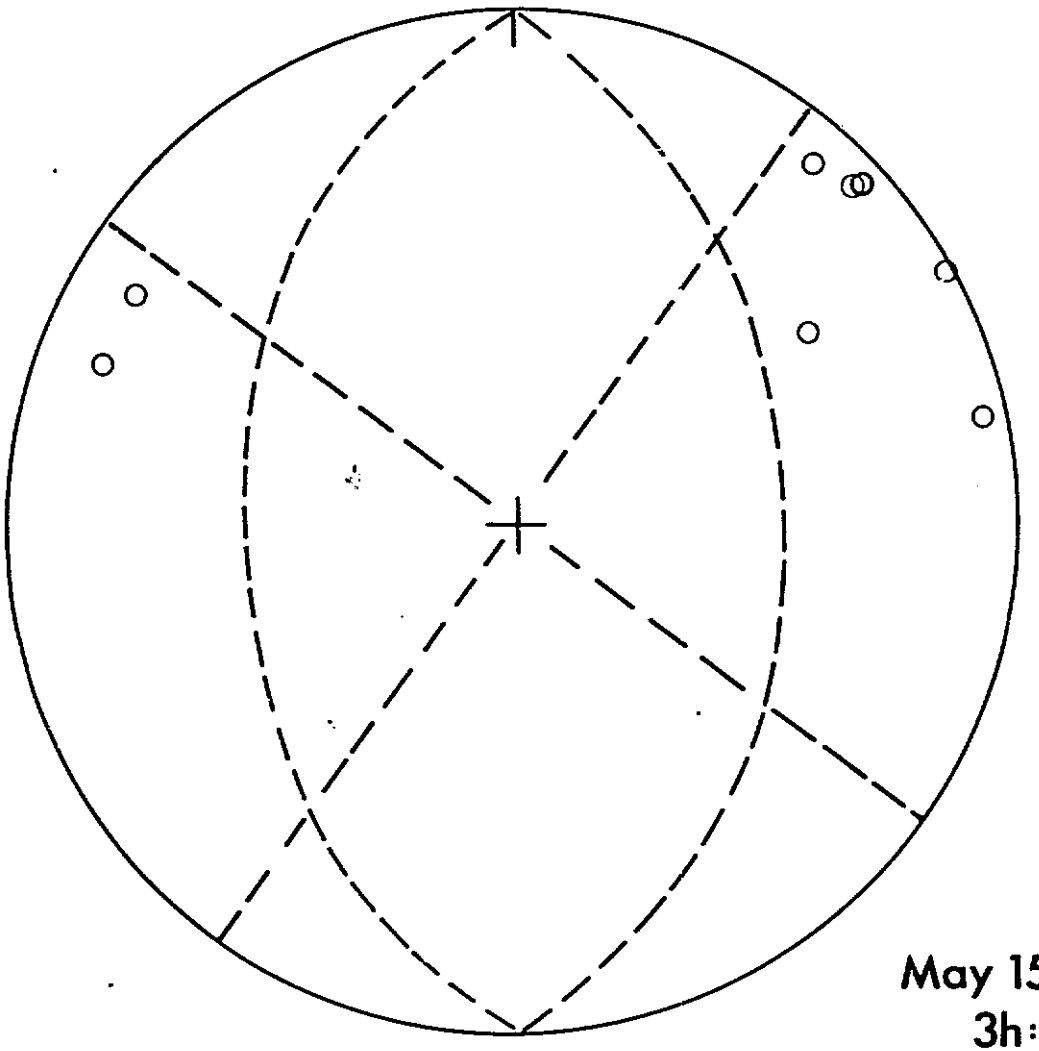

May 15, 1980
3h:52'

Event in the
High Andes
Near Station
PAM

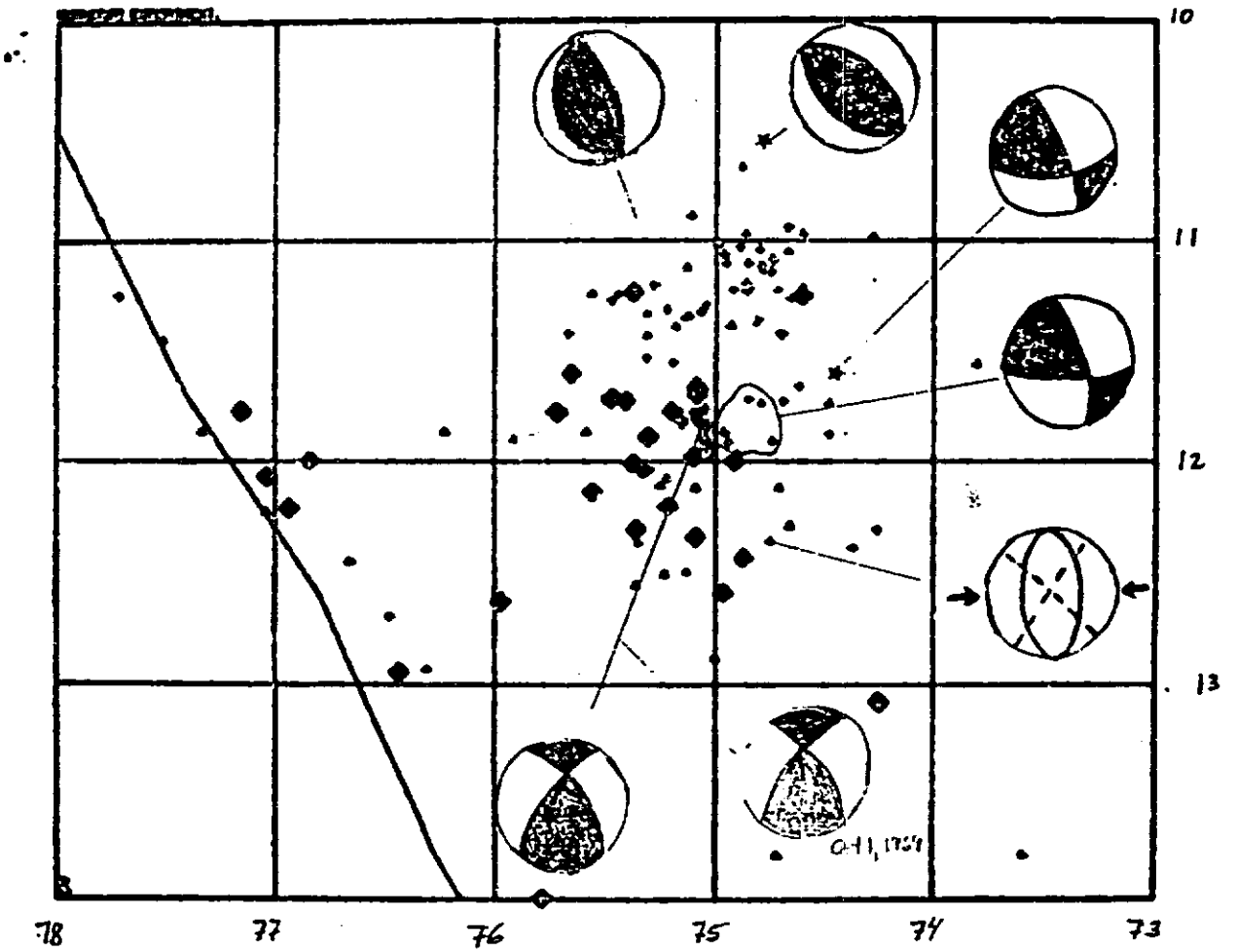

Fig. 13

May 15, 1976

Teleseismic Event
in the Sub-Andes

May 15, 1980 7h:57′
May 20, 1980 2h:48′
May 24, 1980 7h:36′
May 25, 1980 23h:20′
June 4, 1980 6h:22′
June 7, 1980 5h:07′

Events in the
Sub-Andes

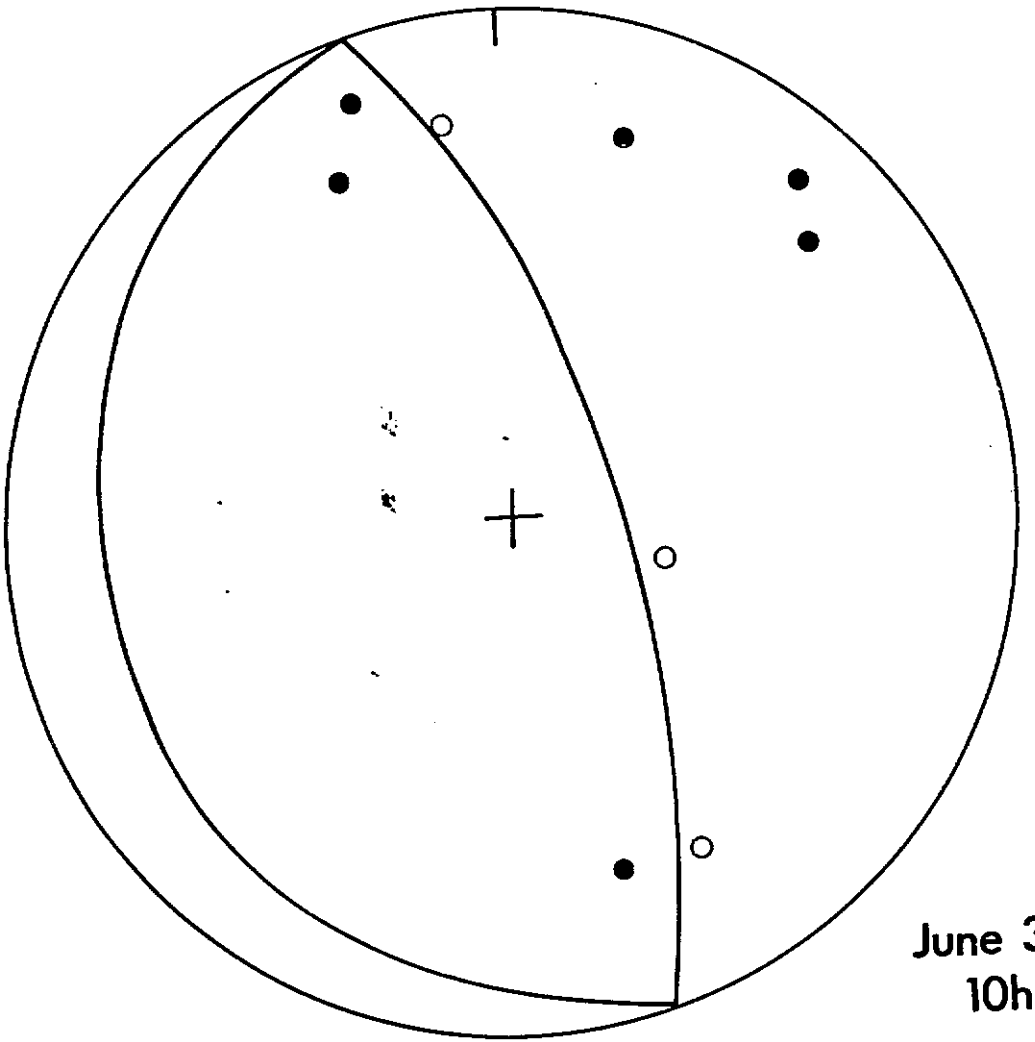

June 3, 1980
10h:43'

Event in the
Sub-Andes

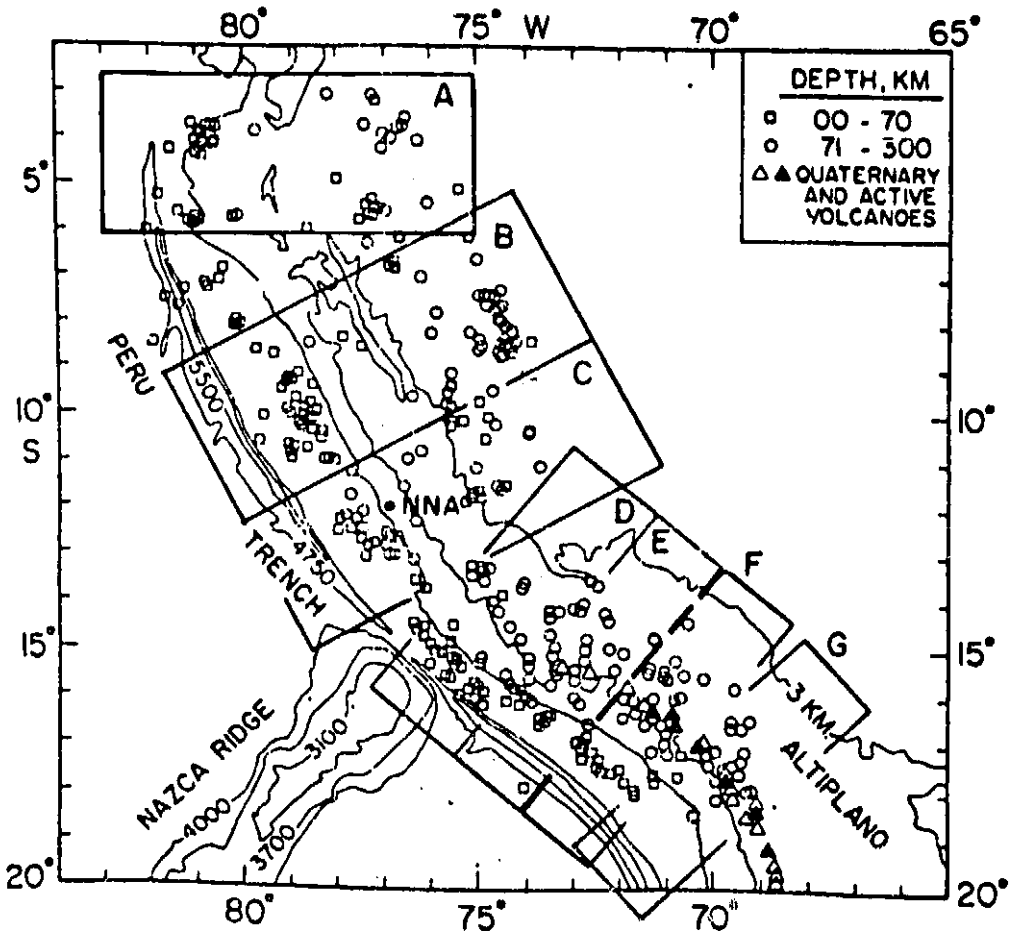

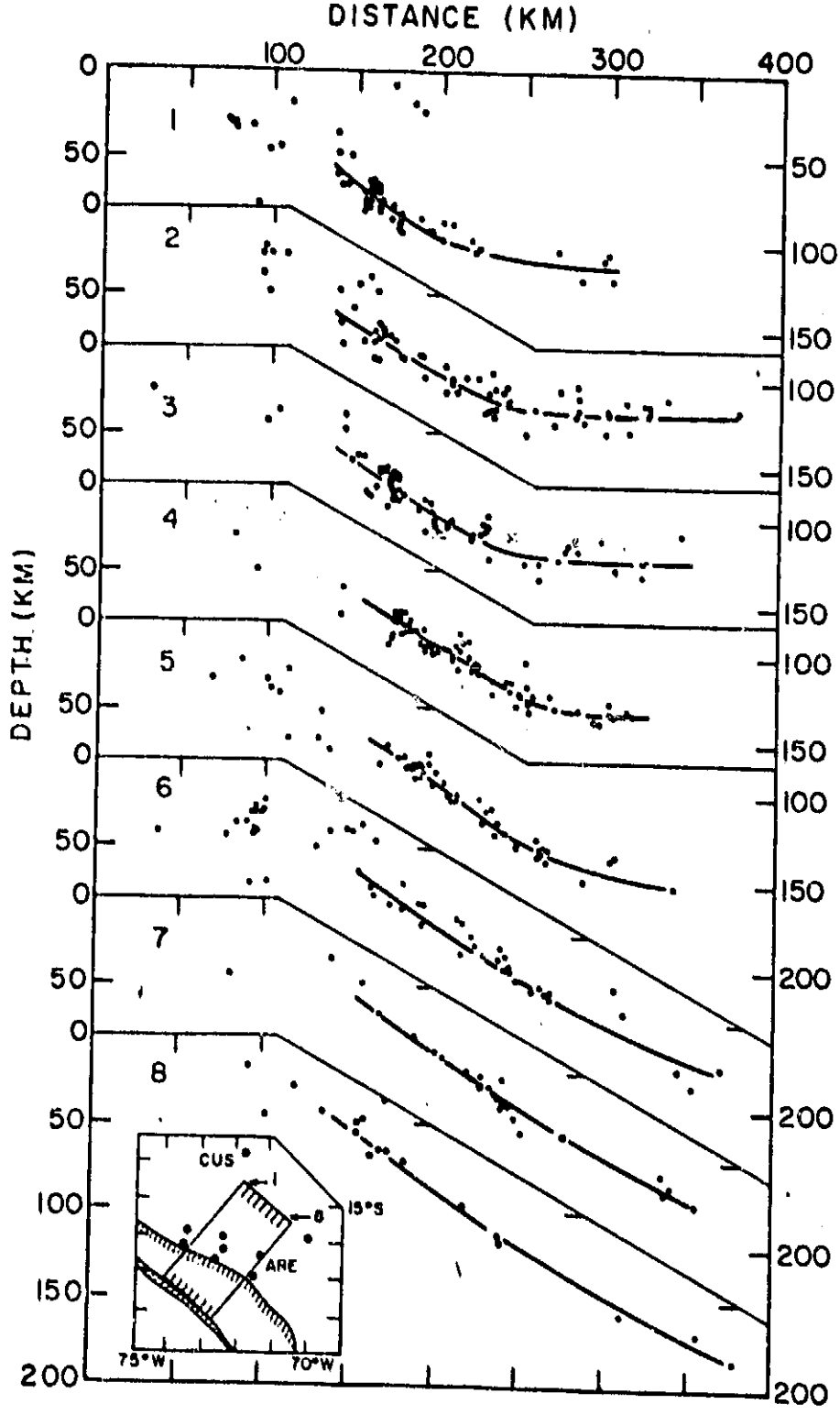

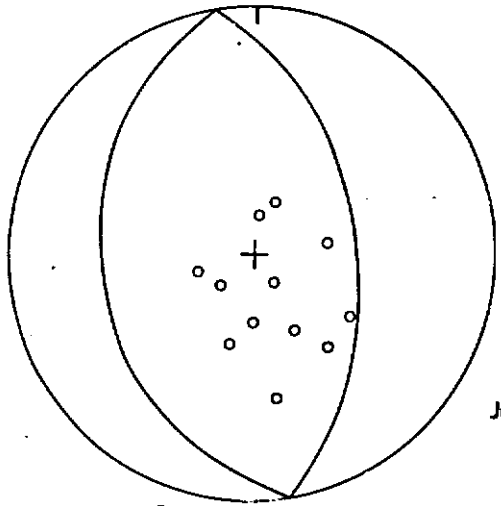

June 10, 1980
12h:06'

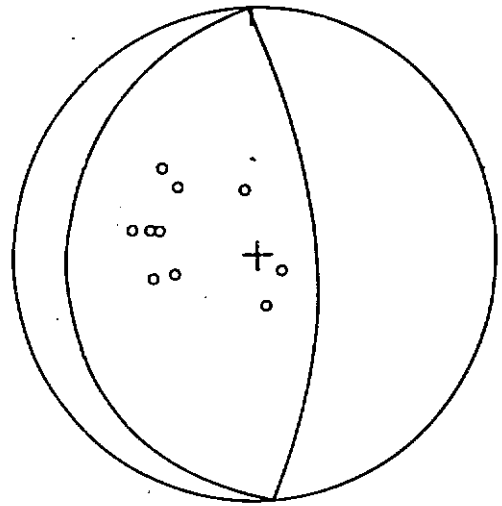

June 10, 198
7h:42

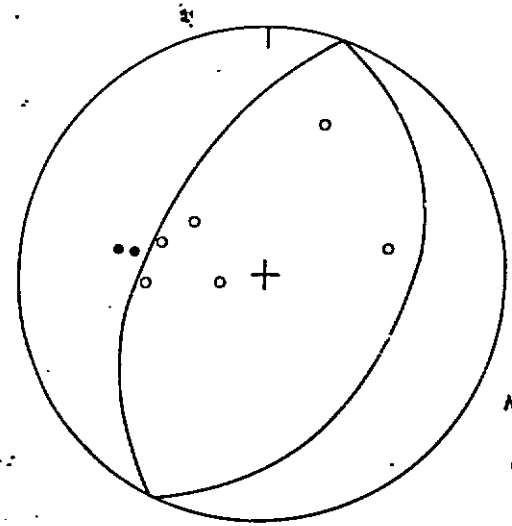

May 22, 1980
2h:28'

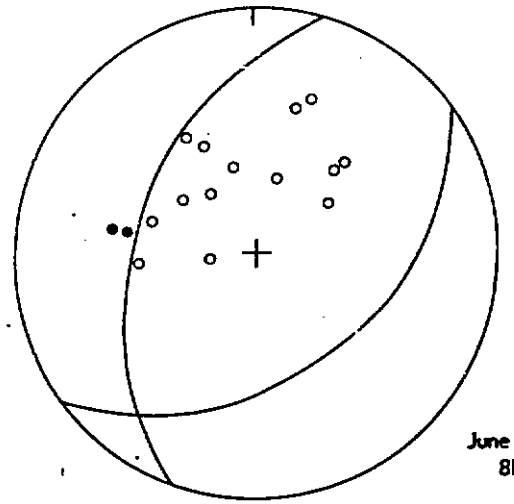

June 10, 1980
8h:47'

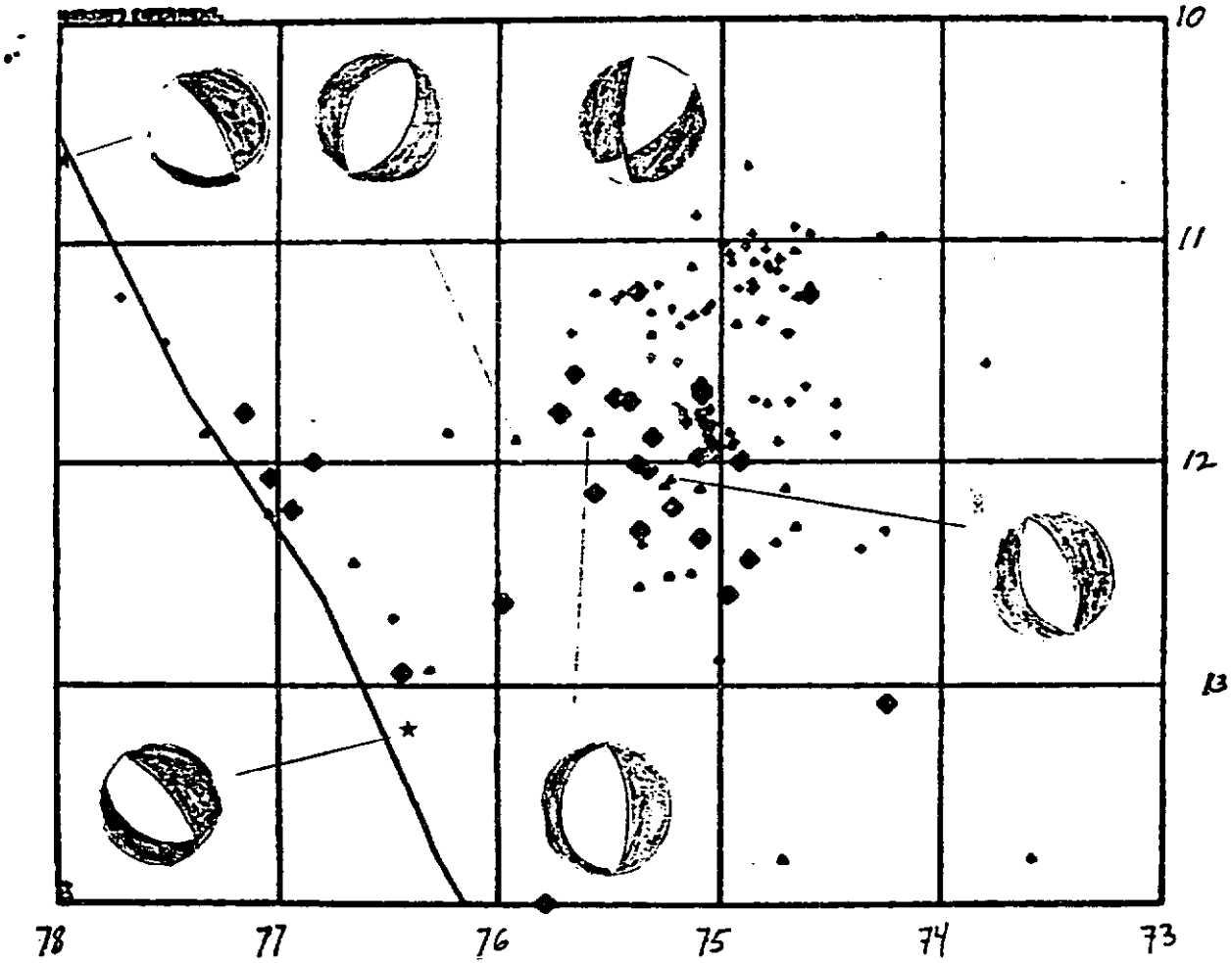

Figure 19

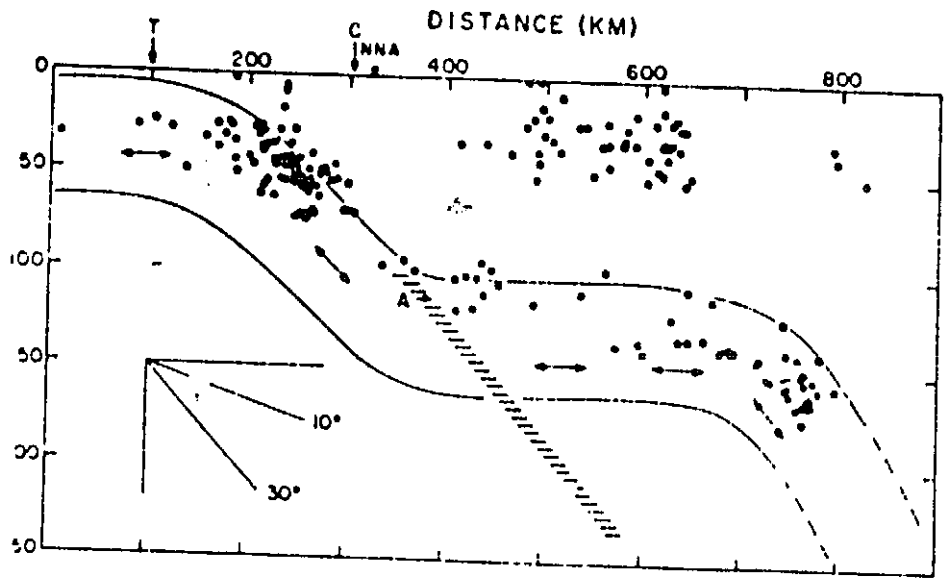

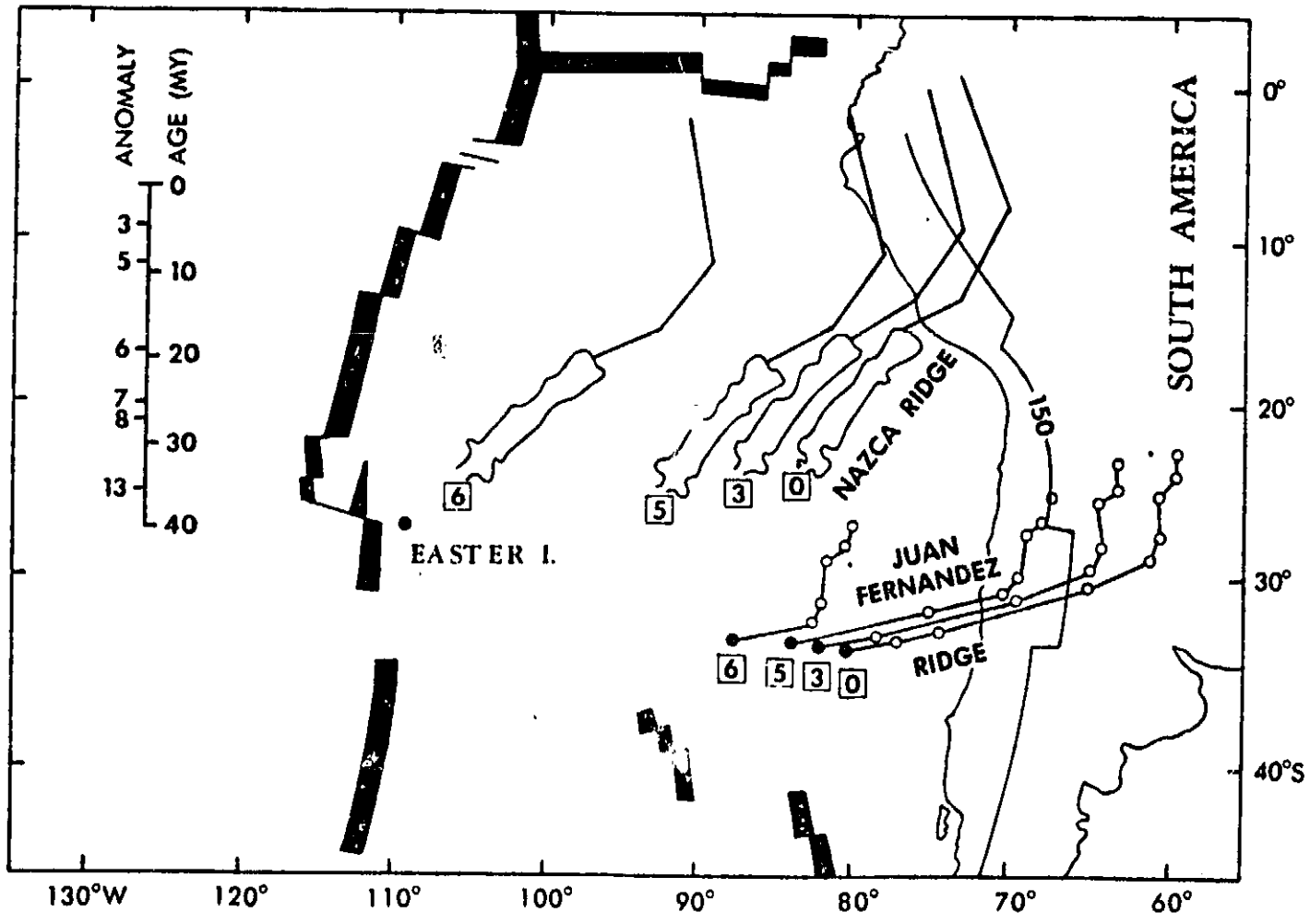

Peter Molnar

Seismicity, Fault Plane Solutions, Depth of Faulting, and Active Tectonics of the Central Andes

Gerardo Suárez

Peter Molnar

B. Clark Burchfiel

Department of Earth and Planetary Sciences

Massachusetts Institute of Technology

Cambridge, Massachusetts 02139

submitted to Journal of Geophysical Research

July, 1982

Abstract

Intracontinental seismicity in the Central Andes of Peru, Ecuador, and southern Colombia, is concentrated along the easternmost flank of the Cordillera beneath the western margin of the sub-Andes. In general, the fault plane solutions of the largest of these events show reverse faulting on steeply dipping planes striking northwest-southeast. Therefore, reflecting crustal shortening perpendicular to the range, probably in response to the horizontal stress applied to the South American plate by the subduction of the Nazca plate. Earthquakes in the sub-Andes occur at depths of between 8 and 38 km indicating that much of the crust deforms in a brittle manner. The style of deformation depicted by these earthquakes does not resemble closely, either, a thin-skinned tectonic regime as that of the Canadian Rockies for example, or a broad zone of deformation with faults extending through the crystalline basement, as that in the Laramide province of Colorado and Wyoming in the western United States. The deformation here seems to reflect the antithetic underthrusting of the Brazilian shield beneath the eastern margin of the Andes. Crustal shortening thickens the crust and creates greater topographic relief until an equilibrium height is attained. New thrust faults are then created farther east, and the deformation in the Andes apparently becomes progressively younger towards the east. In contrast with the sub-Andes, the active tectonics of portions of the High Andes are characterized

by normal faulting on planes parallel to the axis of the range. Thus there seems to be a delicate balance between the compressive stress, which is applied to the mountain belt in the direction of subduction causing thrust faulting in the sub-Andes, and the gravitational body forces acting on the topographically higher parts and the crustal root of the Andes, which may cause normal faulting in the High Andes. The seismicity in the High Andes, however, is low, and unless deformation occurs in a ductile manner, the tectonic activity of this region is mild compared to that in the sub-Andes.

Introduction

The Andes are important as a contemporary example of a mountain belt formed as a result of subduction of oceanic lithosphere beneath a continental plate. They are frequently used as the type example of a tectonic environment in which many ancient orogenic belts formed [eg. Dewey and Bird, 1970]. "Andean margins" are characterized by a voluminous magmatic arc bounded on one side by a trench, and on the other side by a fold and thrust belt. They are inferred to have been present along some continental margins during the closing of oceanic terranes that ultimately led to continental collisions.

Western North America is interpreted to have been an "Andean margin" during the late Mesozoic and early Tertiary, when the Farallon plate or other oceanic plates were subducted beneath it [Burchfiel and Davis, 1972; 1975; Hamilton, 1969], much as the Nazca plate presently plunges beneath western South America. The variability of structural development along strike in both North and South America, however, allows the generic term "Andean margin" to embrace a broad spectrum of tectonic styles. Specifically, differences between the tectonic development of western Canada, with its classic thin-skinned fold and thrust belt [Bally et al, 1966; Price and Mountjoy, 1970] , and the broad zone of late Cretaceous-early Tertiary Laramide deformation with faults extending through the crystalline crust of the western United States in Colorado and Wyoming [eg. Burchfiel and

Davis, 1972; 1975; Sales, 1968; Stearns, 1978], are as great as the differences, for instance, in the tectonic style of the Alps, a collisional orogen, and the High Atlas, an intracontinental zone of deformation. Yet, the late Cretaceous and early Tertiary structures in both Canada and the United States formed in a setting typically classified as an "Andean margin". Moreover, the structure and history of the Andes shows similar and equally large variations in tectonic style along strike. Even though knowledge of Andean geology is still limited, it is clear that the Pampean ranges in central Argentina, represent a broad zone of deformation characterized by faults that extend into crystalline basement. They are clearly different from the wide belt of folds and thrust faults that appear to affect only the Paleozoic sedimentary cover in Bolivia in what can be interpreted as a thin-skinned tectonic style [Jordan et al, 1982]. Accordingly, before the concept of "Andean margin" can contribute more to the understanding of older belts than simply to suggest cartoon-like analogies, a more comprehensive understanding of the tectonics of different parts of the Andes is required.

The purpose of this paper is to contribute some new data bearing on the active tectonics of the Central Andes (Peru, Ecuador and southern Colombia), and to summarize these data in light of plausible mechanisms of how the Andes might have formed and evolved. We are concerned primarily with evidence of recent faulting, particularly reflected by intracontinental earthquakes and geologic evidence of Quaternary faulting.

In the Central Andes, local seismic station coverage is scanty and routine determination of hypocentral depths are frequently grossly in error [eg. James et al, 1969]. Using synthetic seismograms of long period body waves, we revise published fault plane solutions [Pennington, 1981; Stauder, 1975; Wagner, 1972] and determine both focal depths and fault plane solutions for others. At epicentral distances of between 30° and 80°, the shape of long period body waves depends upon both the depth of the hypocenter and the orientation of the nodal planes, and is not very sensitive to changes in the local structure of the upper mantle. Thus, focal depths and fault plane solutions can be constrained by a visual comparison between observed long period P waves and synthetic waveforms on a trial-and-error basis.

The Central Andes: an Overview

The main morphological units in the Central Andes are, from the trench eastward: the coastal plains, the Cordillera Occidental, the Altiplano, the Cordillera Oriental, and the sub-Andes (Figure 1). A brief description of the geology and tectonic evolution of each region is taken from recent reviews of central Andean geology [Audebaud et al, 1973; Dalmayrac et al, 1980; Gansser, 1973; Megard, 1978; Zeil, 1979].

The Coastal Plains

In northern Peru, the coastal plain is a narrow and arid strip of land not wider than 40 km. Limited on the west by the coastline and to the east by the Cordilleran batholith, it is formed mainly of gently folded volcanic and sedimentary rocks of Mezozoic age. In southern Peru, the coastal plains widen and strongly folded crystalline basement rocks crop out. The Precambrian coastal massif in southern Peru, generally called the Arequipa block, contains rocks as old as 1.8 to 2.0 b.y. [Cobbing et al, 1977; Dalmayrac et al, 1977] and was subjected to deformation in Precambrian, Paleozoic and Mesozoic times [Shackleton et al, 1979].

The Cordillera Occidental

The western Cordillera consists mainly of volcanic and plutonic rocks of Mezozoic and Cenozoic age and shallow water marine deposits of Mesozoic age. It forms a continuous and impressive structural entity parallel to the coast and is the locus of most of the late Cenozoic volcanism. The main structural unit is the immense Coastal Batholith extending from about 6° to 16° S parallel to the coast (Figure 2). Plutons ranging in composition from gabbro to syenogranite [Cobbing and Pitcher, 1972; Cobbing et al, 1977] were emplaced episodically from 100 to 30 m.y. ago [Pitcher, 1975]. The plutons become younger and show an increase in silicic content eastward [Bussel et al, 1976; Stewart et al, 1974]. Cenozoic volcanic rocks are widespread in

the western Cordillera and massive ignimbrites of Neogene age are present [Dalmayrac et al, 1980]. Volcanic activity began to wane about 11 m.y. ago and stopped rather abruptly 5 m.y. ago [Noble and McKee, 1977]. This cessation of Quaternary volcanism has been interpreted as marking the begining of shallow plate subduction under Peru [Barazangi and Isacks, 1976;1979; Megard and Philip, 1976]. East and north of the Cordillera Blanca, structures developed in the Mesozoic rocks are similar to those of a foreland fold and thrust belt. The folds and thrusts in this region are generally of flexural-slip type with both broad-rounded hinges and chevron geometry. The Mesozoic limestones were thrust eastward on gentle west-dipping faults, while the underlying Jurassic shales formed tight flexural-slip folds [Dalmayrac, 1978; Dalmayrac et al, 1980; Wilson et al, 1967]. The tectonic style implies detachment of the Mesozoic cover from an older substratum and extensive east-west shortening [Coney, 1971]. In the western part of the belt, volcanic rocks of Oligocene-Miocene age unconformably overlie deformed Mesozoic rocks and limit the age of deformation to late Cretaceous and early Cenozoic time [Dalmayrac, 1978; Wilson et al; 1967]. The folded belt is truncated and limited on its western side by the granitic plutons of the Cordillera Blanca emplaced 3 to 12 m.y. ago [Stewart et al, 1974].

In central Peru, the Mesozoic sedimentary rocks east of the coastal batholith are tightly folded in chevron folds. Fracture cleavage present in the late Cretaceous red beds is absent in the

overlying Tertiary volcanic rocks indicating a late Cretaceous to early Tertiary age of deformation [Megard, 1978].

In southern Peru, the Mesozoic sedimentary rocks are almost completely covered by Cenozoic volcanic rocks and the amount and age of deformation of the Mesozoic rocks is not well known. Recently, Vicente et al [1979] mapped a sub-horizontal east-directed thrust fault with a minimum displacement of 15 km, in the area near Arequipa (Figure 2). The thrust fault places rocks as old as Precambrian on Mesozoic sedimentary rocks. Although this thrust fault is now west of the active volcanoes, when thrusting occurred during the late Cretaceous, it lay east of the volcanic arc active then.

The Altiplano and Central High Plateau

The high plateau of central Peru and the Altiplano in southern Peru are bounded to the west by the coastal batholith, and to the east by the Cordillera Oriental. North of about 10° S, the central high plateaus disappear and the western and eastern Cordillera are adjacent. The width of the high plateau in central Peru is 10 to 50 km wide and increases considerably in the south to nearly 200 km near Lake Titicaca in the Altiplano. The thick sequences of Paleozoic and Mesozoic marine sedimentary rocks that are present in the high plateau and the Altiplano apparently were deposited in deep, northwest-trending basins [eg. Harrington, 1962; Lohman, 1970; Wilson, 1963] and later were capped by late Cretaceous to late Eocene red beds.

The tectonic style in the central high plateaus is variable along strike. In the region around Huancayo in central Peru (Figure 2), zones of tight folds and thrust faults form narrow belts (10 to 30 km wide) that are separated by zones of open folds and undeformed rocks of similar width [Lepry and Davis, 1982; Megard, 1978]. These belts of intense deformation anastomose along strike. The geometry of folds and some faults suggests local detachment from their substratum [Lepry and Davis, 1982]. Where exposed, Paleozoic or Precambrian rocks appear to be involved in some of the structures.

Much of the Altiplano in southern Peru is covered by a thick sequence of mildly deformed continental molasse deposited during the Oligocene and Miocene [eg. Newell, 1949]. Folding is less severe than in central and northern Peru and the Tertiary sedimentary rocks are generally deformed in broad concentric folds cut by reverse faults [eg. Chanove et al, 1969]. Northwest of Lake Titicaca, the thrust faults suggest that the sedimentary cover was detached from its underlying basement and deformed during late Cretaceous and early Cenozoic time [Chanove et al, 1969; Laubacher, 1978].

Cordillera Occidental

The eastern Cordillera is a broad zone underlain largely by pre-Mesozoic rocks located east of the central high plateaus. Precambrian crystalline rock and Paleozoic plutonic rocks crop out in large areas of the eastern Cordillera, particularly in

central Peru. The sedimentary rocks are composed of a thick section of mainly Paleozoic shallow marine and continental strata that are folded and frequently cut by reverse faults.

Precambrian rocks are generally low-grade meta-sedimentary rocks (phyllites or fine-grained schists) that are weakly to strongly foliated [Dalmayrac et al, 1980; Megard, 1978]. Only locally do the Precambrian crystalline rocks reach amphibolite to granulite grade. Lower Paleozoic rocks range from Ordovician to Devonian in age, and are generally unmetamorphosed to weakly metamorphosed. The upper Precambrian and lower Paleozoic rocks are the oldest rocks exposed in the eastern Andes and they form a very anisotropic and weak upper crust. Published material [eg. Dalmayrac et al, 1980; Megard, 1978] attributes deformation of these rocks to a middle to late Paleozoic ("Hercynian") event. The presence of this deformation and the existence of Paleozoic batholiths suggests subduction along the western margin of South America was active at this time.

The sub-Andes

The sub-Andean zone consists of a belt of folded sedimentary rocks parallel to the mountain chain between the high Andes and the Brazilian shield. The limit between the Cordillera Oriental and the sub-Andes is generally shown to be formed by a zone of west-dipping thrust or reverse faults [Ham and Herrera, 1963]. The rocks consist of shallow water and continental sedimentary rocks deposited intermittently from Paleozoic to Pliocene time.

No evidence of Andean magmatism has been found in the sub-Andes. The thickness of the sedimentary cover is not well known. In northern Peru, where exploration for oil has been active, depths of up to 10 km have been reported in some basins [Audebaud et al, 1973; Rodriguez and Chalco, 1975].

The upper-Tertiary sedimentary rocks are poorly dated and the deformation of the sub-Andes is difficult to date precisely [eg. Audebaud et al, 1973]. In Peru, the sub-Andes are formed by a series of folds and faults active from at least the Pliocene to the present. Deformation is usually interpreted as the result of crustal shortening expressed by cylindrical folds cut by steep, west-dipping reverse faults that pass from the sedimentery rocks into the underlying basement [eg. Audebaud et al, 1973; Megard, 1978]. The age and intensity of tectonic deformation is typically shown to decrease steadily to the east [eg. Dalmayrac et al, 1980]. Published cross sections are mostly schematic because data from drill holes or seismic profiles have not generally been available. Dense vegetation limits the exposure; the outcrops are small and fa planes commonly are not exposed well enough to determine their dips. In northern Peru, oil exploration has produced a more detailed three dimensional picture of the structure of the sub-Andes [Rodriguez and Chalco, 1975; Touzett, 1975]. Here, the sub-Andes can be interpreted as a thin-skinned fold-and-thrust belt.

Shallow Seismicity in South America

Epicenters of well located shallow earthquakes (less than 50 km deep) occurring along the western margin of South America in the last 20 years or so define two distinct loci of seismic activity [Barazangi and Isacks, 1976; 1979 To the west, one belt lies parallel to the coastline and marks the boundary where the Nazca plate subducts under South America [Stauder, 1975]. The other belt of seismic activity occurs within the overriding continental plate and follows a trend parallel to the mountain chain. The majority of these crustal events take place in the transition zone between the eastern Cordillera and the western margin of the sub-Andes. The distribution of epicenters of crustal events shows a remarkable quiescence of seismic activity in the high Andes and in the eastern part of the sub-Andes (Figure 3). There is also a paucity of seismic activity in the forearc region, a feature commonly observed in other areas of the world [eg. Yamashina et al, 1978].

The spatial distribution of intracontinental seismicity shows variations along strike as well [Jordan et al, 1982]. The most seismically active areas occur under Peru and southern Ecuador, between 2° and 13° S, and under northern Argentina, between 28° and 33° S (Figure 3). These regions correspond roughly to the two areas where telesesmic data suggest that subduction of the Nazca plate under South America takes place at the unusually shallow dip of about ten degrees [Barazangi and Isacks,

1976; 1979; Megard and Philip, 1976]. In the Central Andes most of the intracontinental earthquakes occur in the eastern part of the Cordillera, beneath the western sub-Andes (Figure 4). Seismicity along the eastern margin of the Altiplano and the Argentinian Puna, beneath which subduction of the Nazca plate occurs at a steeper angle (~30°), also shows the existence of a seismic sub-Andean margin, though less active than the two regions mentioned above (Figure 3). A remarkable segment of quiesence is found along the eastern margin of the Altiplano of southern Peru and northern Bolivia, between 13° and 18° S (Figure 4).

Fault Plane Solutions and Depth of Foci

Data and Method of Analysis

We studied all intracontinental events in the central Andes sufficiently large that a fault plane solution could be obtained with data from the World Wide Seismographic Station Network (WWSSN) between 1962 and 1978 (Table 1). Constraints on the fault plane solutions and the depths of foci were obtained synthesizing long period P waves for a spectrum of solutions and focal depths, and comparing them to the observed waveforms, as others have done elsewhere [eg. Jackson and Fitch, 1981; Kanamori and Stewart, 1976; Rial, 1978; Trehu et al., 1981].

In this study, a point source embedded in semi-infinite half space was used to synthesize all available long period P waves at WWSSN stations within an epicentral distance of 30° to 80°. Body waves at these distance ranges have paths that lie almost entirely within the lower mantle and are not affected by the local structure of the upper mantle [eg. Langston and Helmberger, 1975]. At epicentral distances between 30° and 80°, P waves do not experience triplification or diffraction near the core-mantle boundary that severely complicate the observed waveforms. Synthetic seismograms were computed in the time domain by convolving the response of a shear dislocation in a semi-infinite half space with a far field source time function, an attenuation operator, and the instrument response. The far-field source time function was assumed to be a symmetric trapezoid for both direct and reflected phases and was adjusted in an ad-hoc manner to fit the observed P waves. Plots of the fault plane solutions and waveforms used in the analysis are shown in the Appendix. Synthesized waveforms are also shown at several hypocentral depths for a few selected stations spanning a range of azimuths. This will permit the reader to judge the uncertainty in the estimates of focal depth (see Appendix).

Constraints on the Fault Plane Solution.

The determination of fault plane solutions for earthquakes in the Andes suffers from a dearth of WWSSN stations to the west.

Only a few stations on islands in the Pacific, with low magnifications, sometimes yield reliable first motions. Thus, since most of the events in the area show reverse faulting, the dip of nodal plane dipping west is generally very poorly constrained (Appendix).

A clear example illustrating this problem is the earthquake of May 15,1976 (event 16). First motions for this earthquake are scarce and allow two different families of fault plane solutions (Figure 5). The solid line depicts an almost pure dip-slip solution with reverse faulting, while the dotted line indicates nearly pure strike-slip motion. Only two stations, WES and OGD in the eastern United States, produced long period P waves large enough to be useful in the visual comparison with synthetic waveforms. WES and OGD are stations in close proximity and rays to them leave the source with similar take-off angles. Thus, the orientation of the fault planes cannot be resolved well. Synthetic waveforms, however, allow us to determine which of the two alternative types of faulting is likely [eg. Langston, 1979]. The strike-slip solution does not produce waveforms that resemble the observed P waves, but synthetic P waves corresponding to the dip-slip mechanism closely resemble the observed wavetrains (Figure 6). It should be pointed out, however, that varying the strike or dip of the nodal planes of the dip-slip solution by as much as 15 degrees will not change appreciably the shape of the synthetic waveforms observed at these two stations.

Errors in Depth Determination

A comparison of focal depths reported in the ISC catalog and those determined in this study using synthetic waveforms shows large discrepancies in many cases (Tables 1 and 2). The problem stems in part from the sparse coverage of the local networks and the poor azimuthal distribution of the WWSSN stations. One of the primary objectives in this paper is the accurate determination of the focal depths of these events.

To illustrate the accuracy of focal depth estimates, Figure 7 shows that for the earthquake of March 20, 1972 (event 13), focal depths shallower than 36 km are clearly unacceptable, for the average crustal velocity used in the calculation. Similarly, for depths larger than about 42 km, the interval between the direct and reflected phases is too large, and the synthetic P waves are too broad (Figure 7). Thus, we consider the focal depth in this case to be 38±2 km, if the average crustal velocity were 6.0 km/sec This would be equivalent to an error in focal depth of about 5%. It is noteworthy that the focal depth reported by ISC was 52 km. The inferred depth is proportional to the assumed velocity of P waves in the crust. Using velocities of 5.5 or 6.5 km/sec, which span the range of plausible crustal velocities, synthetic seismograms for a given depth at these three stations are not significantly different from one another (Figure 8). Thus, our ignorance of the crustal velocity adds roughly another 5 to 10 % uncertainty to the estimated focal depth.

Discussion of Results

Of the seventeen earthquakes studied, ten occurred along the transition zone between the sub-Andes and the Cordillera Oriental. The rest are distributed among the high Andes (four), the forearc in Ecuador (two), and the Brazilian shield in Colombia (one).

Events in the Forearc

As discussed above, the forearc in the Central Andes is, in general, seismically quiet. Of the events studied only two earthquakes beneath the coast of Ecuador occured in the forearc. They are two of the largest earthquakes studied. The focal depth of event 15 is about 22 km. Therefore, this event probably occurred above the inclined seismic zone, which lies at a depth of about 35 km in the region just south of where event 16 occurred [Barazangi and Isacks, 1979]. The fault plane solution for this event shows thrust faulting on a north or northeast trending plane. Thus, this event may reflect crustal shortening along the western margin of the Andean cordillera and not simple underthrusting of the Nazca plate beneath the arc, as most events along the margin do. Thus, it might be part of a process of tectonic erosion of the continental margin due to subduction [eg. Plafker, 1972].

The solution for event 10 also shows thrust faulting on a north trending plane that dips approximately 45° either east or

west. The focal depth of event 10 is 32 km, and it is not clear if it lies within or above the inclined seismic zone. The dip of 45° of the east-dipping nodal plane appears to be too steep for this event to occur along the shallow-dipping plate boundary (Figure 10). This boundary appears to be shallower beneath Ecuador than it is farther south in Peru. Nevertheless, it is very poorly defined by teleseismic data (see Figure 5 in Barazangi and Isacks [1979]). Thus, the depth of event 10 (30 km) is sufficiently deep that it is difficult to ascribe it to internal deformation of the overriding plate or attribute it to slip on the main inclined seismic zone.

The Brazilian Shield

The fault plane solution of event 14 in the Brazilian shield indicates strike-slip motion with the P axis oriented in an east-west direction. The orientation of the P axis parallel to the direction of subduction suggests that the Brazilian shield experiences compression in that direction and in response to convergence. This is consistent with the solutions of 5 shallow events in cratonic South America showing P axes oriented approximately east-west [Mendiguren and Richter, 1978].

Tectonics of the sub-Andes

Most of the earthquakes studied are concentrated along the eastern flank of the Andes on the western edge of the sub-Andes.

They occur beneath regions of low topographic elevation and consistently show thrust faulting approximately parallel to the mountain belt (Figure 9). In most cases, the nodal planes dip at steep angles, between 30° and 60° (Figure 12), and we cannot determine which of the two nodal planes was the fault plane. The events are too small for the body waves to show azimuthal differences in pulse shapes due to the finiteness of the source that could be used to select the fault plane. Moreover, the lack of local stations did not permit the recording and accurate locating of aftershock sequences. Nevertheless, because most of the thrust faults in the sub-Andes dip west [Dalmayrac, 1978; Dalmayrac et al, 1980; Megard, 1978], we presume that the west dipping nodal planes are the fault planes (Figures 10 and 11). Although west dipping nodal planes are usually the more shallow dipping of the two nodal planes, the dips are still much steeper than those associated either with decollement in a thin-skinned tectonic environment as in the Canadian Rockies [Bally et al, 1966; Price and Mountjoy, 1970], or with surface exposures of large crystalline nappes, such as those in Norway [Gee, 1975]. At first glance, the steep dips appear to be more reminiscent of faults active in the early Tertiary (Laramide) in the Rocky Mountains of Colorado and Wyoming [eg. Brewer et al, 1979; Smithson et al, 1979], or of those deduced from fault plane solutions of earthquakes in the Tien Shan [eg. Tapponnier and Molnar, 1979] or the Zagros Mountains [Jackson and Fitch, 1981; McKenzie, 1972].

The earthquakes studied in the sub-Andes are relatively deep, ranging in depth from 8 to 38 km, compared with those in the Zagros Mountains with focal depths of 10 to 15 km [Jackson and Fitch, 1981]. Thus, they indicate that most of the crust and possibly the uppermost mantle are involved in the deformation. The inferred depth of the deepest event is between 36 and 40 km. Unfortunately, we are not aware of any studies of crustal thickness in the sub-Andes that resolves the question of whether these deeper events occurred in the uppermost mantle or in the lower crust. None of those studied here, however, occurred as deep as 80 km, as suggested by Stauder [1975]. Regardless of the depth of the Moho, it is clear that the earthquakes occurred in the crystalline basement and not in the overlying sedimentary cover. This fact is consistent with the inference that the earthquakes do not result from slip along a decollement between the crystalline basement and overlying sedimentary strata.

Relating the earthquakes to specific faults identified from geologic field work is difficult, both because of inaccuracies in the locations of the earthquakes and because of a lack of detailed geologic studies of the sub-Andes. The best studied segment of the the sub-Andes is in Central Peru [Audebaud et al, 1973; Dalmayrac, 1978; Megard, 1978]. Numerous west dipping thrust, or reverse, faults can be inferred from the juxtaposition of rocks of different ages. Typically, faults are drawn dipping at steep angles (60° to 70°). The descriptions of these regions are not sufficiently detailed, however, for us to know why steep

instead of shallow dips have been inferred. In the regions that we have seen, albeit only during a cursory field reconnaissance, the fault planes generally were not exposed and faults could be inferred only from the juxtaposition of rocks of very different ages. The style of internal deformation of the rocks near the faults suggested that they are thrust faults. From the gentle west-dipping cleavage present in Mezozoic and Cenozoic limestones and red sandstones and from the shallow west dips of some minor faults, we suspect that many of the thrusts dip at more shallow angles (less than 20°) than are shown in published cross sections.

One of the basic questions to be addressed by this study is to what extent does the deformation in the sub-Andes resemble that of the Canadian Rockies during the late Cretaceous in one extreme, or the Colorado-Wyoming Rockies during the early Tertiary in the other. The steep-dipping faults that cut the basement of the sub-Andes resembles the type of faulting in the Colorado-Wyoming Rockies, where the basement is clearly involved and some fault planes are quite steep (≥30°) [Brewer et al, 1980; Smithson et al, 1979]. Nevertheless, the similarity is far from perfect. In particular, whereas the ranges in Colorado and Wyoming apparently are bounded and uplifted by one or two faults, the sub-Andes seem to be cut by numerous faults over a broad zone that has experienced deformation in the late Cenozoic. More importantly, the earthquakes in the sub-Andes occur only in the western margin of the province, while at the surface the most

recently deformed rocks appear to be on the eastern side. Thus, while the basement beneath the transition from the Cordillera Oriental and the sub-Andes undergoes crustal shortening, the youngest deformation of the cover occurs some 50 to 100 km to the east.

To reconcile these two observations, one can infer that the cover is, in fact, detached, so that the relatively steep thrusts in the basement flatten when they reach the overlying sedimentary rocks. In this respect, the style of deformation would resemble that of the Canadian Rockies. In the Canadian Rockies, faults dipping steeply at the surface flatten with depth and detach the sedimentary cover from the underlying basement. The earthquakes in the central Andes give no hint of a similar process; the nodal planes are too steep and the events are too deep, clearly having occurred within the basement. Moreover, there is no obvious systematic change with depth of the dips of the nodal planes as might be expected if fault surfaces curved smoothly with depth. It is also possible that shortening on steep faults in the basement is decoupled along a gently dipping decollement from the shortening in the sedimentary cover rocks; displacement in the decollement would then be largely aseismic. Thus, the earthquakes and brittle deformation of the basement in Peru may occur in a setting different from the wide zone of detached sedimentary rocks in the Canadian Rockies.

Perhaps, the earthquakes indicate deformation of the basement below and west of a detached sub-Andean terrane, and if

there were a sequence of thick and competent sedimentary rocks in the sub-Andes of central Peru, they would show a style of deformation similar to that of the Canadian Rockies. Thus, the shortening in the basement would occur west of the surficial expression of shortening in the sedimentary cover, and the two areas would be related by a gently dipping aseismic(?) decollement. Considering the weak and foliated nature of the Precambrian crystalline rocks that crop out in the Cordillera Oriental, it is possible that part of this crystalline basement is also detached from a deeper and more rigid substratum. Alternatively, one can infer that some of the faults active in the basement continue into the overlying cover so that the eastward progression of deformation is then only approximate. Regardless, despite some similarities to both, the style of deformation in the Peruvian sub-Andes as a whole seems to differ from that of both the Colorado-Wyoming Rocky Mountains and the Canadian Rockies.

The present regime of steep basement-involved thrust faults is similar to the style of basement deformation that probably prevailed in the high Andes during their formation. Throughout much of Peru, the sedimentary cover is tightly folded, sometimes in localized zones of concentrated deformation and with occassional steep faults [eg. Coney, 1971; Lepry and Davis, 1982; Megard, 1978]. Except for a portion in north-central Peru, neither a preferred vergence nor large overthrusts can be recognized. Therefore, it is appropriate to suggest that the

active tectonic regime that we observe today in the sub-Andes is similar to the process that produced extensive crustal shortening and is responsible for the formation of the Central Andes.

Rate and amount of crustal shortening. This interpretation motivates a comparison of the rate of crustal shortening obtained by adding the seismic moments of earthquakes with that implied by the geologic history. The definition of seismic moment is:

$$M_o = \mu S u \qquad (1)$$

[Aki, 1966], where M_o is the scalar seismic moment, S is the surface area of the fault, u is the average slip of the fault, and μ the shear modulus. Thus, the cumulative slip on a single fault can be estimated by simply summing the seismic moments of earthquakes causing slip on the fault [eg. Brune, 1968; Davies and Brune, 1971]. In the central Andes, however, seismic energy release does not occur along a single major fault. Instead, earthquakes occur on fault planes with different orientations distributed over a large seimogenic volume. In this case, it is more appropriate to follow Kostrov (1974) and use the seismic moment tensors to calculate the strain resulting from the motion of all the faults in the region (eg. Wesnousky et al, 1982; Chen and Molnar, 1977).

The seismic moment tensor for an arbitrary shear dislocation may be expressed as,

$$M_{ij} = \mu S(u_i \eta_j + u_j \eta_i) \qquad (2)$$

where ν_i are the direction cosines of the vectors normal to the fault plane, and u_i is the average slip in vectorial form. The principal values of the moment tensor, $-M_o$,0, and $+M_o$, correspond to the P, B, and T axes of fault plane solutions (Gilbert, 1970). Kostrov (1974) showed that the mean rate of irrotational strain in a volume, V, over a period of time, t, due to slip on N different faults within that volume is,

$$\dot{\epsilon}_{ij} = \frac{1}{2\mu Vt} \sum_{n=1}^{N} M_{ij}^{n} \qquad (3)$$

In the Central Andes, the areal dimensions of the deformed volume are about 2000 km in length and 250 km in width. We assume a thickness of 38 km corresponding to the deepest intracontinental earthquake studied.

Diagonalizing $\dot{\epsilon}_{ij}$ yields the principal directions of the average strain rate. Crustal shortening is computed by multiplying the horizontal component of the principal compressive strain rate times the width of the deformed body in that direction. In the Central Andes, the principal value of compressive strain rate is 6×10^{-9} yr^{-1} oriented about 95° west of north with a dip of 4° This orientation is consistent with the direction of subduction of the Nazca plate beneath South America. The average rates of crustal shortening are between 1.0 and 1.7 mm/yr. The smaller figure is obtained by not including event 10 in the calculations. As discussed above, it is possible that event 10 occurs in the main thrust contact between the Nazca and South American plate and not be the result of crustal deformation of the continental

plate. These rates of crustal shortening are lower bounds since they assume that the deformation is being taken up only by brittle fracture, and disregard the possibility of fault creep and viscoelastic deformation. The rates also include only contributions from earthquakes with magnitudes between 5.4 and 6.3. Combining the frequency-magnitude ($\log N=a-b\cdot Ms$) and moment-magnitude ($\log M_o=1.5\cdot Ms+16$) [Hanks and Kanamori, 1979] relations, where N is the number of earthquakes, Ms is the surface wave magnitude, and Mo the seismic moment, the contribution due to earthquakes smaller that magnitude 5.4 can be estimated [eg. Molnar 1979]. Assuming a value of b equal to 1, the contribution to the total moment by events with $Ms < 5.4$ is only 37% of that of events with magnitudes between 5.4 and 6.3. Thus, average crustal shortening rates would increase to 1.4 to 2.1 mm/yr.

The total amount of crustal shortening can be estimated assuming that crustal volume is conserved, and excess material beneath the mountainous topography and in the root of the Andes correspond to South American crust that subsequently has been substantially shortened. Assuming an average elevation of 4 km and a crustal thickness of 60 km [James, 1971], then for a crust originally 35 km thick, we obtain 190 km of crustal shortening. This estimate neglects the loss of crustal material through erosion or addition by magmatic processes. Even if 10 km of material had been eroded from the top of the Andes over a width of 250 km, these estimates of crustal shortening would increase

by only 35%. Thus, we do not consider ignoring erosion to be important for the significance of the following calculations. More problematic is the quantity of mantle-derived plutonic rocks in the Andes. To our knowledge there are no reliable estimates of the amount of such rocks in the Peruvian Andes, and we simply ignore them, recognizing that the amount of crustal shortening estimated here is an upper bound. For contrast, from the structures and style of deformation in a geologic cross section traversing the Central Andes, Megard [1978] suggests crustal shortening to be of the order of 100 km.

Shortening of 190 km of Andean crust at a rate of 1.4 to 2.1 mm/yr would require 90 to 135 m.y. Although subduction probably occurred throughout most of the Mezozoic [eg. Helwig, 1973], paleogeographic interpretations have indicated the presence of a major transgression ending in the late Cretaceous [eg. Audebaud et al, 1973; Zeil, 1979]. Therefore, much of the present Andes were at sea level about 70 to 80 m.y. ago and the present topography and thickened crust must have formed since then.

Because of the short record of seismicity, our ignorance of recurrence rates, and the unavoidable approximate assumptions made in estimating the rate and amount of crustal shortening, the agreement between the average rates of shortening inferred from the seismic moments of 16 years of seimicity and from about 70 m.y. of geologic history is not a strong argument that the present tectonics of the sub-Andes are similar to those of the Andes as a whole throughout the last 70 my or so. However, agreement

within order of magnitude suggests that if most of the topography, and implicitly the associated crustal root as well, developed in latest Cenozoic time as often presumed [eg. Audebaud et al, 1973], then the Andes must have been built by some process other than crustal shortening.

Earthquakes in the High Andes

Thrust faulting at high elevation. Only four large earthquakes occurred in the high Andes in the last twenty years: event 17, in Ecuador, events 7 and 8 in the Cordillera Oriental of southern Peru, and event 11 in the northern Altiplano (Figure 9). These earthquakes are shallow; focal depths never deeper than 16 km. In fact, among all of the earthquakes studied here only event 7 is known to have produced a surface break in the Andes. Events 7 and 8 occurred near the Huaytapallana fault, which crops out at an elevation of about 4600 m above sea level. The fault scarp indicates reverse faulting with a component of left-lateral strike-slip motion on a plane dipping about 60°NE and striking N50°W [Philip and Megard, 1976]. In the basins just west of this fault, Dollfus and Megard [1968] reported folding of Quaternary glacial terraces. The strike of the folds is in a direction N30°W and is consistent with the strain pattern deduced from the fault.

Event 11 is the only large earthquake in the Altiplano large enough to be studied. It has a focal depth of 8 km and the fault plane solution indicates almost pure strike-slip motion with

north-south oriented T axes. In Ecuador, event 17 occurs at a depth of 16 km. Event 17 shows a thrust mechanism with the P axes oriented approximately east-west.

Normal faulting in the high Andes. Although thrust faulting is the prevalent style of deformation throughout much of Andes, normal faulting has been documented in a number of localities in the high Andes. Normal faults clearly offset Quaternary glacial moraines along the eastern margin of the Cordillera Blanca of central Peru [Dalmayrac, 1974; Yonekura et al, 1979]. Yonekura et al [1979] recognize a system of normal faults on the satellite imagery more than 100 km long (Figure 13). The strike of the faults is roughly parallel to the Andes indicating a component of extension perpendicular to the mountain range. Furthermore, in the Altiplano of southern Peru and northern Bolivia, normal faults offset Quaternary sediments [Lavenu, 1979; 1980; Mercier, 1981]. During field work in the summer of 1980, we discovered another clear, recently active normal fault near the northern edge of the Altiplano. The fault scarp is not prominent on satellite imagery, but it is clear on aerial photographs (Figure 14), and from the ground (Figure 15).

The only large earthquake recorded in areas where normal faulting has been reported is the 1946 Ancash earthquake [Richter, 1958]. The epicenter is located about 100 km east of the Cordillera Blanca. Silgado [1951] described the scarps produced by this event and concluded that normal faulting

occurred on a plane dipping west at about 45 degrees. Moreover, the fault plane solution (Figure 16). [Hodgson and Bremner, 1953] shows normal faulting with one of the nodal planes parallel to the strike of the fault scarps observed by Silgado [1951]. It has been suggested that normal faulting was also the cause of both the 1949 Ambato earthquake in the high Andes of Ecuador (B. Foxall personal communication, 1982) and the 1958 Maipu earthquake in Chile [Jordan et al, 1982].

Implications of Normal and Thrust Faulting in the High Andes. The coexistance of normal faulting at high elevation and thrust faulting at the eastern edge of the mountain belt, within a few tens of kilometers of each other, can be explained by variations in the stress field that must balance the gravitational body force acting on the regions of high elevation and their associated crustal roots [Dalmayrac and Molnar, 1981]. To balance the lateral variations in the gravitational body force, there must be a gradient in stress. This balance can be maintained if the horizontal compressive stress exceeds the vertical stress in regions of low elevation, where thrust faulting prevails. Alternatively, the vertical compressive stress can exceed the horizontal stress in regions of high altitude (and thickened crust), where normal faulting occurs. In portions of the central Andes both seem to occur concurrently. For topography in the form of a ridge on an elastic half space, the horizontal compressive stress induced by gravity acting on the ridge approaches a maximum on the flanks of

the ridge and is mimimum at the peak [McTigue and Mei, 1981]. For large characteristic slopes, the horizontal stress can become purely tensile at the peak of the ridge (Figure 17).

The two segments of the Central Andes where thrust faulting and crustal shortening are observed in the high Andes coincide with the regions where aseismic oceanic ridges are being subducted: the Galapagos-Carnegie ridge in Ecuador and the Nazca ridge in southern Peru. It is qualitatively easy, to ascribe an excess horizontal compressive stress to resistance to subduction of the buoyant ridges beneath these portions of the Andes as has been suggested before to explain other phenomena [eg. Kelleher and McCann, 1976; Pilger, 1981; Vogt et al, 1976].

Implications For Andean Evolution

In some ways, the active tectonics and tectonic setting are analogous to those present in the Himalaya and Tibet [Molnar and Tapponnier,1975; 1978; Molnar et al, 1977]. Thrust faulting on the margins of Tibet occurs concurrently with normal faulting in the highest part of the plateau. The stress needed to cause slip on a thrust fault at low elevations apparently is less than that required to uplift the topography beyond a certain elevation. Consequently, the region of elevated topography seems to grow laterally instead of increasing its elevation.

The near absence of thrust faulting, and in some cases extension along much of the high Andes, suggest that no significant amount of crustal shortening is taking place there. Unless deformation occurs in a ductile fashion, the active tectonic regime of the High Andes is mild compared to that in the sub-Andes, and the rates of extension or shortening are probably low. This tectonic style comprising extension in some areas and shortening in others, suggests a delicate balance between the compressive forces applied to the flanks of the Andes by the converging Nazca plate and Brazilian Shield and the gravitational force applied to the elevated crust and its thickened root. It appears that the Andes transmit the stresses applied by one side to the other, much as Tibet seems to do between India and Eurasia [Molnar and Tapponnier, 1978]. Thus, the forces driving the plates together apparently are not elevating the portion of the Andes that is already at high altitudes, increasing the large amount of gravitational potential energy already stored there. Instead, they seem to do work breaking the crust where it is thinner, underthrusting the Brazilian shield beneath the eastern margin of the mountain belt. This has the effect of thickening the crust where it is thin causing topographic relief to grow progressively towards the east. In this manner, when the elevation reaches a critical height, faults are progressively created farther east and new material is constantly appended to the central Andes along their eastern margin, maintaining an average equilibrium topography (Figure 18).

This mode of tectonic evolution would reconcile two important observations: 1) The eastward migration of deformation inferred from the geologic record, and 2) the alignement of the majority of the intracontinental earthquakes along a narrow zone of deformation beneath the western edge of the sub-Andes, in the transition zone to the Cordillera Oriental. Crustal earthquakes in other tectonically active areas of the world usual occur at depths of less than 15 km [eg. Chen and Molnar, 1981; Meissner and Strelhau, 1982]; the lower crust apparently deforming in a ductile manner. The presence of earthquakes in the lower crust beneath the sub-Andes, at depths of 20 to 38 km, indicates the presence of cold crustal material subject to brittle deformation. The existence of cold and brittle material at these depths suggests the presence of an abnormally low geothermal gradient in the sub-Andes, which in turn, is probably due to the underthrusting of shallow and cold basement rocks from the Brazilian shield under the eastern margin of the Andes.

Extension in the high Andes is probably due to body forces produced by gravity and to buoyancy forces exerted by the crustal root of the Andes [Dalmayrac and Molnar, 1981] . This delicate balance of thrust faulting along the eastern piedmont and extension in the highest part of the Cordillera helps maintain an average equilibrium topography. In this scenario, one can imagine that the cessation of subduction along the western margin of the mountain belt may reduce the horizontal compressive stress

required to support the topography. The Andes might then collapse by extensive normal faulting.

Summary

Comparing synthetic and observed long period P waves we determined fault plane solutions and depths of foci of all earthquakes occuring in the central Andes of Peru, Ecuador, and southern Colombia, sufficiently large to be studied with data form the WWSSN. In general, fault plane solutions indicate thrust faulting along nodal planes striking northwest-southeast in a direction parallel to the mountain belt. Nodal planes dip at high angles of about 30° to 60° degrees. The fault plane solutions of these intracontinental earthquakes seems to reflect deformation of the South American plate probably due to the convergence with the Nazca plate. Most of the earthquakes occur on the western margin of the sub-Andes, in the transition zone from the sub-Andes to the Cordillera Oriental, beneath regions of low elevation (~1000 m). The focal depths of earthquakes range from 10 to 38 km, suggesting the lower crust and possibly the uppermost mantle are involved in the deformation. The earthquakes in the sub-Andes are too deep, and their nodal planes are too steep, to associate them with decollement of the sedimentary rocks from the underlying basement in a thin-skinned tectonic environment. A few earthquakes occur in the Cordillera Oriental. Earthquakes

there are shallow with the focal depths of none of the four events studied exceding 16 km. Two events that occurred in the Cordillera Oriental in southern Peru are the only two earthquakes in the last 20 years associated with surface fault breaks [Philip and Megard, 1976]. With only two large earthquakes in the coastal region of Ecuador, the forearc in the central Andes appears to be relatively aseismic. The thrust solutions for these indicate that the crust is undergoing east-west shortening that may be associated with tectonic erosion of the western margin of the South American plate.

While thrust faulting at high angles is prevalent on the eastern side, normal faulting has been documented in a number of localities in the High Andes. The normal faults trend in a direction parallel to the mountain belt, suggesting some extension takes place in a direction normal to the strike. They occur in areas of high topographic relief and faulting associated with one earthquake (the 1946, Ancash earthquake) reflects this extensional regime.

Excess crustal material in the topography and the root of the Andes indicates that as much as 190 km of crustal shortening may have taken place. A summation of the seismic moment of earthquakes in the sub-Andes yields a rate of shortening of 1.4 to 2.1 mm/yr. If these rates were comparable to those in the geologic past, the formation of the Andean topography and crustal root would have occurred in the last 90 to 135 my. Unless the deformation is aseismic and ductile, no significant amount of

crustal shortening is taking place in the High Andes. Most of the shortening, as reflected by the seismicity, takes place in the western sub-Andes. We infer that underthrusting of the Brazilian shield along the eastern side of the massif thickens the crust and creates topographic relief. New faults are successively created farther east when the topography reaches a critical height, so that the mountain belt grows eastward in areal extent.

Acknowledgements

We are grateful to B. Dalmayrac, G. Laubacher, A. Lavenu, R. Marocco, and F. Megard for useful discussions on Andean geology and for helpful hints in planning our visit to geologically interesting areas of Peru and Bolivia. J. Nabelek kindly made available his programs to synthesize body waves. J. Stock helped to digitize data for events 3 and 4. Discussions with D. Davis are gratefully appreciated. One of us (GS) would like to thank K. Aki for his generous support and encouragement, and CONACYT (Consejo de Ciencia y Tecnologia, Mexico) for partial support. This research was supported by NASA's Geodynamics Program under contract NAG5-19.

C-2

References

Aki, K., Generation and propagation of G waves from the Niigata earthquake of June 16, 1964, 2, Estimation of earthquake moment, released energy, and stress-strain drop from G wave spectrum, Bull. Earthquake Res. Inst. Tokyo, 44, 73-88, 1966.

Audebaud, E., R. Capdevilla, B. Dalmayrac, J. Debelmas, G. Laubacher, C. Lefevre, R. Marocco, C. Martinez, M. Mattauer, F. Megard, J. Paredes, and P. Tomasi, Les traits geologiques essentiels des Andes Centrales (Perou-Bolivie), Revue de Geographie Physique et de Geologie Dynamique (2), 15, 73-114, 1973.

Bally, A.W., P.L. Gordy, and G.A. Stewart, Structure, seismic data and orogenic evolution of the southern Canadian Rocky Mountains, Bull. Can. Petr. Geol., 14, 337-381, 1966.

Barazangi, M., and B.L. Isacks, Spatial distribution of earthquakes and subduction of the Nazca plate beneath South America, Geology, 4, 686-692, 1976.

Barazangi, M., and B.L. Isacks, Subduction of the Nazca plate beneath Peru: evidence from spatial distribution of earthquakes, Geophys. J.R. astr. Soc., 57, 537-555, 1979.

Brewer, J.A., S.B. Smithson, J.E. Oliver, S. Kaufman, and L.D. Brown, The Laramide orogeny: Evidence from COCORP deep crustal seismic profiles in the Wind River mountains, Wyoming, Tectonophys., 62, 165-189, 1980.

Brune, J.N., Seismic moment, seismicity, and rate of slip along major fault zones, J. Geophys. Res., 73, 777-784, 1968.

Burchfiel, B.C., and G.A. Davis, Structural framework and evolution of the southern part of the Cordilleran orogen, western United States, Am. J. Sci., 272, 97-118, 1972.

Burchfiel, B.C., and G.A. Davis, Nature and controls of Cordilleran orogenesis, western United States: Extension of an earlier synthesis, Am. J. Sci., 275-A, 363-396, 1975.

Bussell, M.A., W.S. Pitcher, and P.A. Wilson, Ring complexes of the Peruvian coastal batholith: a long standing subvolcanic regime, Can. J. Earth Sci., 13, 1020-1030, 1976.

Chanove, G., M. Mattauer, and F. Megard, Precisions sur la tectonique tangentielle des terrains secondaries du massif de Pirin (NW du Lac Titicaca, Perou), C.R. Acad. Sci. Paris, 268, ser D, 1698-1701, 1969.

Chen, W.P., and P. Molnar, Depth distribution of earthquake foci and its possible implications for the rheological structure of the crust and upper mantle, (abs.), EOS, 62, 397, 1981.

Chen, W.P., and P. Molnar, Seismic moments of major earthquakes and the average rate of slip in central Asia, J. Geophys. Res., 82, 2945-2969, 1977.

Cobbing, E.J., and W.S. Pitcher, The coastal batholith of central Peru, Q.J. geol. Soc. Lond., 128, 421-460, 1972.

Cobbing, E.J., W.S. Pitcher, and W.P. Taylor, Segments and super-units in the coastal batholith of Peru, J. Geol., 85, 625-631, 1977.

Coney, P.J., Structural evolution of the Cordillera Huayhuash, Andes of Peru, Geol. Soc. Am. Bull., 82, 1863-1884, 1971.

Dalmayrac, B., Geologie de la Cordillere orientale de la region de Huanuco: sa place dans une transversale des Andes du Perou central (9°S à 30°S), Travaux et Documents de l'ORSTOM, 161 pp., Office de la Recherche Scientifique et Technique Outre-Mer, Paris, France, 1978.

Dalmayrac, B., and P. Molnar, Parallel thrust and normal faulting in Peru and constraints on the state of stress, Earth. Plan. Sci. Lett., 55, 473-481, 1981.

Dalmayrac, B., J.R. Lancelot, and A. Leyreloup, Two-billion-year granulites in the late Precambrian metamorphic basement along the southern Peruvian coast, Science, 198, 49-51, 1977.

Dalmayrac, B., G. Laubacher, and R. Marocco, Geologie des Andes Peruviennes, Caracteres generaux de l'evolution geologique des Andes peruviennes, Travaux et Documents de l'ORSTOM, Editions de l'Office de la Recherche Scientifique et Technique Outre-Mer, Paris, France, 1980.

Davies, G.F., and J.N. Brune, Regional and global fault rates from seismicity, Nat. Phys. Sci., 229, 101-107, 1971.

Dewey, J.F., and Bird, J.M., Mountain belts and the new global tectonics, J. Geophys. Res., 75, 2625-2647, 1970.

Dollfus, O., and F. Megard, Les formations Quaternaires du basin de Huanayo et leur neotectonique (Andes centrales peruviennes), Rev. Geograph. Phys. Geol. Dynamique (2), X, 5, 429-440, 1968.

Gansser, A., Facts and theories on the Andes, Q.J. geol. Soc. Lon., 129, 93-131, 1973.

Gee, D.G., Nappe displacement in the Scandinavian Caledonides, Tectonphys., 47, 393-419, 1978.

Gilbert, F., Excitation of the normal modes of the earth by earthquake sources, Geophys. J.R. astr. Soc., 22, 223-226, 1970.

Ham, C.K., and L.J. Herrera, Jr., Role of subandean fault system in tectonics of eastern Peru and Ecuador, in Childs, O.E., and Beebe, R.N., eds., Backbone of the Americas, Am. Assoc. Petr. Geol. Mem., 2, 47-61, 1963.

Hamilton, W., The volcanic central Andes - a modern model for the Cretaceous batholiths and tectonics of western North America, Oregon Dept. Geology and Mineral Industries, Bull., 65, 175-184, 1969.

Hanks, T.C., and H. Kanamori, A moment magnitude scale, J. Geophys. Res., 84, 2348-2350, 1979.

Harrington, H.J., Paleogeographic development of South America, Bull. Am. Assoc. Petr. Geol. Bull., 46, 1173-1814, 1962.

Helwig, J., Plate tectonic model for the evolution of the Central Andes: Discussion, Geol. Soc. Am. Bull., 84, 1493-1496, 1973.

Hodgson, J.H., and P.C. Bremmer, Direction of faulting in the Ancash, Peru, earthquake of November 10, 1946, from teleseismic evidence, Seism. Soc. Am. Bull., 43, 121-125, 1953.

Jackson, J., and T. Fitch, Basement faulting and the focal depth of the larger earthquakes in the Zagros Mountains (Iran), 64, 561-586, 1981.

James, D.E., Andean crustal and upper mantle structure, J. Geophys. Res., 76, 3246-3271, 1971.

James, D.E., I.S. Sacks, E. Lazo, and O. Aparicio, On locating local earthquakes using small networks, Seis. Soc. Am. Bull., 59, 1201-1212, 1969.

Jordan, T.E., B.L. Isacks, R.W. Allmendinger, J.A. Brewer, V.A. Ramos, and C.J. Ando, Andean tectonics related to geometry of subducted Nazca plate, submitted to Geol. Soc. Am. Bull., 1982.

Kanamori, H., and G.S. Stewart, Mode of strain release along the Gibbs fracture zone, Mid-Atlantic ridge, Phys. Earth Planet. Int., 11, 312-332, 1976.

Kelleher, J., and W. McCann, Buoyant zones, great earthquakes and unstable boundaries of subduction, J. Geophys. Res., 81, 4885-4896, 1976.

Kostrov, V.V., Seismic moment and energy of earthquakes, and seismic flow of rock, Izv. Acad. Sci. USSR, Phys. Solid Earth, 1, 23-44, 1974.

Langston, C.A., A single station fault plane solution, Geophys. Res. Lett., 6, 41-44, 1979.

Langston, C.A., and D. Helmberger, A procedure for modeling shallow dislocation sources, Geophys. J. Roy. Astron. Soc., 42, 117-130, 1975.

Laubacher, G., Geologie de la Cordillera Oriental et de l'Altiplano au Nord et Nord-ouest du Lac Titicaca, Geologie des Andes Peruviennes, Trauvaux et Documents de l'ORSTOM, 95 pp., Office de la Recherche Scientifique et Technique Outre-Mer, Paris, France, 1978.

Lavenu, A. Neotectonique des sediments plio-quaternaires du nord de l'Altiplano bolivien (Region de La Paz-Ayo-Ayo-Umala), Cah. O.R.S.T.O.M., ser. Geol., X, No. 1, 115-126, 1978.

Lavenu, A., and O. Ballivian, Estudios neotectonicos de las cuencas de las regiones de Cochabamba, Sucre, Tarija - Cordillera Oriental boliviana, Rev. Acad. Nac. Cien. Bolivia, 2, No. 3, 107-129, 1979.

Lepyr, L.A., and G.H. Davis, Influence of 'soft' basement on ramp thrusting in the Yauli dome foreland region, Cordillera Occidental, Peru, submitted to Geol. Soc. Am. Bull., 1982.

Lohman, H.H., Outline of the tectonic history of Bolivian Andes, Am. Assoc. Petr. Geol. Bull., 54, 735-757, 1970.

McKenzie, D., Active tectonics of the Mediterranean region, Geophys. J.R. astr. Soc., 30, 109-185, 1972.

McTigue, D.F., and C.C. Mei, Gravity-induced stresses near topography of small slope, J. Geophys. Res., 86, 9268-9278, 1981.

Megard, F., Etude geologique des Andes du Perou central, Office de la Recherche Scientifique et Tecnique Outre-Mer, Mem. 86, 310 pp., 1978.

Megard, F., and H. Philip, Plio-Quaternary Tectono-Magmatic zonation and plate tectonics in the central Andes, Earth Plan. Sci. Lett., 33, 231-239, 1976.

Meissner, R., and J. Strehlau, Limits of stresses in continental crusts and their relation to depth-frequency distribution of shallow earthquakes, Tectonics, 1, 73-89, 1982.

Mendiguren, J.A., and F.M. Richter, On the origin of compressional intraplate stresses in South America, Phys. Earth Plan. Int., 16, 318-326, 1978.

Mercier, J.L., Extensional-compressional tectonics associated with the Aegean Arc: comparison with the Andean Cordillera of south Peru-north Bolivia, Phil. Trans. R. Soc. Lond., 300, 337-355, 1981.

Molnar, P., Earthquake recurrence intervals and plate tectonics, Bull. Seis. Soc. Am., 69, 115-133, 1979.

Molnar, P., and P. Tapponnier, Cenozoic tectonics of Asia: effects of a continental collision, Science, 189, 419-426, 1975.

Molnar, P., and P. Tapponnier, Active tectonics of Tibet, J. Geophys. Res., 83, 5361-5375, 1978.

Molnar, P., W.P. Chen, T.J. Fitch, P. Tapponnier, W.E.K. Warsi, and F.T. Wu, Structure and tectonics of the Himalaya: A brief summary of relevant geophysical observation, in Himalaya: Sciences de la Terre, pp. 269-294, Centre National de la Recherche Scientifique, Paris, 1977.

Newell, N.D., Geology of the Lake Titicaca region, Peru and Bolivia, Geol. Soc. Am. Mem., 36, 111 pp., 1949.

Noble, D.C., and E.J. McKee, Spatial distribution of earthquakes and subduction of the Nazca plate beneath south: Comment, Geology, 5, 576-578, 1977.

Pennington, W.D., Subduction of the Eastern Panama Basin and seismotectonics of Northwestern South America, 86, 10753-10770, 1981.

Philip, H., and F. Megard, Structural analysis of the superficial deformation of the 1969 Pariahuanca earthquakes (central Peru), Tectonophys., 38, 259-278, 1977.

Pilger, R.H., Plate reconstructions of aseismic ridges, and low angle subduction beneath the Andes, Geol. Soc. Am. Bull., 92, 448-456, 1981.

Pitcher, W., On the rate of emplacement of batholiths, Q.J. Geol. Soc. Lond., 581-591, 1975.

Plafker, G., Alaskan earthquake of 1964 and Chilean earthquake of 1960: implications for arc tectonics, J. Geophys. Res., 77, 901-925, 1972.

Price, R.A.,. and E.W. Mountjoy, Geologic structure of the Canadian Rocky Mountains between Bow and Athabaska Rivers - a progress report, Geol. Assoc. Canada Spec. Paper, 6, 7-25, 1970.

Rial, J.A., The Caracas, Venezuela, earthquake of July 1967: A multiple-source event, J. Geophys. Res, 83, 5405-5414, 1978.

Richter, C.F., Elementary Seismology, W.H. Freeman, San Francisco, 768 pp., 1958.

Rodriguez, A., and A. Chalco, Cuenca Huallaga, Resena geologica y posibilidades petroliferas, Bol. Soc. Geol. Peru, 49, 187-212, 1975.

Sales, J.K., Cordilleran foreland deformation, Am. Assoc. Petroleum Geol. Bull., 52, 2016-2044, 1968.

Shackleton, R.M., A.C. Ries, M.P. Coward, and P.R. Cobbold, Structure, metamorphism, and geochronology of the Arequippa Massif of coastal Peru, 136, 2, 195-214, 1979.

Silgado, E., The Ancash, Peru, earthquake of November 10, 1946, Bull. Seism. Soc. Am., 41, 83-100, 1951.

Smithson, S.B., J.A. Brewer, S. Kaufman, J.E. Oliver, and C.A. Hurich, Structure of the Laramide Wind River uplift, Wyoming, from COCORP deep reflection data and from gravity data, J. Geophys. Res., 84, 5955-5972, 1979.

Stauder, W., Subduction of the Nazca plate under Peru as evidenced by focal mechanisms and by seismicity, J. Geophys. Res., 80, 1053-1064, 1975.

Stearns, D.W., Faulting and forced folding in the Rocky Mountain foreland, in Matthews, V., III, ed., Laramide Folding Associated with Basement Block Faulting in the Western United States, Geol. Soc. Am. Memoir, 151, 1-37, 1978.

Stewart, J.S.W., J.F. Evernden, and N.J. Snelling, Age determinations from Andean Peru: a reconnaissance survey, Geol. Soc. Am. Bull., 85, 1107-1116, 1974.

Tapponnier, P., and P. Molnar, Active faulting and tectonics in China, J. Geophys. Res., 82, 1977.

Touzett, G., Evaluacion geologica del yacimiento petrolifero Agua Caliente, Bol. Soc. Geol. Peru, 48, 9-24, 1975.

Trehu, A.M., J.L. Nabelek, and S.C. Solomon, Source characterization of two Reykjanes Ridge earthquakes: surface waves and moment tensors; P waveforms and nonorthogonal nodal planes, J. Geophys. Res., 86, 1701-1724, 1981.

Vicente, J.C., F. Sequeiros, M.A. Valdivia, and J. Zavala, El sobre-escurrimiento de Cincha-Lluta: Elemento del accidente mayor andino al NW de Arequipa, Bol. Soc. Geol. Peru, 61, 67-100, 1979.

Vogt, P.R., A. Lowrie, D.R. Bracey, and R.N. Hey, Subduction of aseismic oceanic ridges: effects on shape, seismicity and other characteristics of

consuming plate boundaries, Geol. Soc. Am. Spec. Paper, 172, 59 pp., 1976.

Wagner, D., Statistical decision theory applied to the focal mechanism of Peruvian earthquakes, Ph.D. dissertation, 176 pp., St. Louis Univ., St. Louis, Mo., 1972.

Wesnousky, S.G., C.H. Scholz, and K. Shimazaki, Deformation of an island arc: Rates of moment-release and crustal shortening in intraplate Japan determined from seismicity and Quaternary fault data, J. Geophys. Res., in press, 1982.

Wilson, J.J., Cretaceous stratigraphy of the central Andes of Peru, Amer. Assoc. Petr. Geol. Bull., 47, 1-34, 1963.

Wilson, J.J., L. Reyes, and J. Garayar, Geologia de los Cuadrangulos de Mollebamba, Tayabamba, Huaylas, Pomabamba, Carhuaz y Huari, Servicio de Geologia y Mineria, Bol. 16, Lima, Peru, 95 pp., 1967.

Yamashina, K., K. Shimazaki, T. Kato, Aseismic belt along the frontal arc and plate subduction in Japan, J. Phys. Earth, 26, 447-458, 1978.

Yonekura, N., T. Matsuda, M. Nogami, and S. Kaizuka, An active fault along the western part of the Cordillera Blanca, Peru, J. Geography Tokyo, 88, 1-19, 1979.

Zeil, W., The Andes a geological review, 260 pp., Gebruder Borntraeger, Berlin-Stuttgart, Germany, 1979.

TABLE 1

LIST OF EARTHQUAKES STUDIED

DATA FROM THE I.S.C. CATALOG

Event	Date	Latitude	Longitude	Origin Time	Depth	Magnitude
1	May 10, 1963	-2.20	-77.60	22^h 22' 42.0"	33	6.7
2	Nov 3, 1963	-3.50	-77.80	3^h 10' 12.7"	33	6.7
3	Feb 9, 1967	2.93	-74.83	15^h 24' 45.3"	36	6.3
4	Jun 19, 1968	-5.55	-77.20	8^h 13' 35.6"	33	6.1
5	Jun 20, 1968	-5.51	-77.30	2^h 38' 30.7"	33	5.8
6	Dec 1, 1968	-10.54	-74.81	13^h 14' 55.0"	33	5.4
7	Jul 24, 1969	-11.84	-75.10	2^h 59' 20.9"	1	5.9
8	Oct 1, 1969	-11.75	-75.15	5^h 5' 50.0"	43	5.8
9	Feb 14, 1970	9.84	-75.55	11^h 17' 16.4"	36	5.8
10	Dec 10, 1970	-3.97	-80.66	4^h 34' 38.0"	15	6.3
11	Oct 5, 1971	-14.20	-73.45	10^h 33' 46.3"	54	5.7
12	Mar 20, 1972	-6.79	-76.76	7^h 33' 48.7"	52	6.1
13	Feb 23, 1973	-2.16	-78.33	4^h 26' 21.1"	44	5.7
14	Sep 27, 1974	2.72	-71.37	4^h 9' 1.6"	44	5.5
15	Apr 9, 1976	0.85	-79.63	7^h 8' 50.0"	19	6.0
16	May 15, 1976	-11.62	-74.45	21^h 55' 55.0"	5	5.9
17	Oct 6, 1976	-0.76	-78.75	9^h 12' 39.0"	33	5.7

TABLE 2

Source Parameters

Event Number	Date	P axis		T axis		Depth (km)	Seismic Moment M_o (dyne-cm)	Number of Stations Used to Estimate M_o
		Trend	Plunge	Trend	Plunge			
1	May 10, 1963	95.4	4.2	5.0	1.42	16	8.65×10^{25}	16
2	Nov. 3, 1963	90.0	5.0	270.0	85.0	18	2.73×10^{25}	24
3	Feb. 9, 1967	260.2	8.7	353.8	22.26	32	1.60×10^{26}	20
4	June 19, 1968	284.3	11.4	150.2	73.8	20	1.96×10^{26}	19
5	June 20, 1968	82.8	12.5	330.4	60.8	16	4.95×10^{24}	16
6	Dec. 1, 1968	80.8	5.0	260.0	85.0	18	5.75×10^{24}	3
7	July 24, 1969	77.0	23.0	205.8	55.9	6	1.81×10^{25}	14
8	Oct. 1, 1969	52.6	21.9	207.4	66.1	5	9.84×10^{25}	17
9	Feb. 14, 1970	260.0	9.0	80.0	81.0	28	9.71×10^{24}	9
10	Dec. 10, 1970	73.0	10.0	253.0	80.0	32	6.76×10^{26}	15
11	Oct. 15, 1971	264.1	0.1	174.1	14.1	8	2.98×10^{24}	6
12	March 20, 1972	267.0	10.0	87.0	80.0	38	4.23×10^{25}	25
13	Feb. 23, 1973	97.8	22.5	321.9	60.0	10	9.47×10^{24}	13
14	Sept. 27, 1974	285.0	5.3	194.8	1.76	6	3.67×10^{25}	1
15	April 9, 1976	264.0	33.0	84.0	57.0	22	9.69×10^{25}	12
16	May 15, 1976	16.5	9.1	281.2	25.4	18	1.25×10^{26}	23
17	Oct. 6, 1976	274.4	24.2	145.2	54.6	16	5.24×10^{24}	2

Figure Captions

Figure 1. Physiographic provinces of the Andes of Peru and northern Bolivia. (1) Coastal Plains, (2) Cordillera Occidental, (3) Altiplano, (4) Cordillera Oriental, (5) Sub-Andean zone. Dark areas indicate plutonic bodies and hachured areas the volcanic rock cover (after Dalmayrac et al, 1980).

Figure 2. Main structural features of the central Andes (after Audebaud et al, 1973).

Figure 3. Shallow focus seismicity in western South America from 1962 to 1979. Squares show the epicenters of earthquakes shallower than 70 km and registered by more than 40 stations reporting P waves to the International Seismological Catalog. Shown also is the 3000 m elevation contour.

Figure 4. Earthquakes shown in Figure 3 plotted on a physiographic map of the Central Andes. Intracontinental seismicity concentrates along the western margin of the sub-Andes in central and northern Peru.

Figure 5. Lower hemisphere equal area projection of the focal sphere for the May 15, 1976 earthquake (event 17). Open circles indicate dilatational first motions and closed circles indicate compressions. Two alternative pairs of nodal planes satisfying the data are shown.

Figure 6. Observed and synthetic long period P waves at stations WES and OGD for the two alternative fault plane solutions shown in Figure 5. The observed P waves are matched better by the dip-slip solution. Each of the strike, dip, and rake of the nodal planes, however, may be varied as much as 10° without changing appreciably the shape of the synthetic pulses.

Figure 7. Comparison of the recorded P waveforms from the event of March 20, 1972 with a suite of synthetic waveforms for different focal depths using the fault plane solution shown in the Appendix. Synthetic P wavesforms for depths shallower than 36 km or deeper than 40 km do not match the observed waveforms well.

Figure 8. Comparison of synthetic P waveforms using mean crustal velocities of 5.5, 6.0, and 6.5 km/sec with the observed P waveforms from the earthquake of March 20, 1972 at the same stations shown in Figure 7.

Figure 9. Map of the central Andes summarizing fault plane solutions and focal depths. Dark areas in lower hemispheric projections of focal spheres indicate quadrants with compressional first motion. Epicenters are plotted as stars and the numbers beside them indicate estimated focal depths in km. Numbers next to balloons correspond to those in Table 1 and Appendix.

Figure 10. Cross section of seismicity accross Ecuador. Black dots show position of earthquakes selected by Barazangi and Isacks [1979] in cross section B-B' These events determine the dip of the slab. The east-dipping nodal plane of event 10 in the forearc, is too steep to be associated with slip on the main-inclined seismic zone. The west-dipping nodal planes of earthquakes in the sub-Andes are also projected on the cross section. The position of the Moho beneath the Andes is drawn so as to maintain isostatic equilibrium but is not constrained by other data

Figure 11. Cross section of seismicity through central Peru (symbols as in Figure 10). The dip of the slab is determined by the earthquakes selected by Barazangi and Isacks [1979] in cross section C-C'. West dipping nodal planes of two of the earth-

quakes studied here from sub-Andes are projected onto the cross section The fault plane of the earthquakes in the high Andes is known to dip east, as observed in the field (Philip and Megard, 1976)

Figure 12. Histogram of the dips of the nodal planes of the earthquakes studied.

Figure 13. LANDSAT image 2194-14345-7 of the area north of the Cordillera Blanca (snow capped range). Steep escarpment to the west of the range defines zone of normal faulting.

Figure 14. Aerial photograph of an active normal fault in the Altiplano of southern Peru. Arrow points to the fault scarp (scale 1:20,000).

Figure 15. Photograph of normal fault shown in figure 14 taken from the ground at a distance of two kilometers south southwest of the fault White arrow in Figure 15 shows position of main river valley in left third of photo. The fault scarp clearly offsets Quaternary sediments and moraines.

Figure 16. Fault plane solution of the November 10, 1946 Ancash earthquake. Open circles indicate dilatational and closed circle compressional first motions (from data collected by Hodgson and Bremner [1953]).

Figure 17. Stress in and near an elastic, two-dimensional ridge subjected to horizontal compression perpendicular to it. The horizontal compressive stress reaches a maximum at the edges of the ridge. At the center of the ridge the value of the horizontal stress decreases, and for large characteristic slopes it may become purely tensile (after McTigue and Mei, 1981).

Figure 18. Sequence of idealized cross sections across the Central Andes through time. (a) Underthrusting of the Brazilian shield east of the incipient mountain belt. (b) and (c) The crust thickens and uplifts the topography to an equilibrium height and a new fault breaks to the east. (d) Present day topography and crustal thickness. Circles indicate earthquakes plotted in Figure 10.

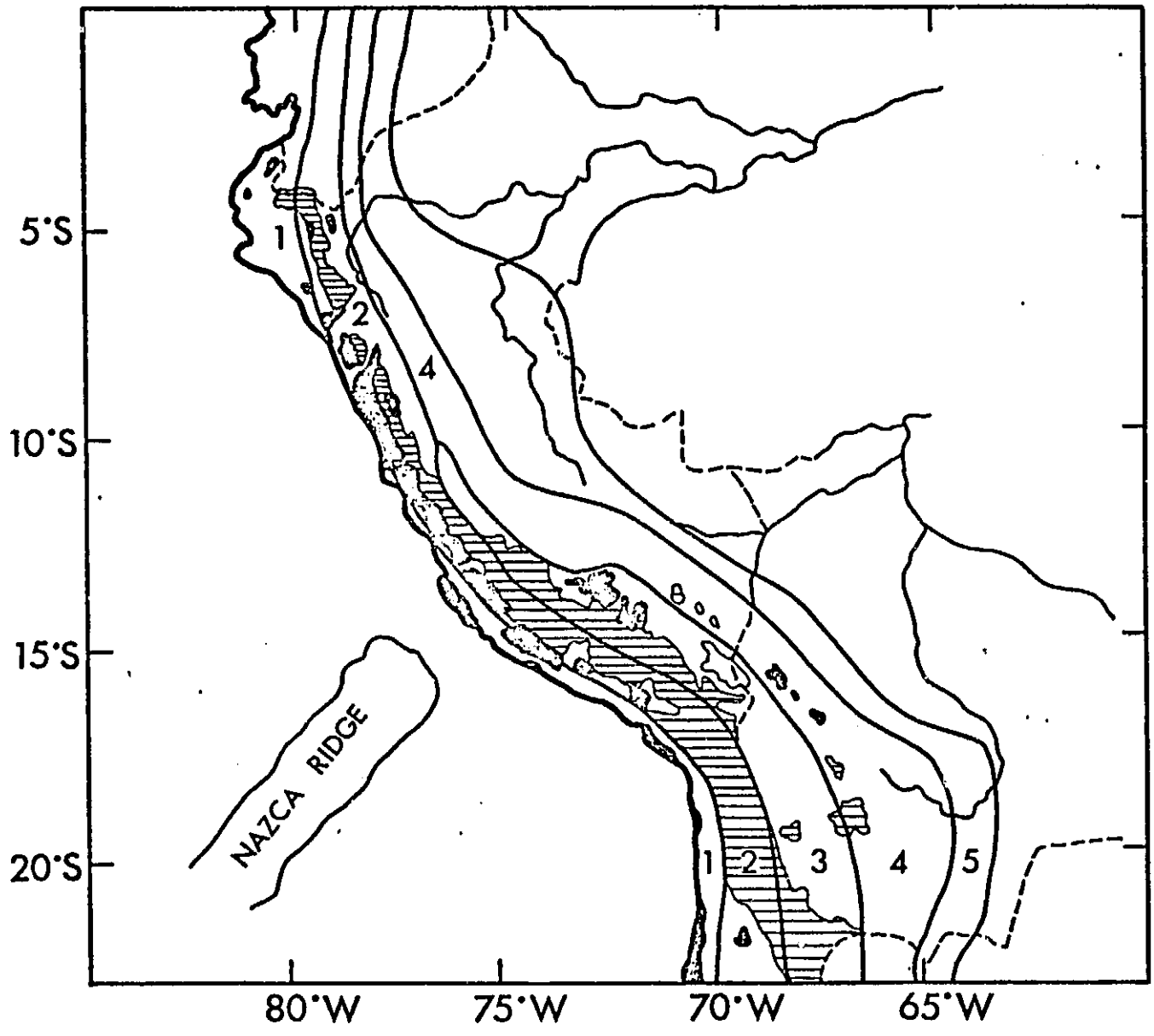

Fig. 1

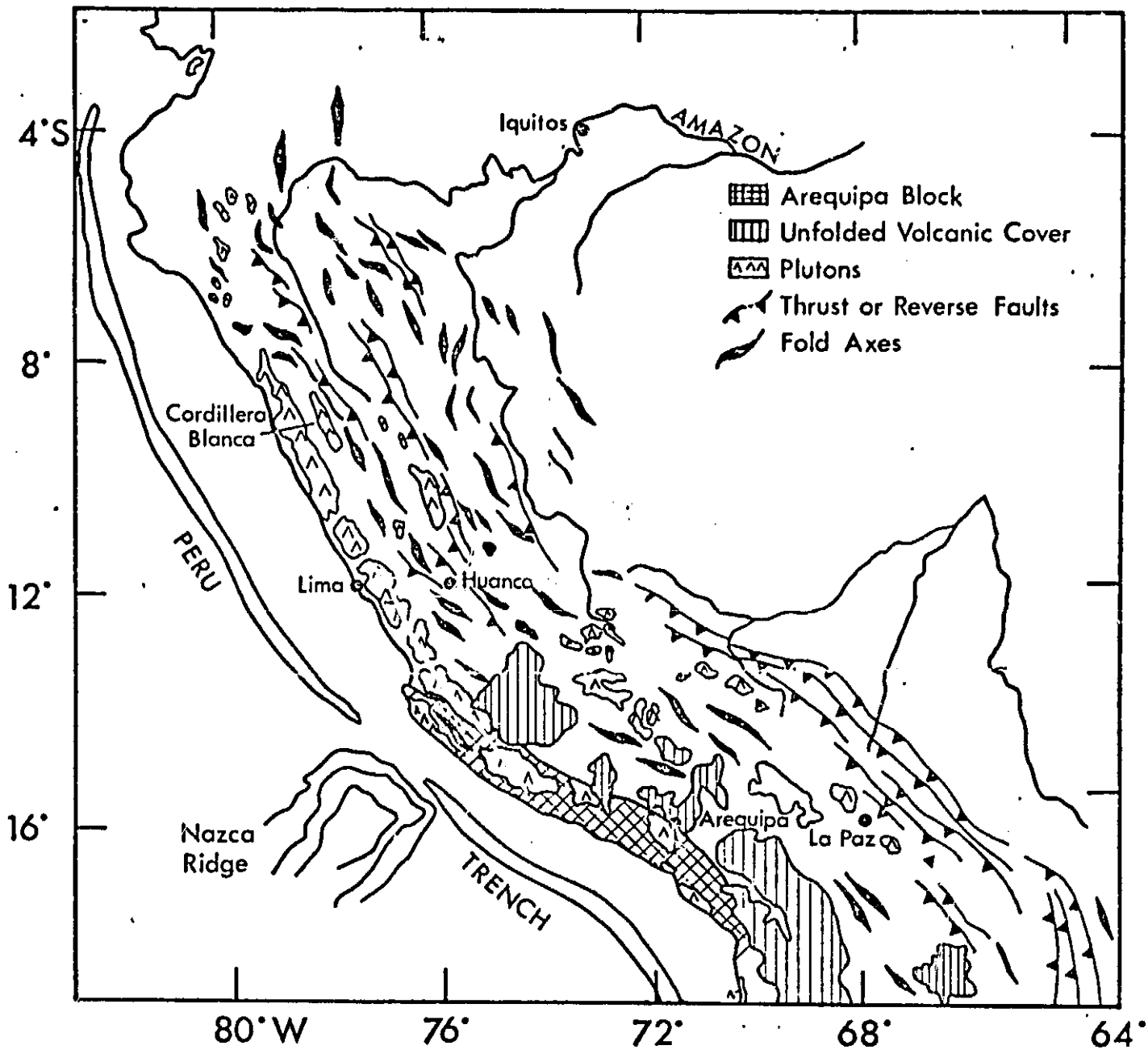

Fig. 2

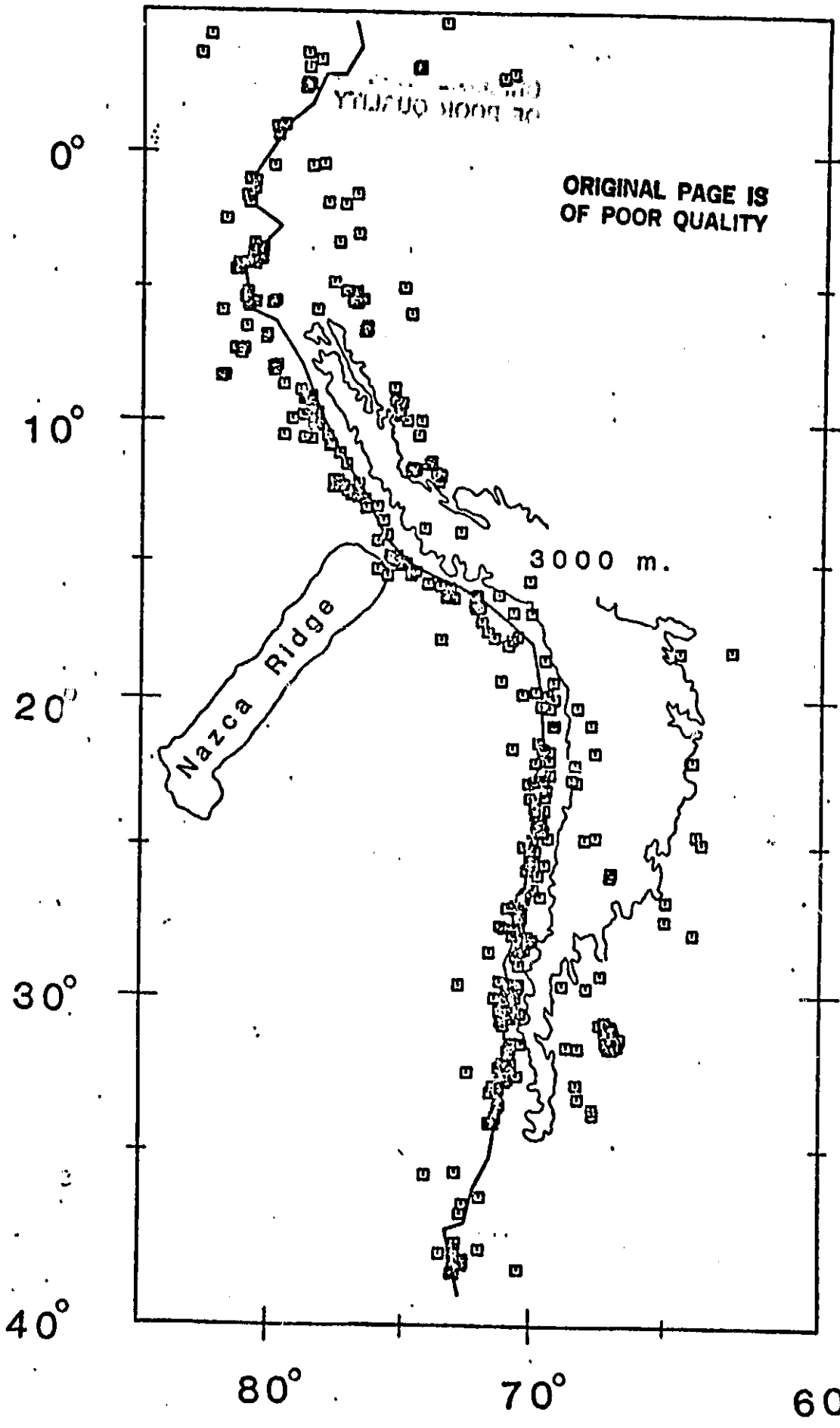
0°
10°
20°
30°
40°
80°
70°
60°
3000 m.
Nazca Ridge
ORIGINAL PAGE IS
OF POOR QUALITY

Fig 3

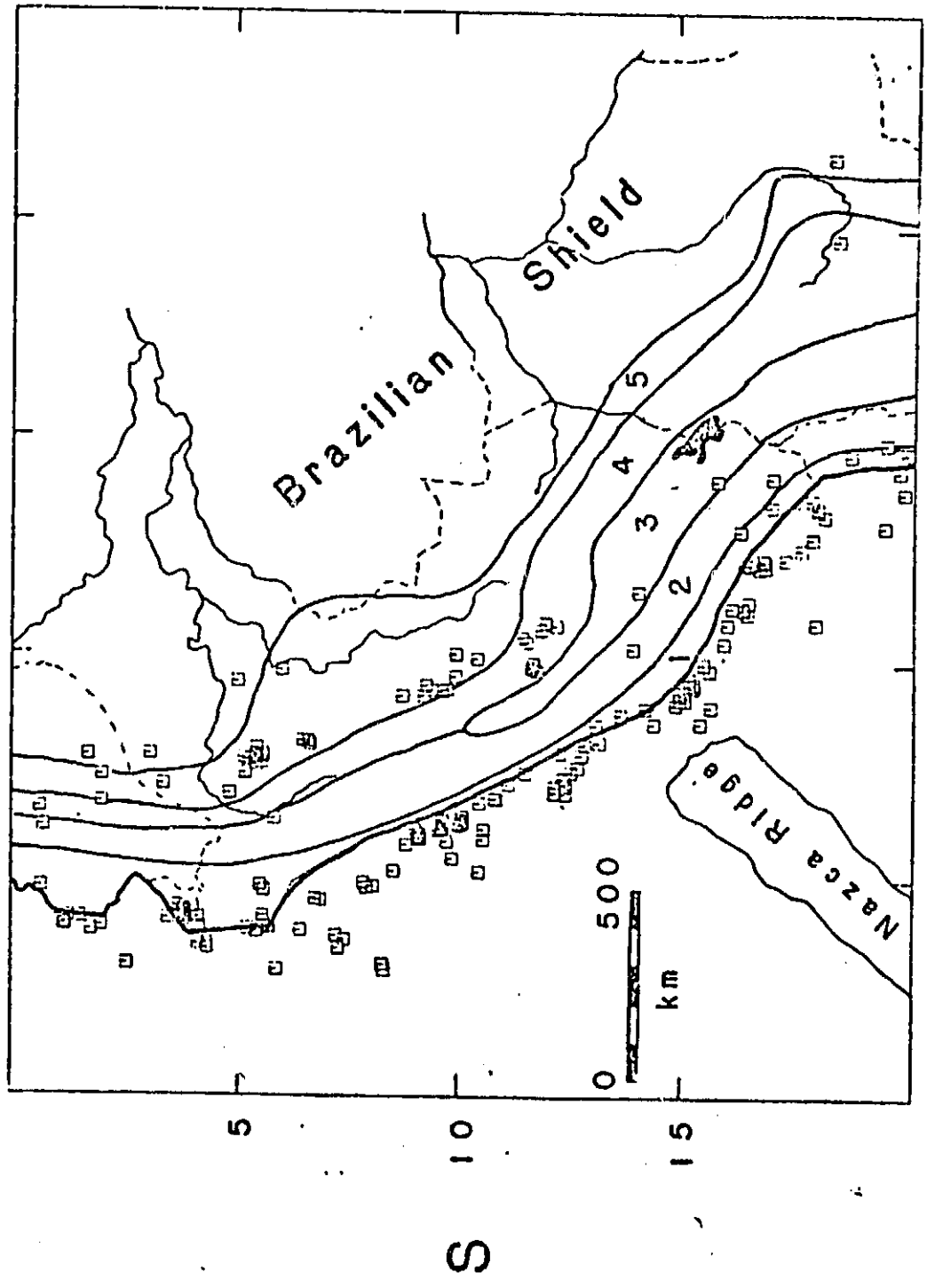

Fig 4

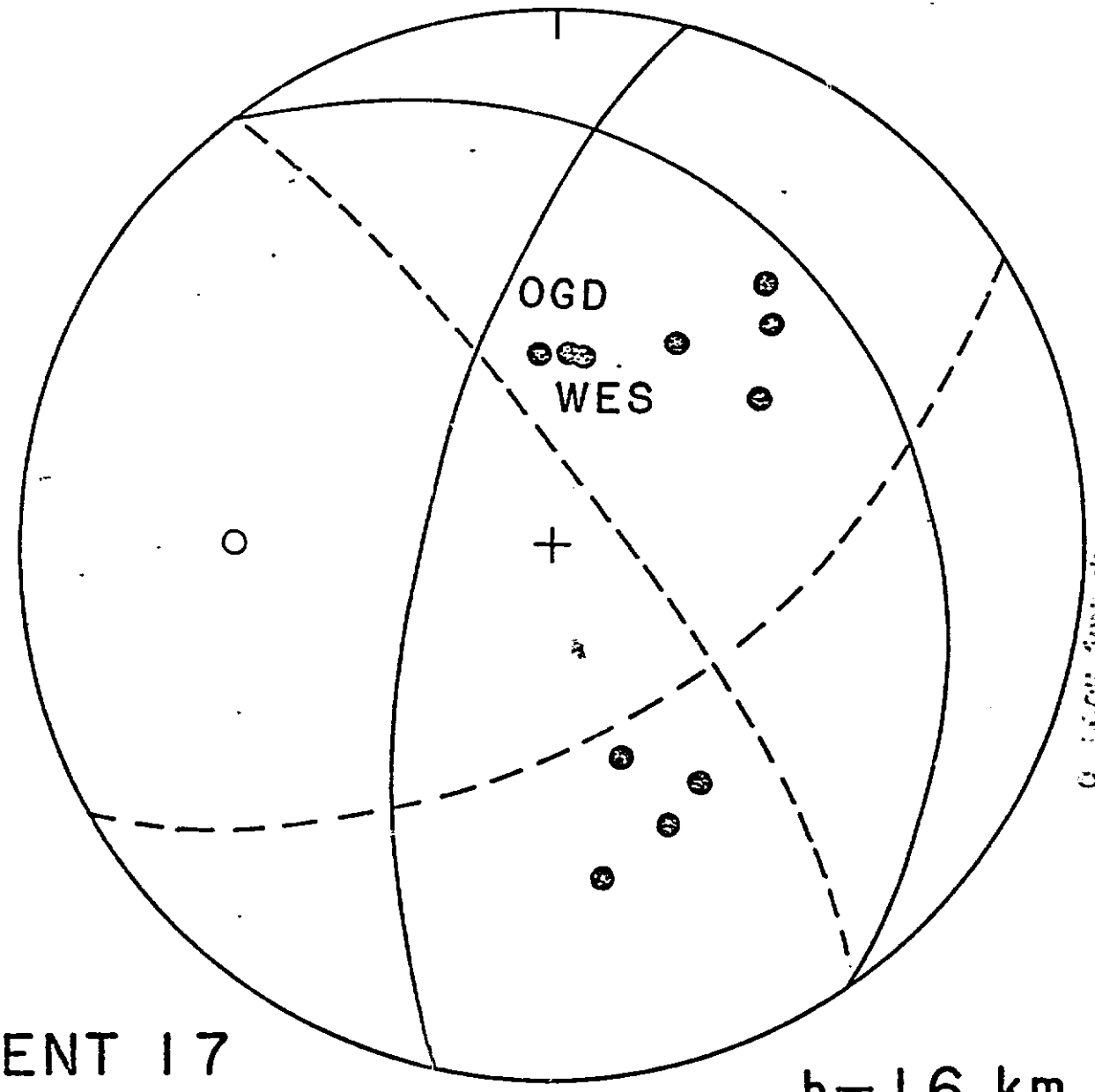

EVENT 17
May 15, 1976

h=16 km.

Fig 5

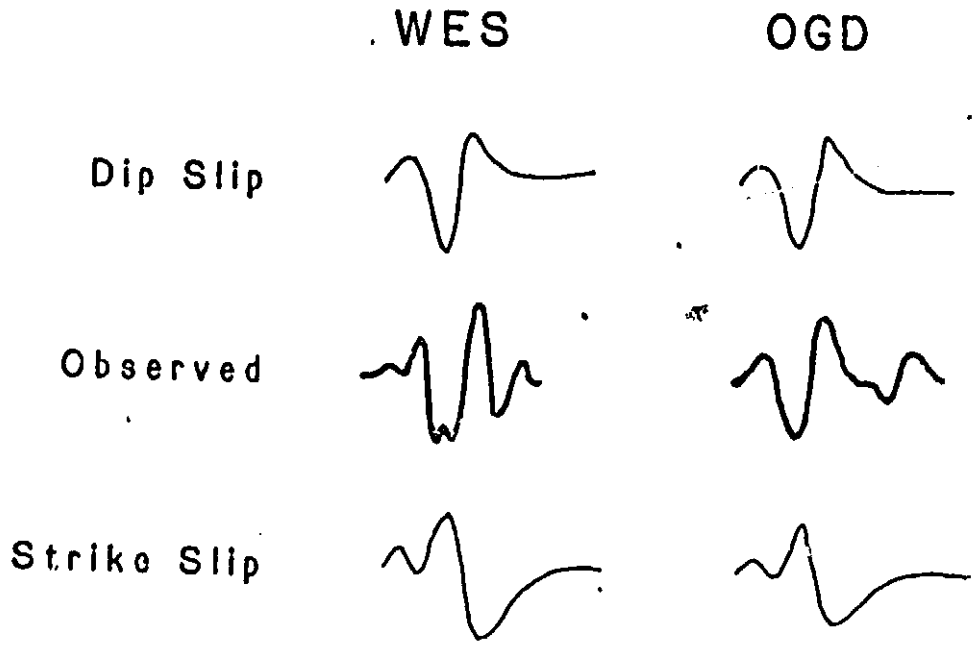

Fig 6

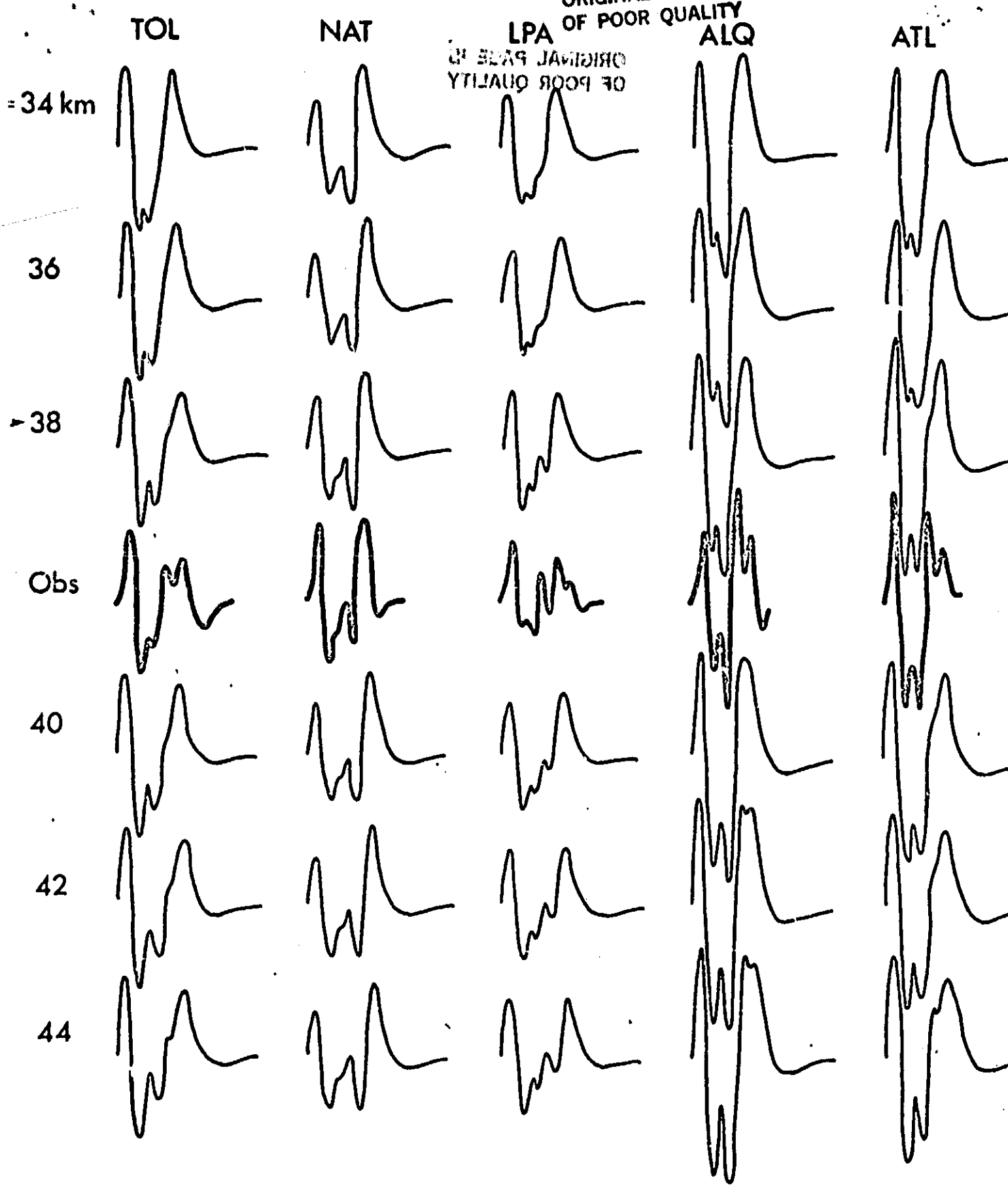

Fig 7

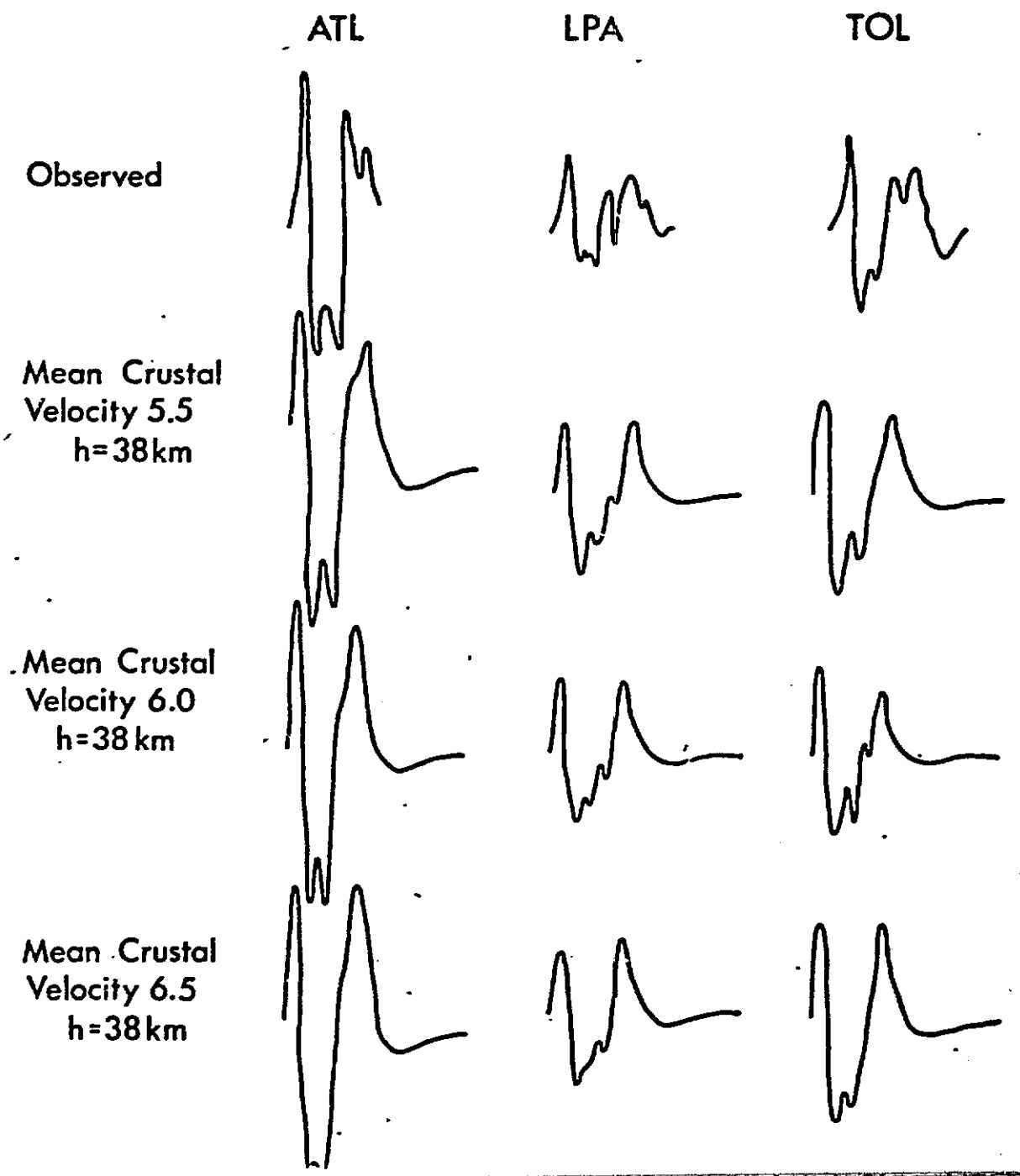

Fig 8

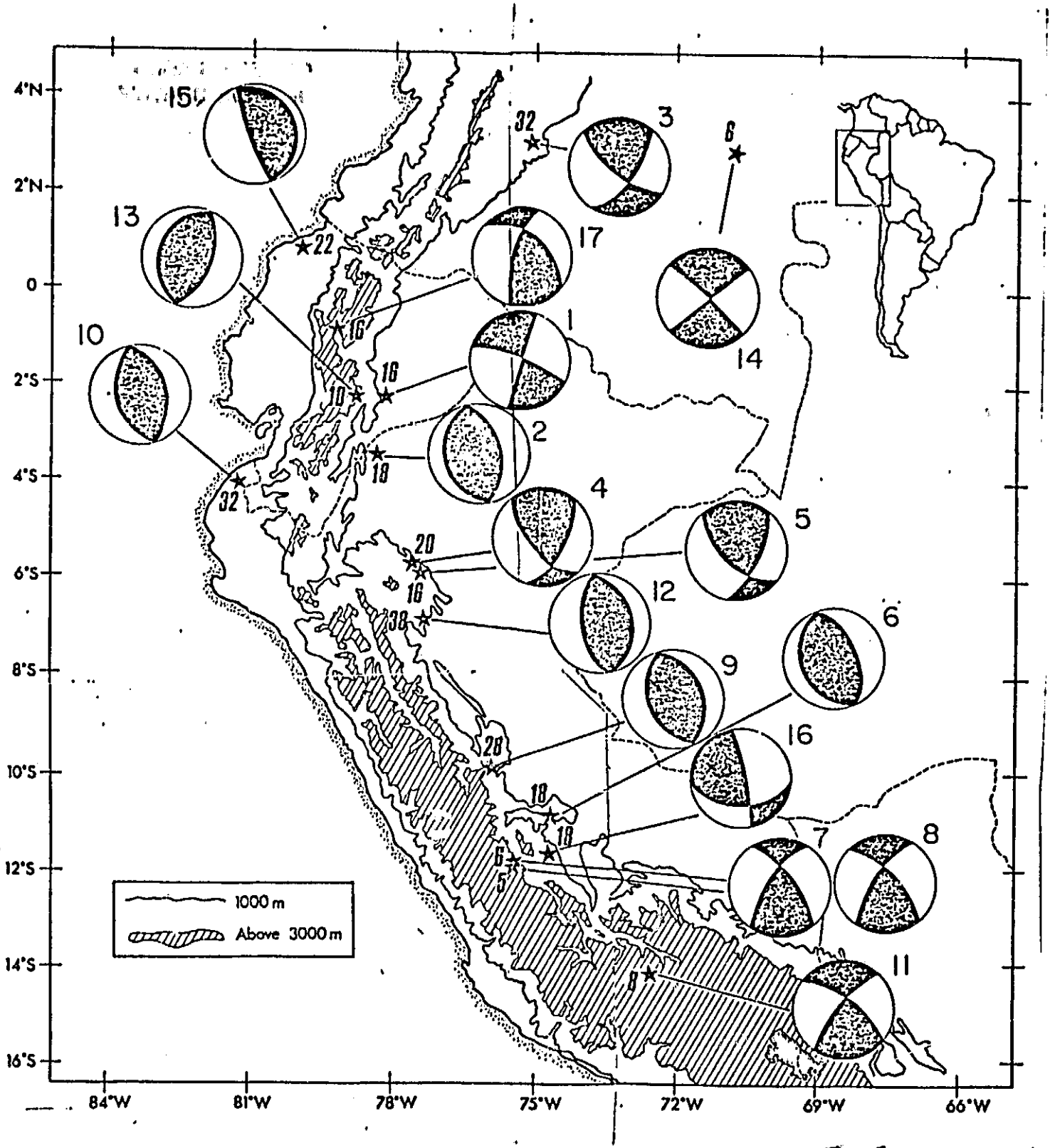

Fig 9

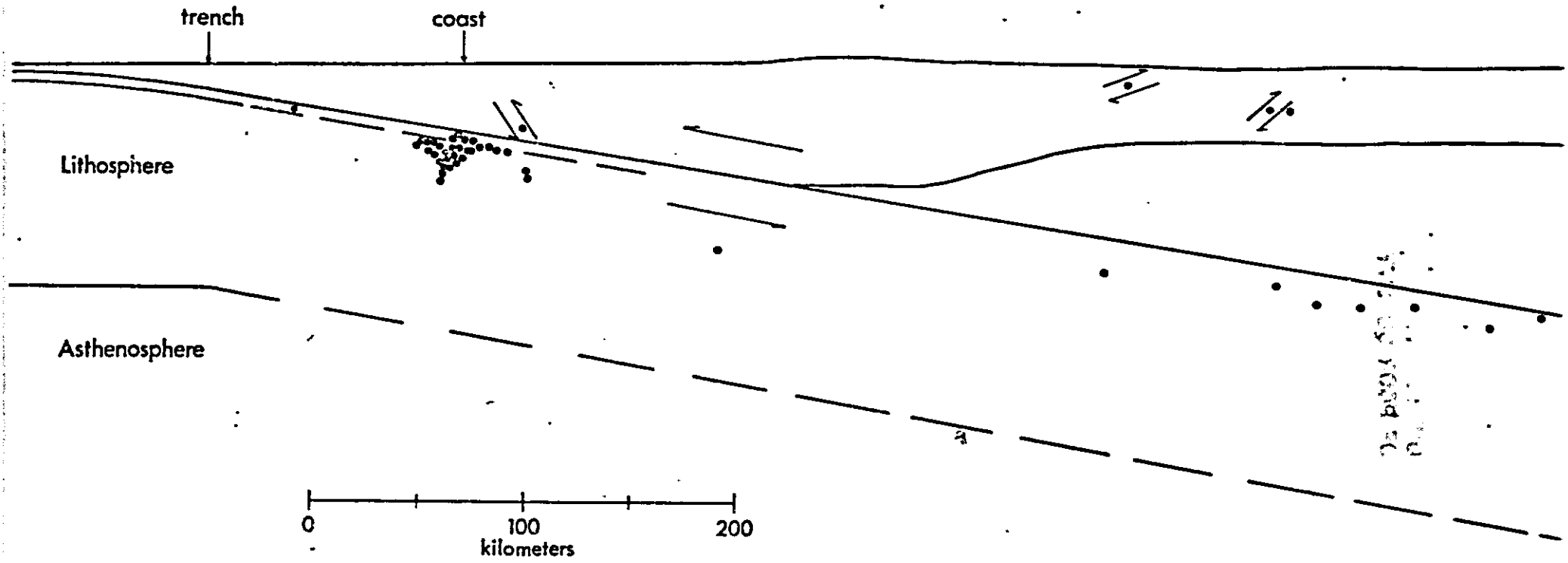

Fig 10

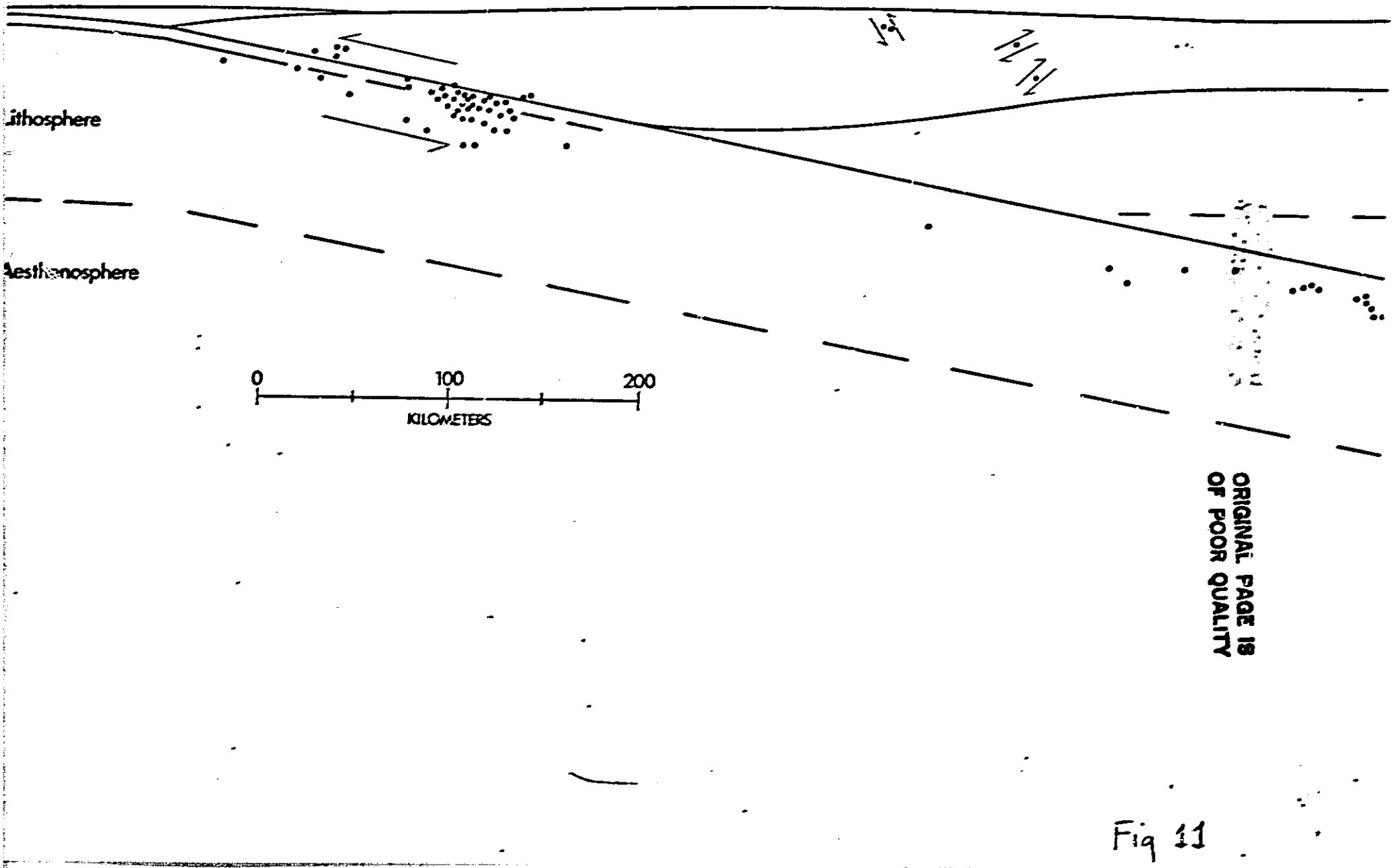

ORIGINAL PAGE IS
OF POOR QUALITY

Fig 11

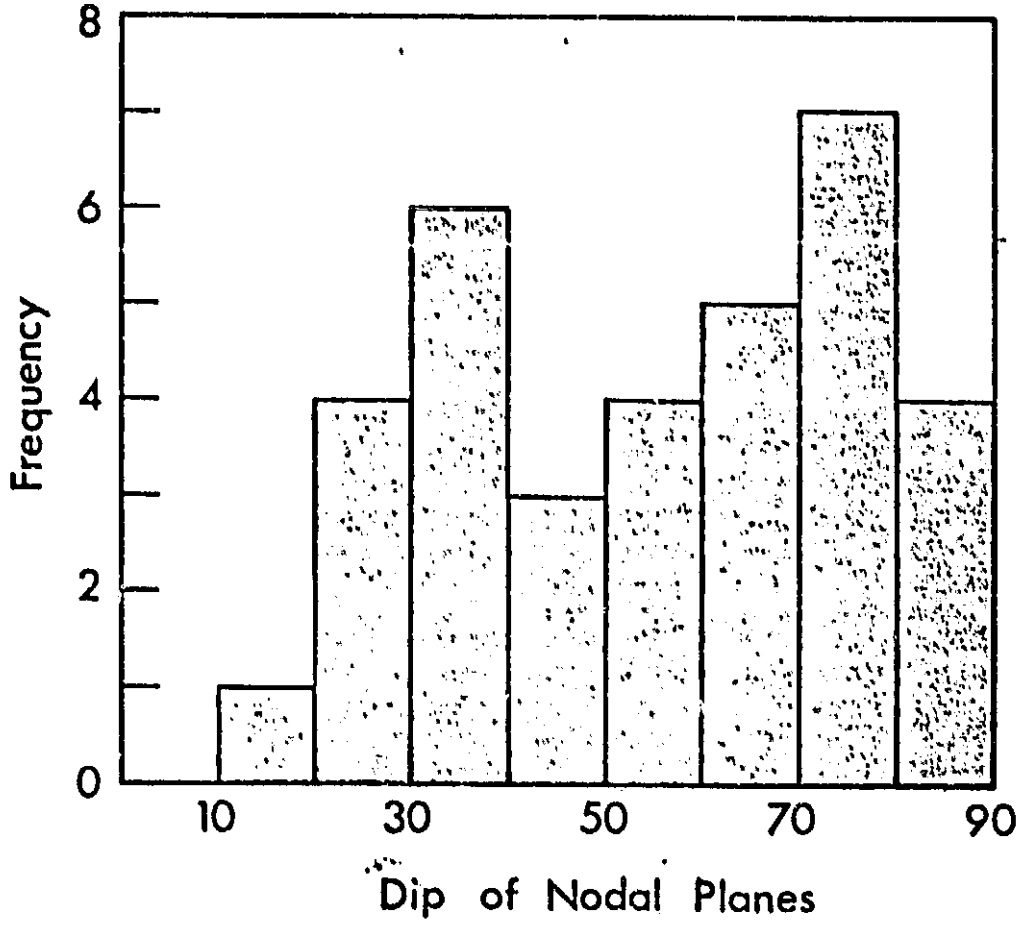

Fig. 12

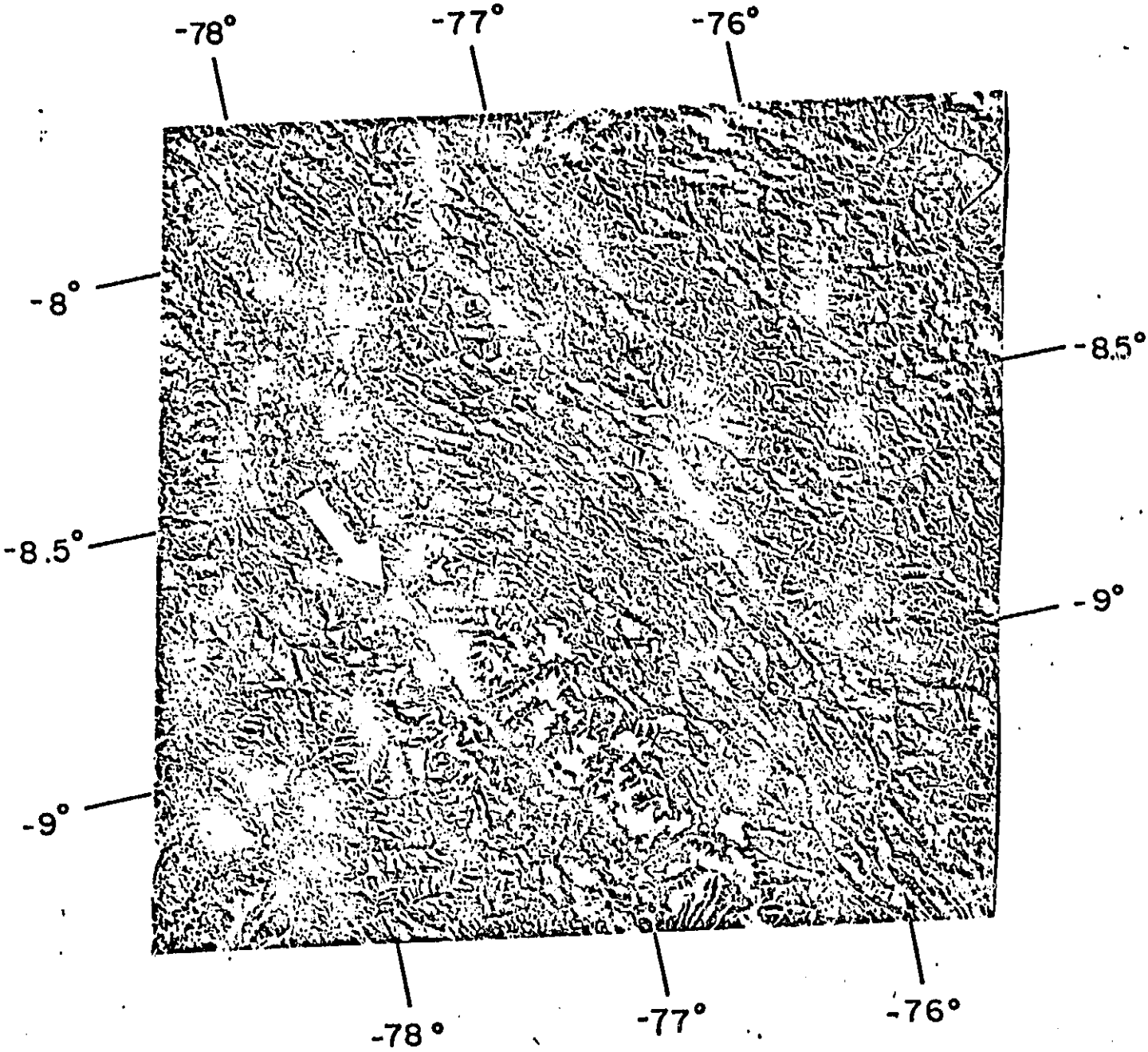

Fig. 13

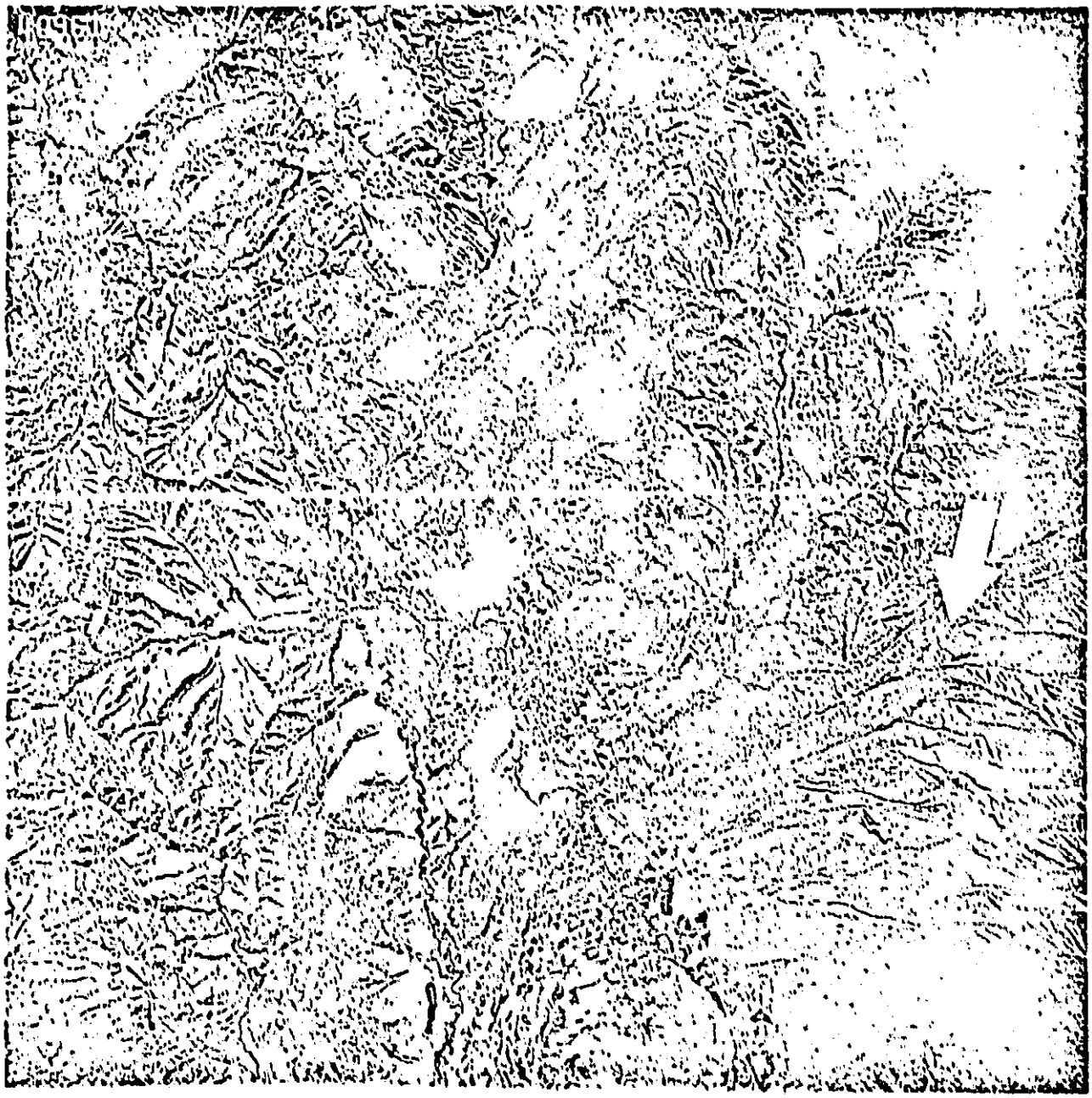

Fig. 14

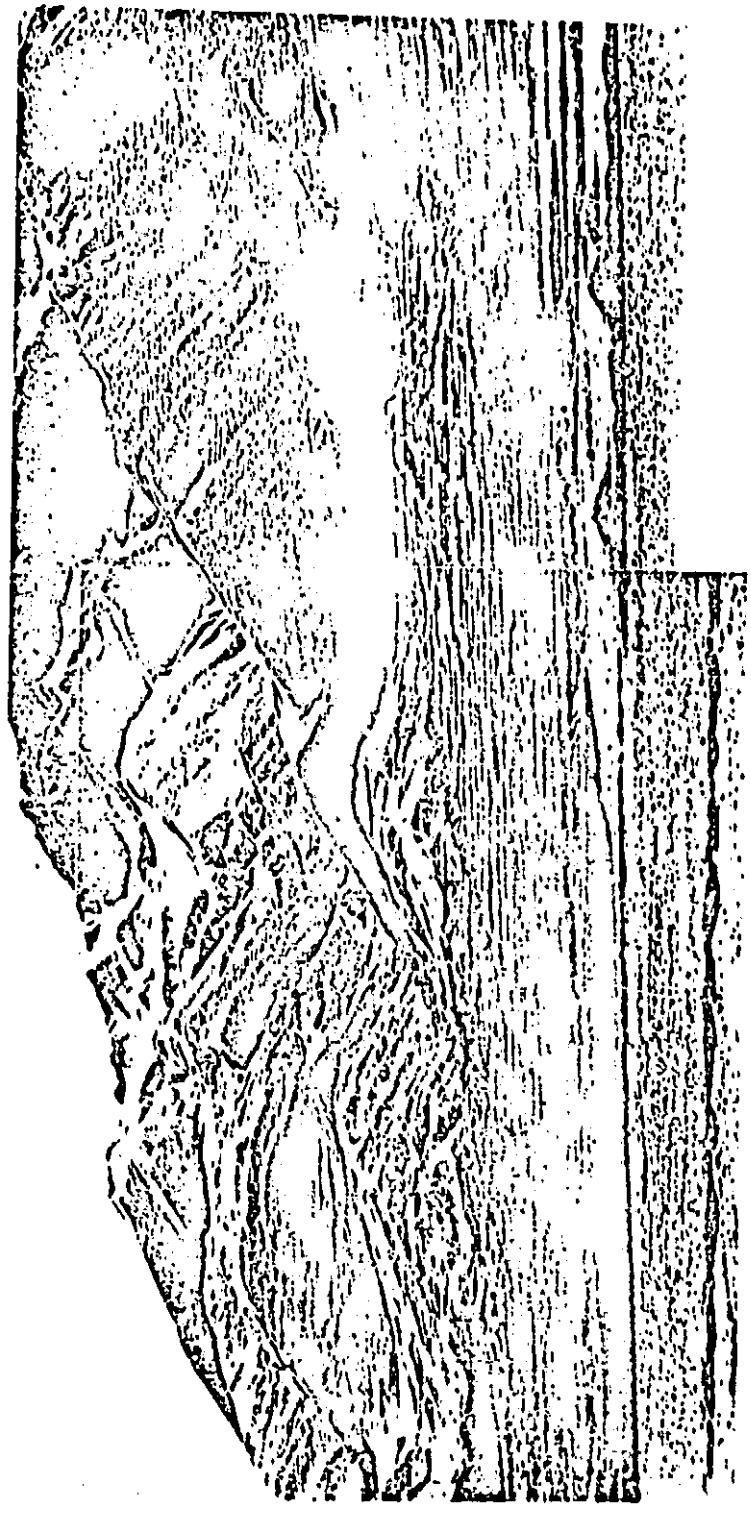

Fig. 15.

Ancash Earthquake
November 10, 1946

O dilatation
● compression

Horizontal Stress (σ_{xx}) Near a Ridge
Due to Tectonic Compression

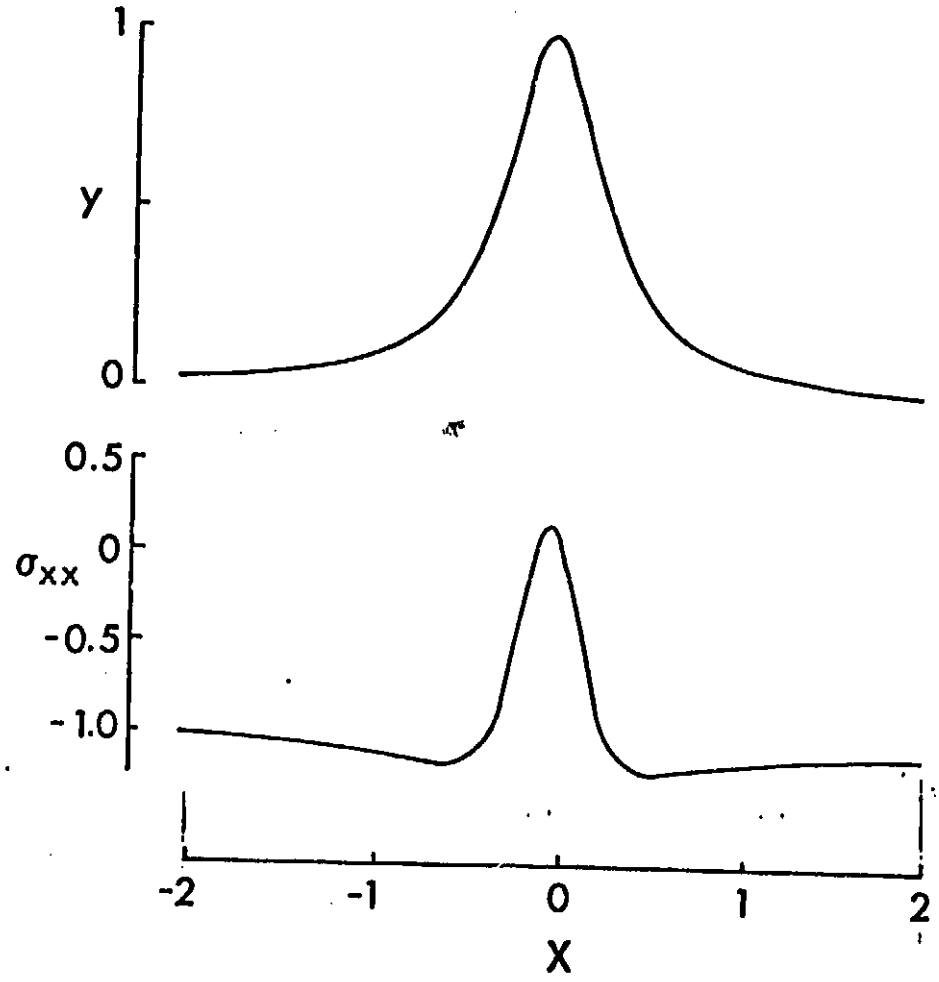

Fig. 17

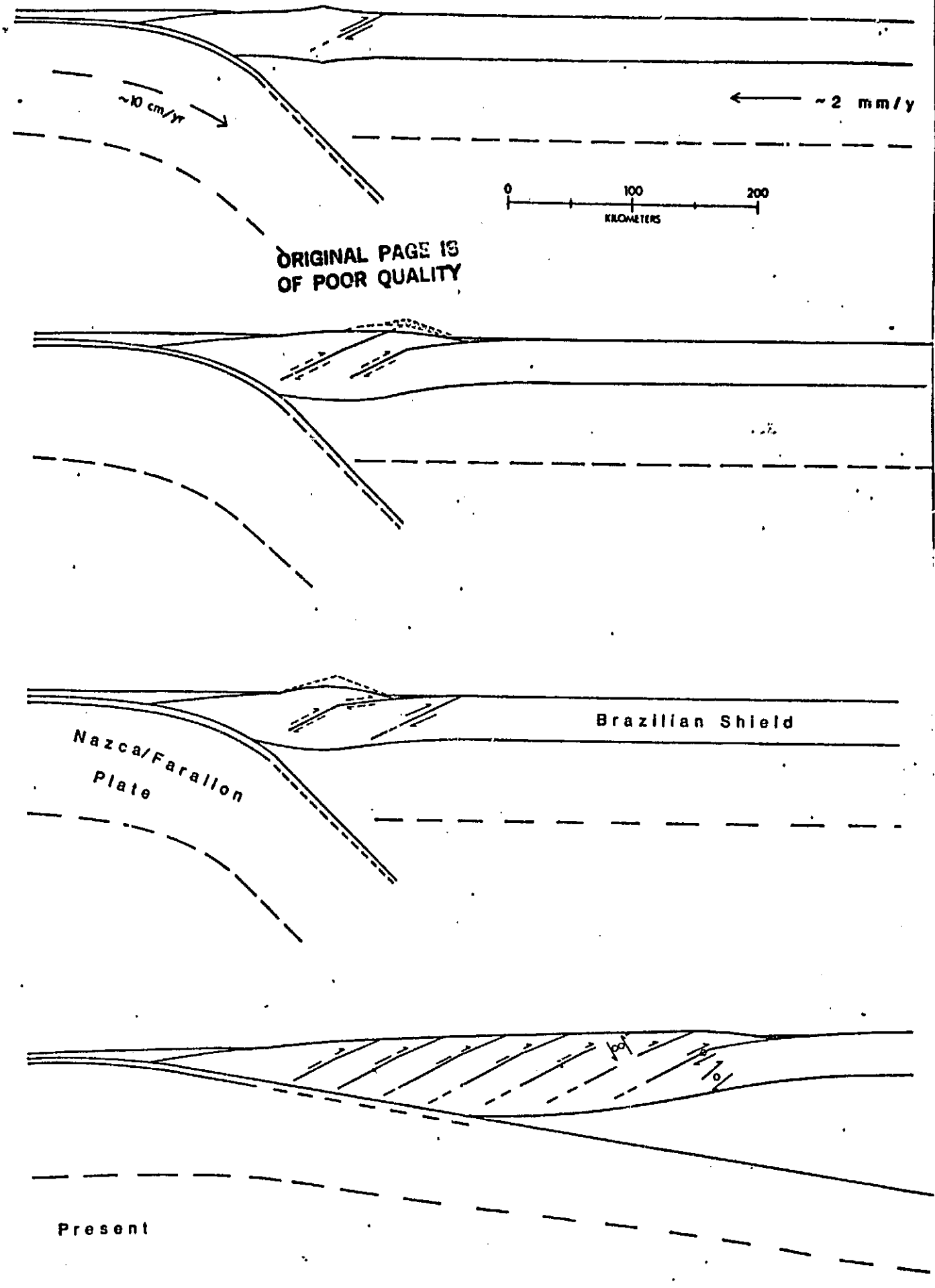

Appendix

Fault plane solutions and synthetic waveforms for the earthquakes listed in Tables 1 and 2. First motion data are plotted on equal area lower hemispheric projections where the solid circles indicate compressional first motions and open circles dilatational first motions. Observed long period P waves and synthetic waveforms for the fault plane solutions shown are also presented for a few stations. Not all the stations used in the analysis are shown since many of them, specially those in North America and Europe, are clustered at similar azimuth and epicentral distance from the source and have very similar waveforms. Synthetic waveforms computed at various focal dephts are also shown versus the observed long period P waves at a few stations spanning a range of azimuths and epicentral distances. Arrow indicates preferred focal depth. + indicates amplitude was reduced in half for plotting purposes.

ORIGINAL PAGE IS
OF POOR QUALITY

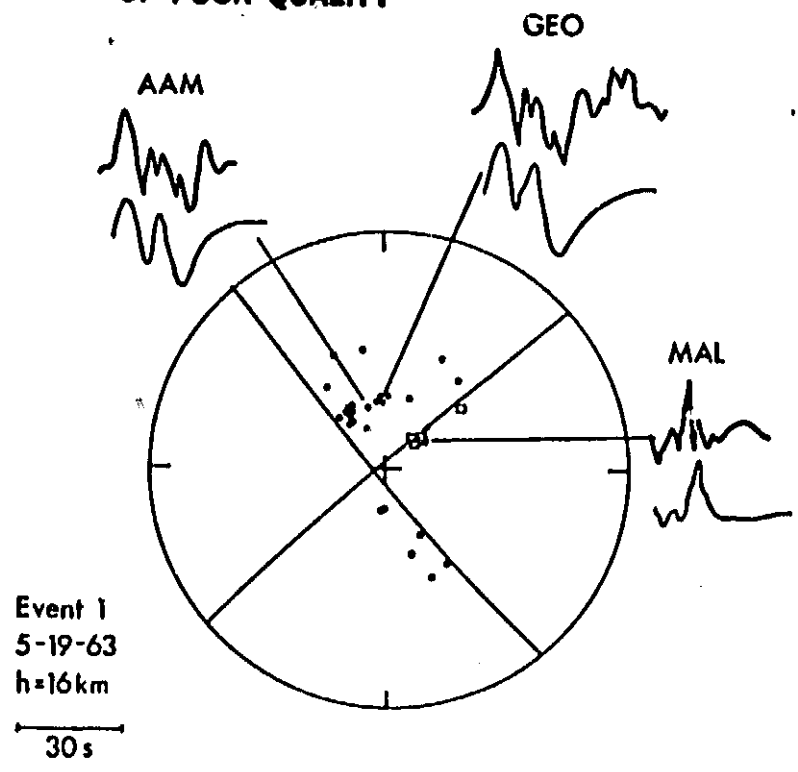

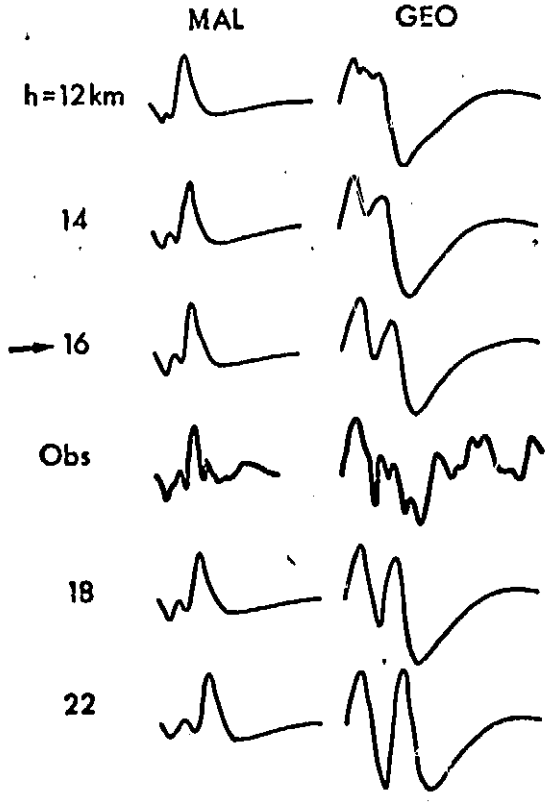

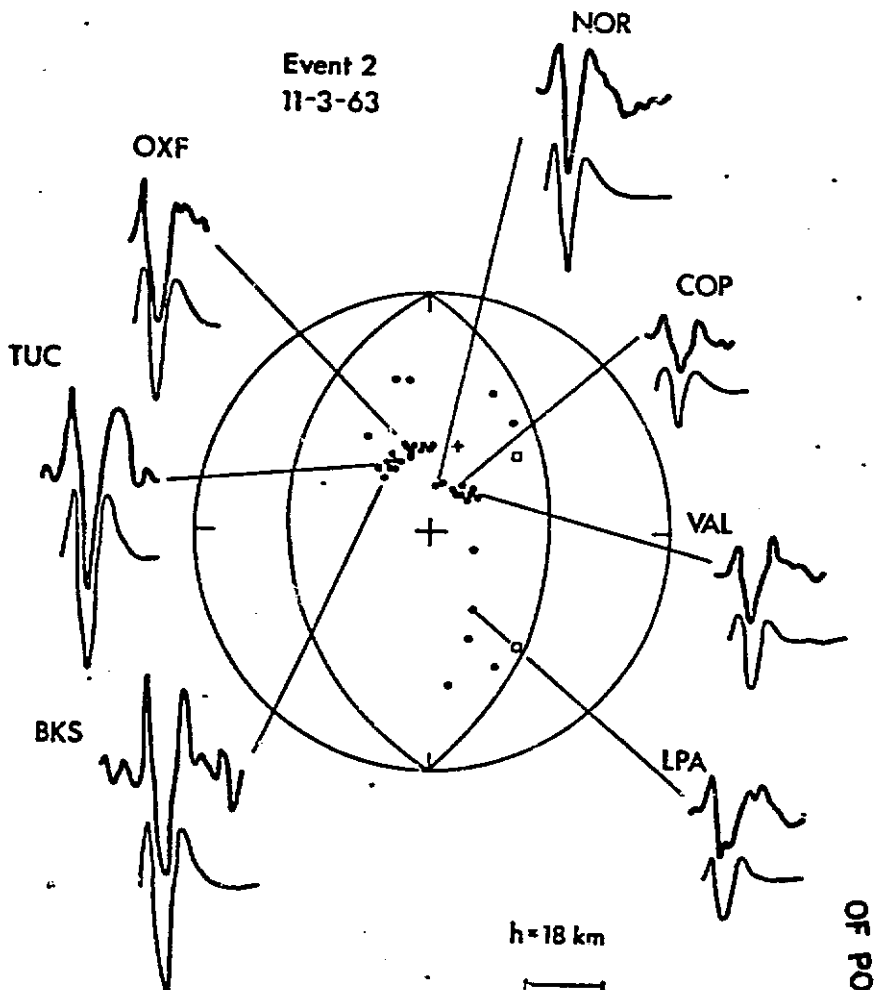

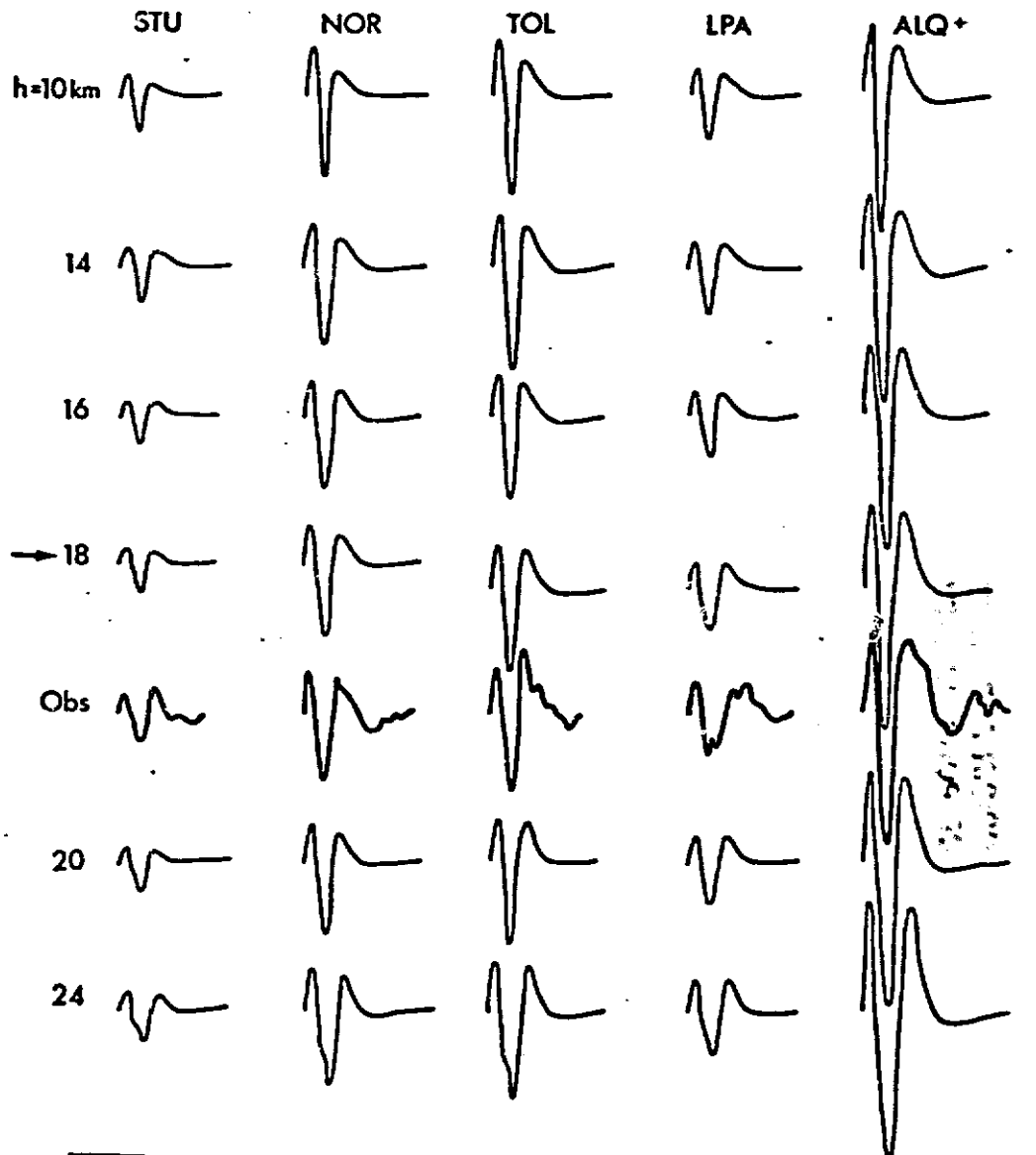

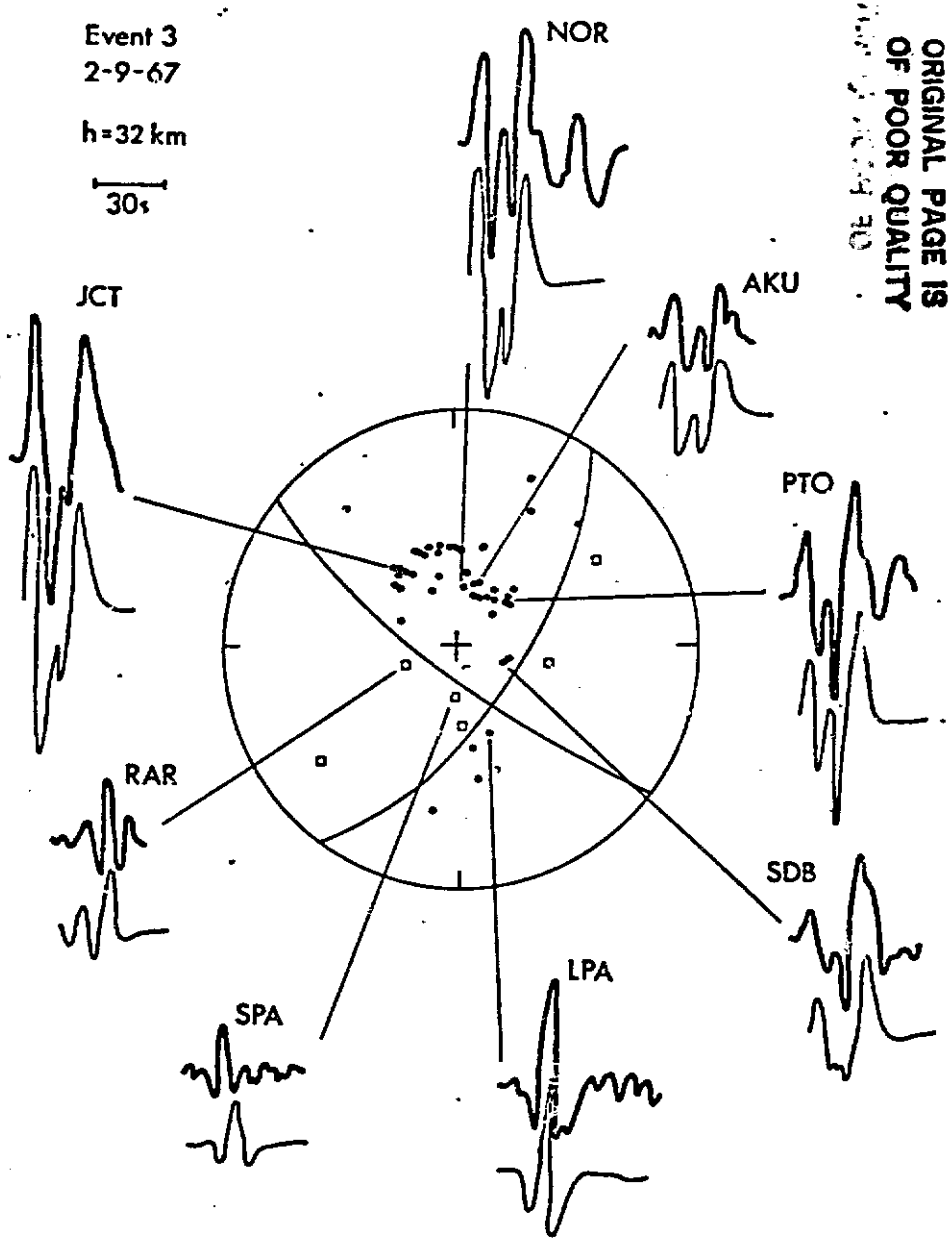

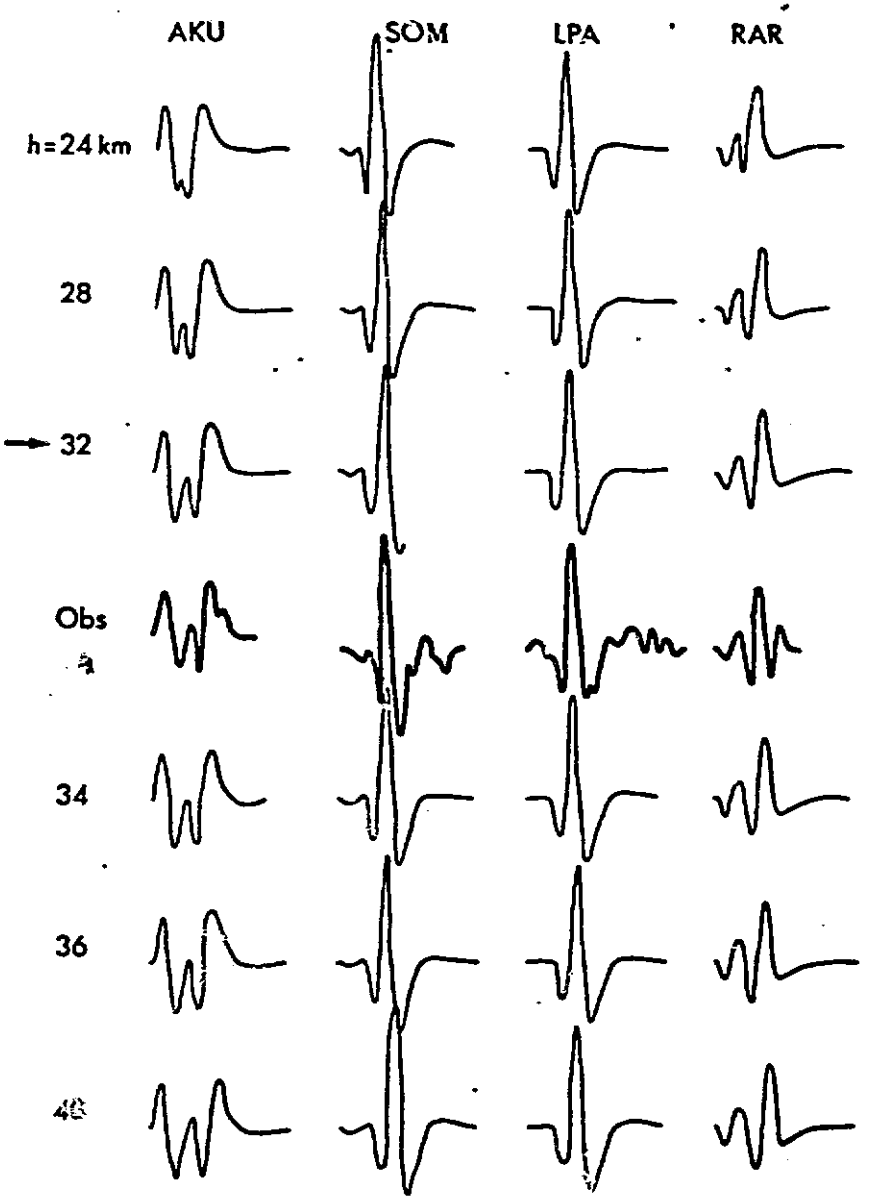

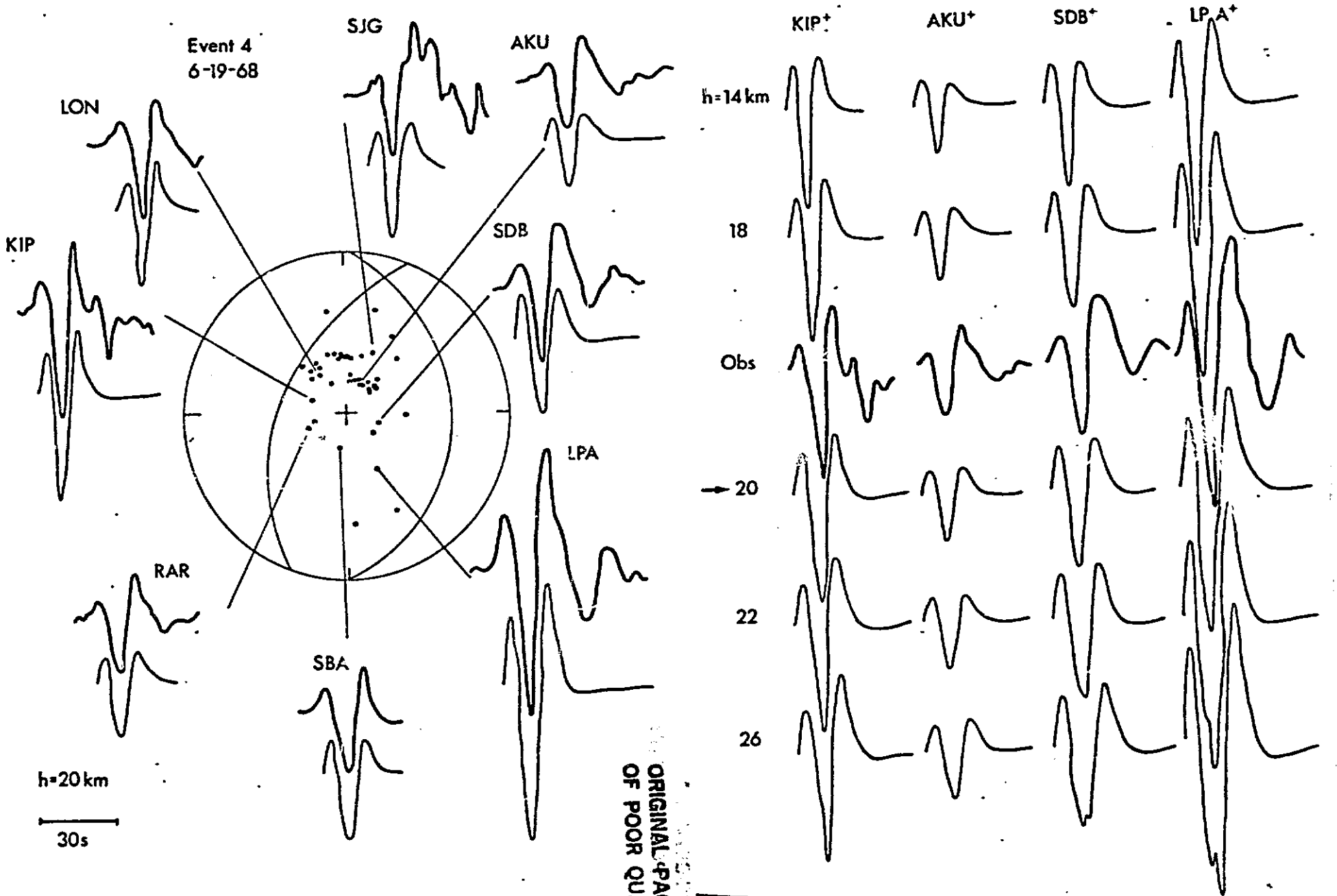

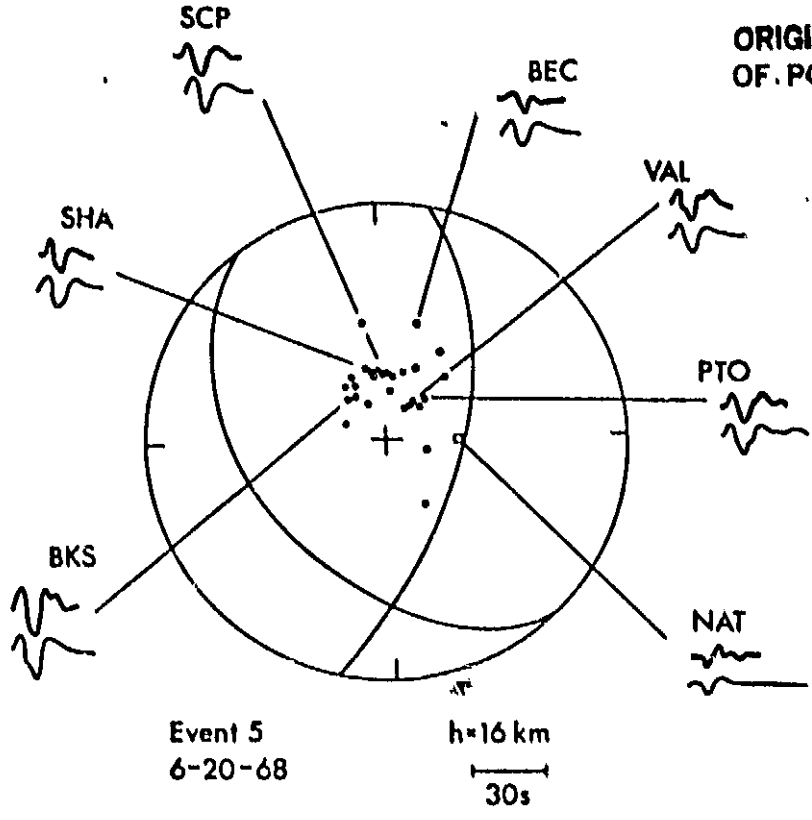

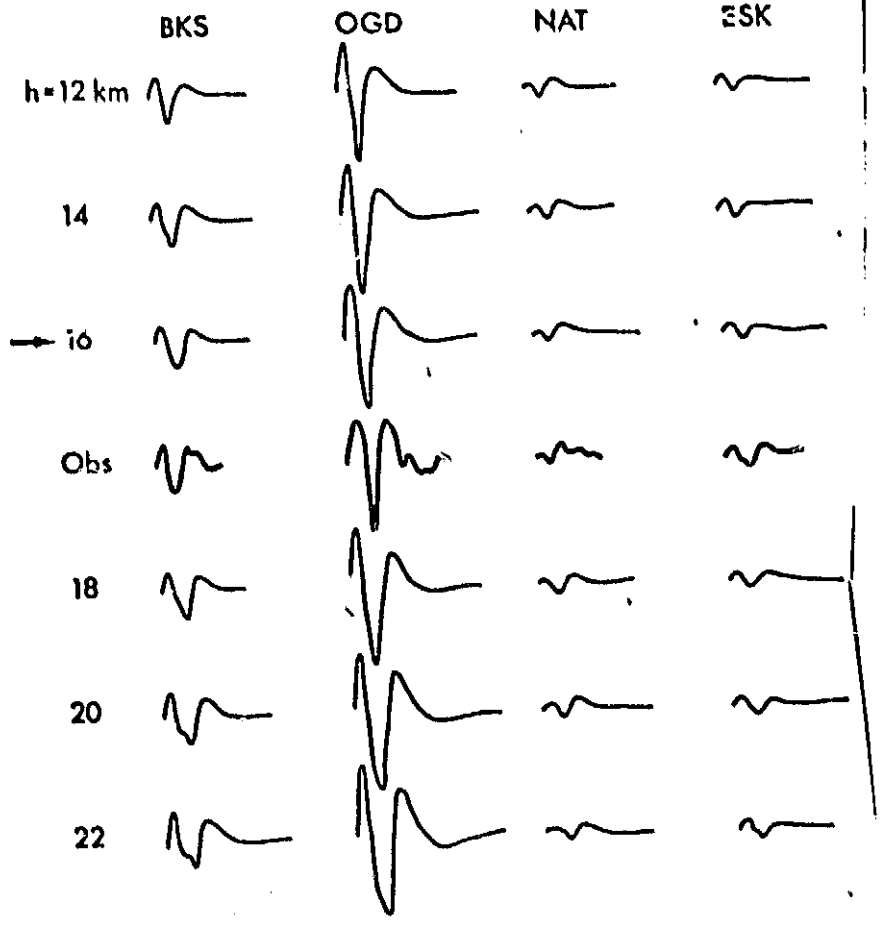

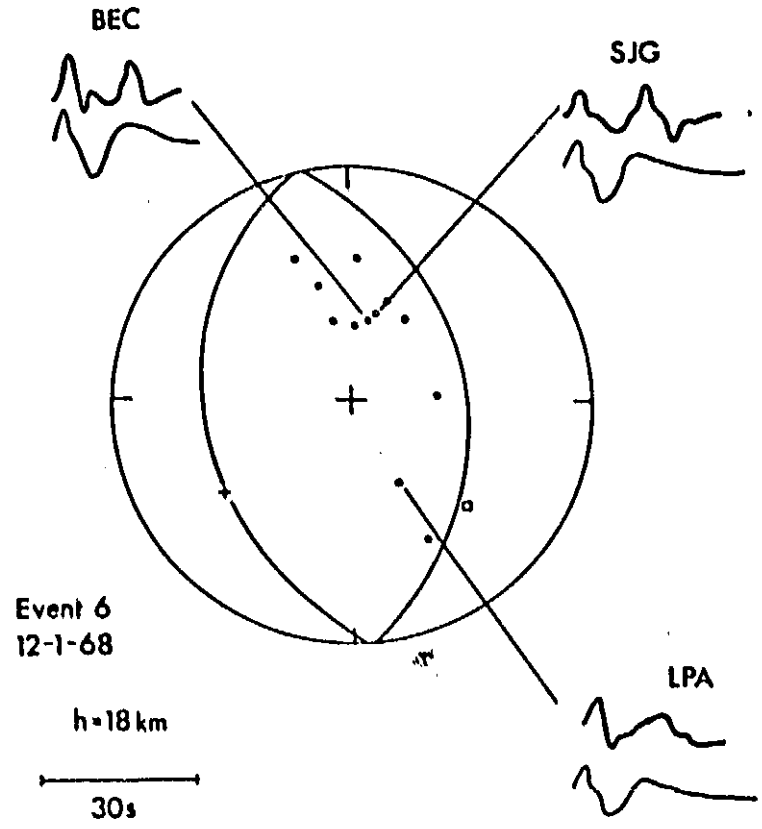

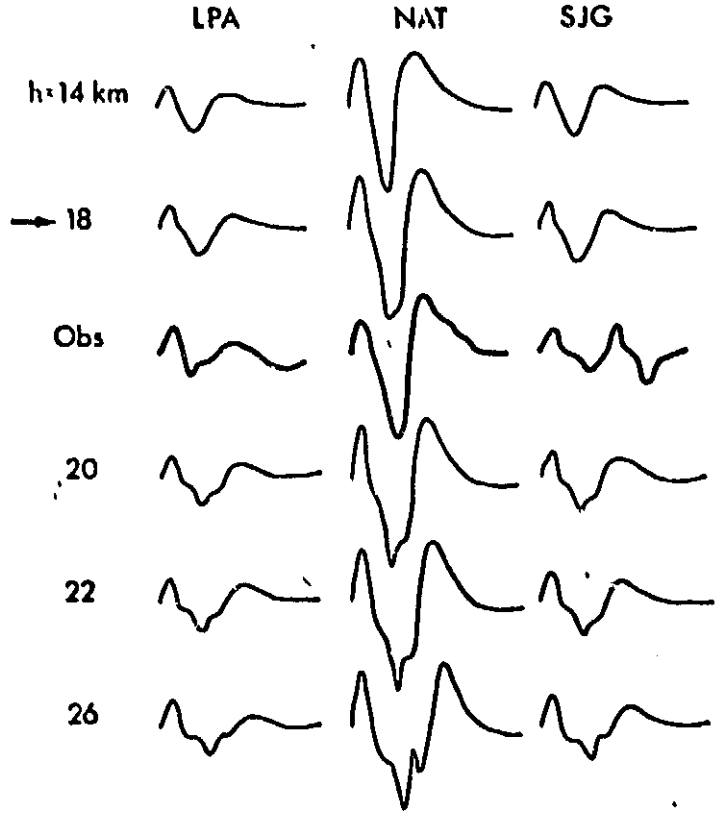

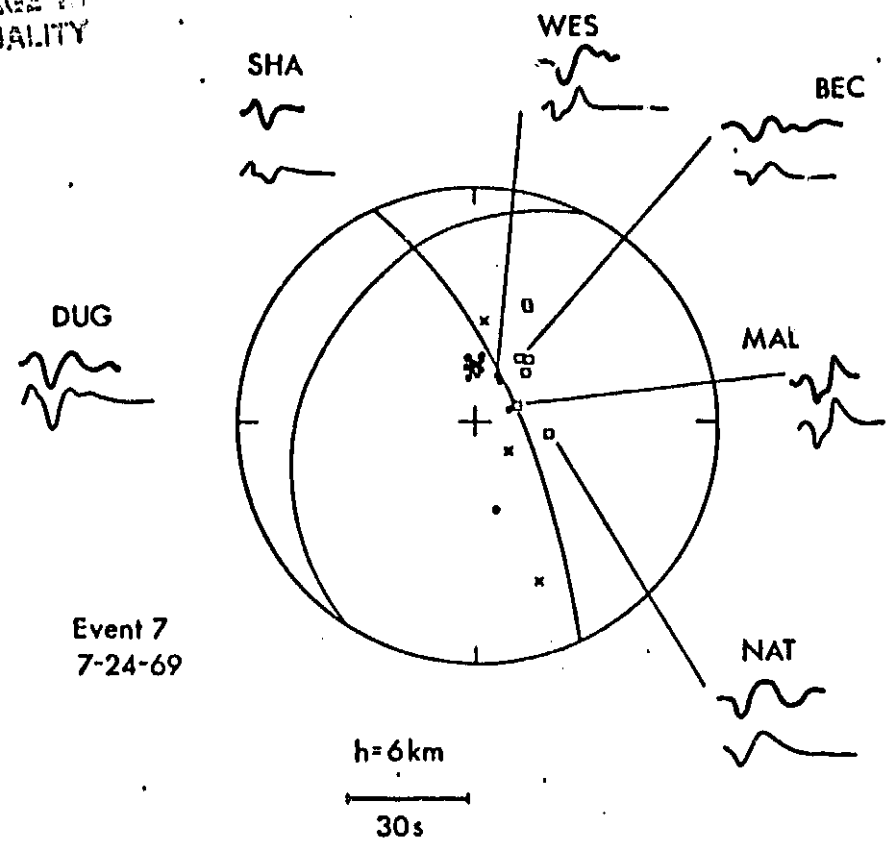

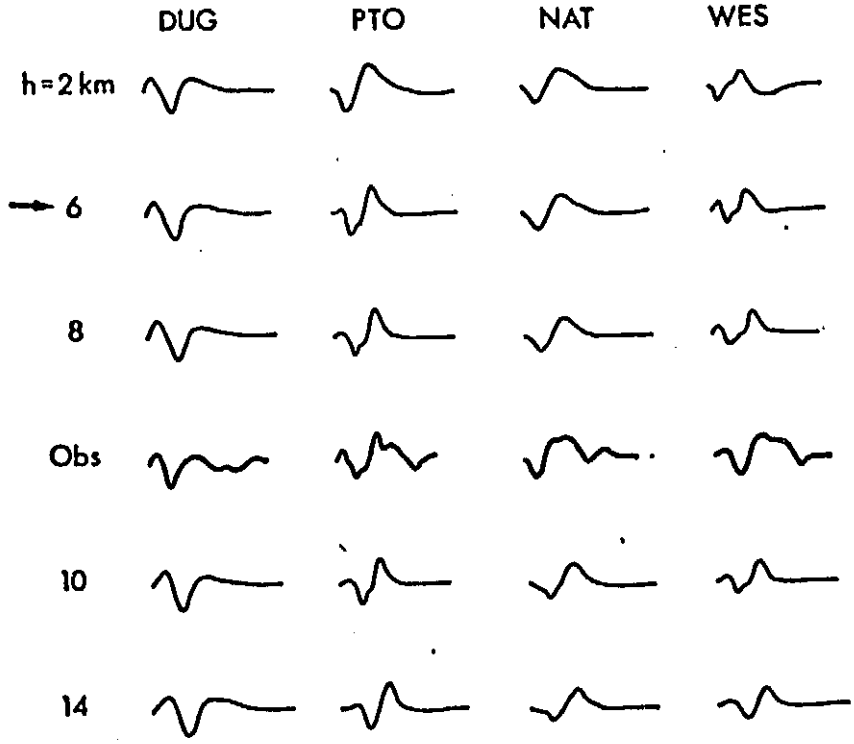

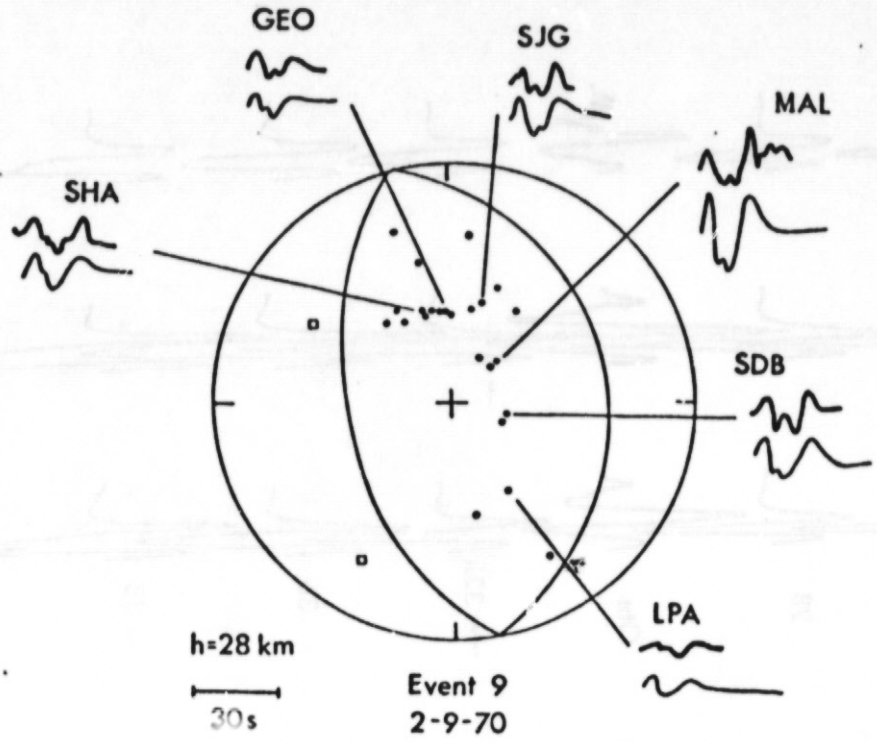

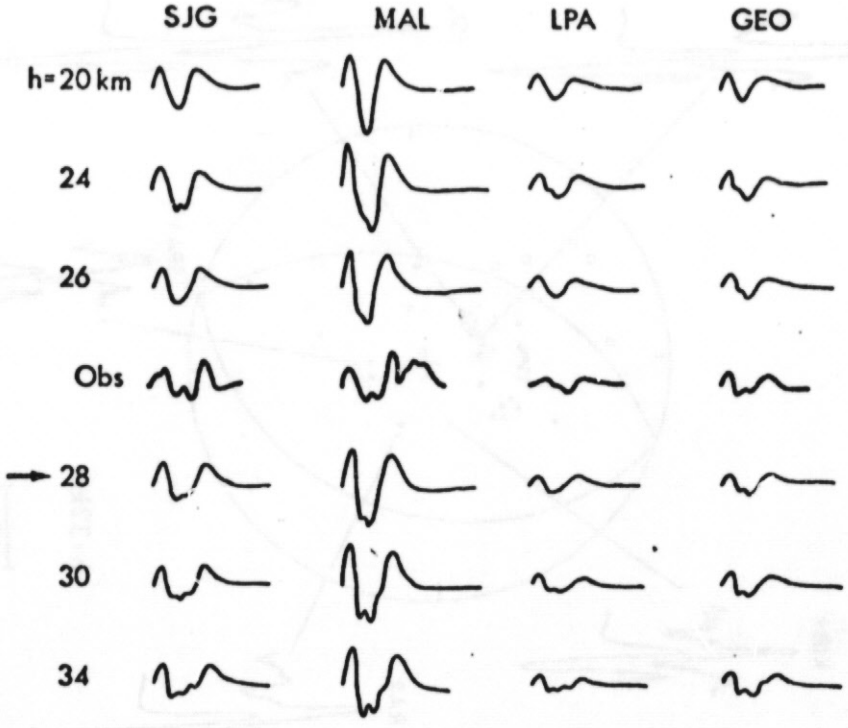

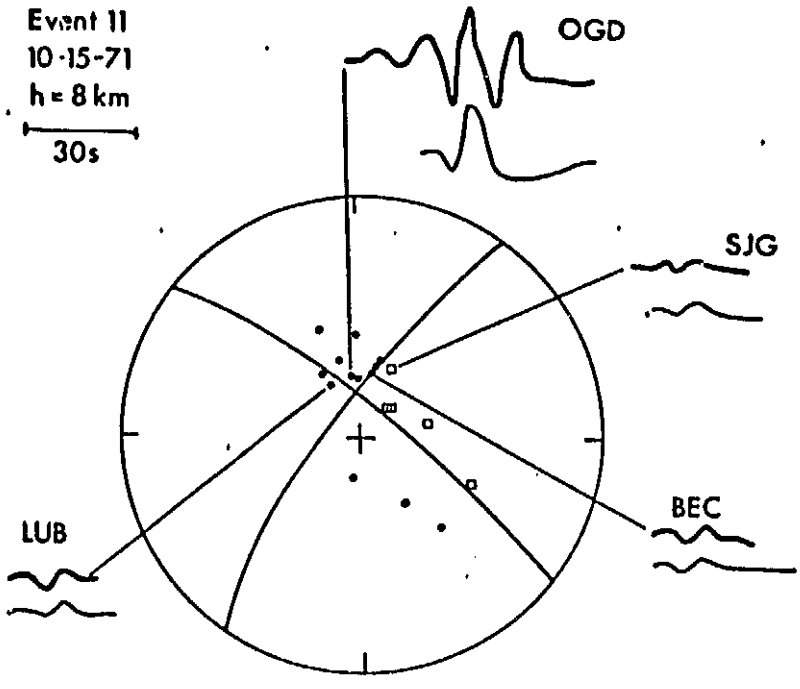

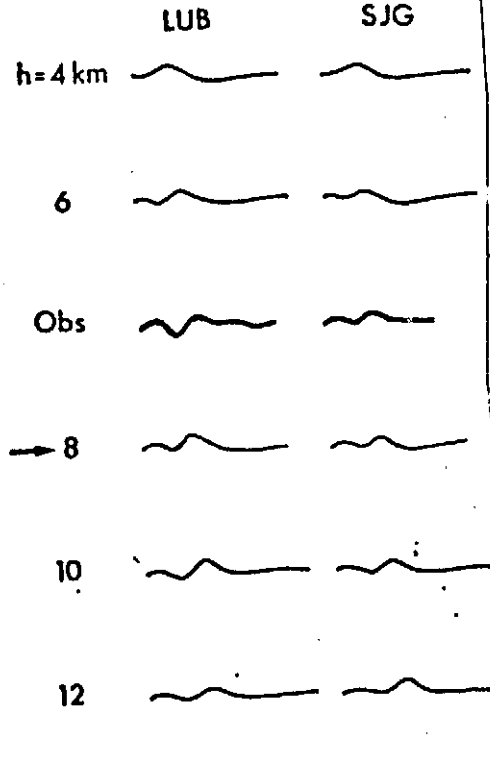

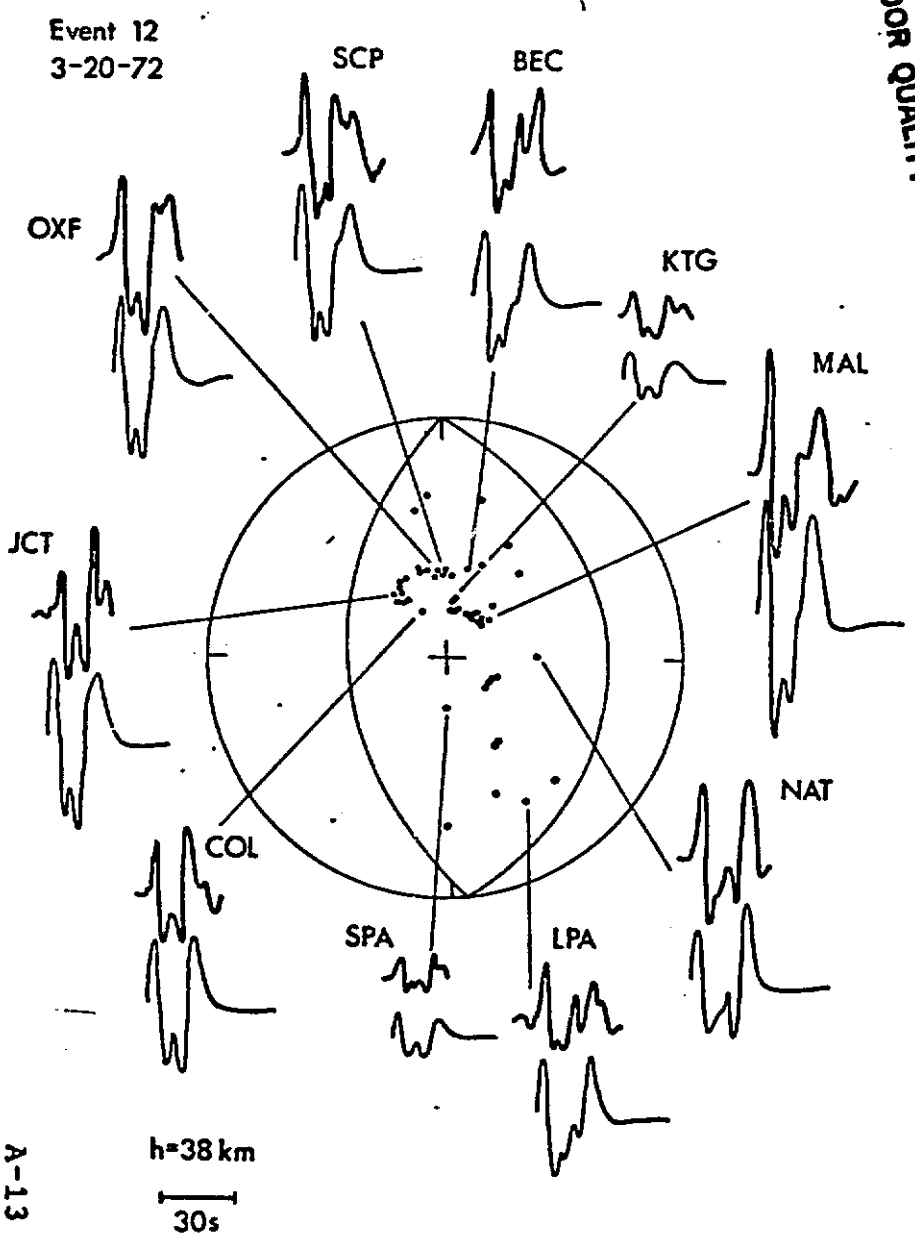

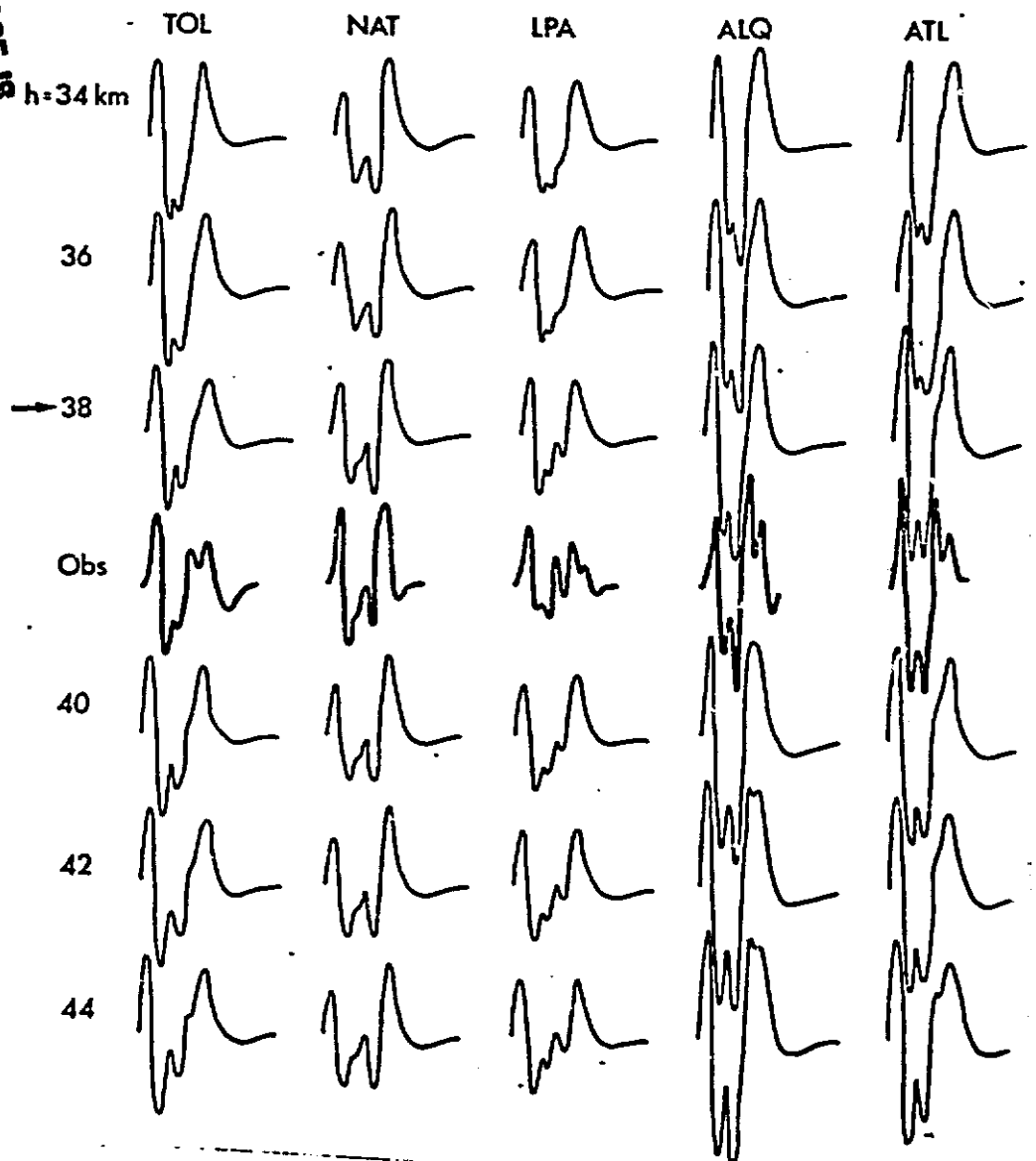

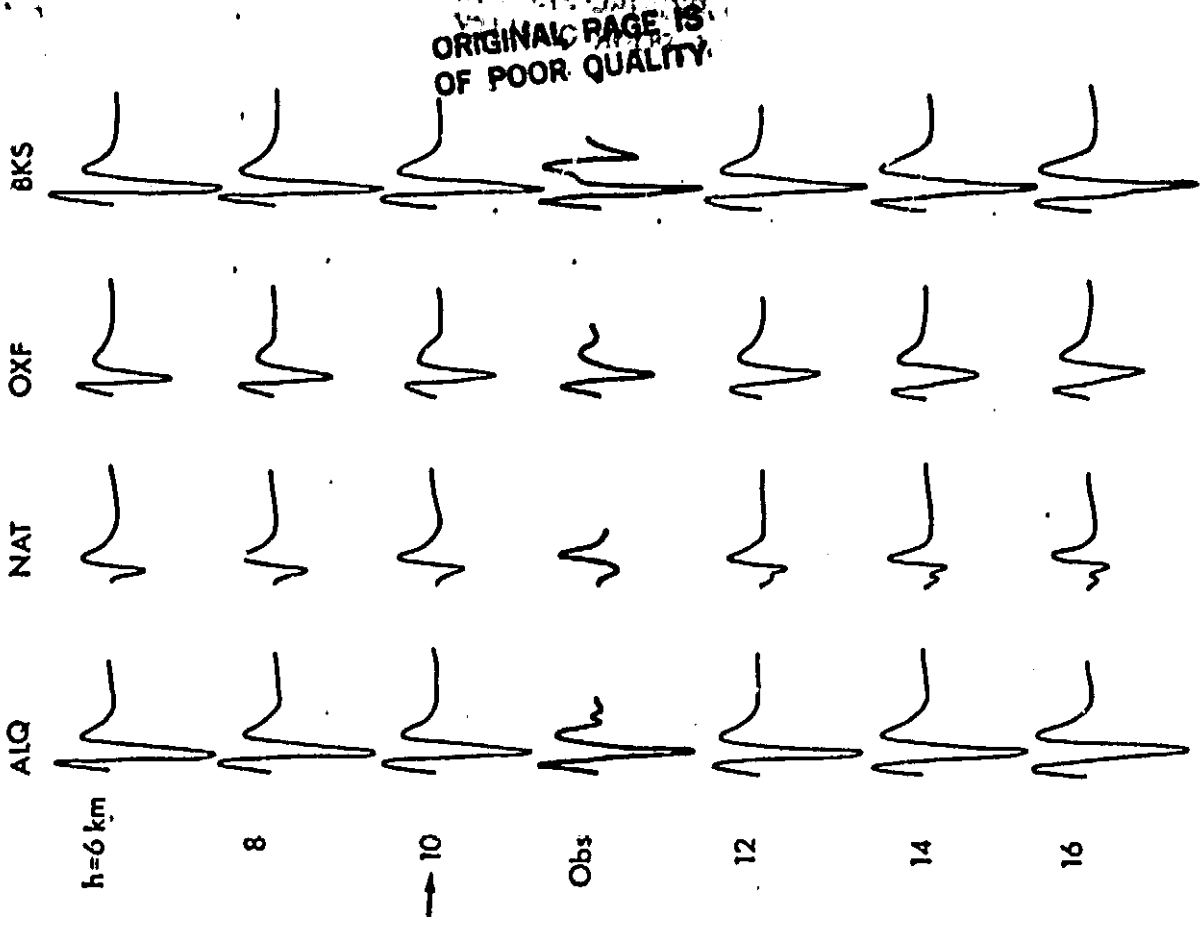

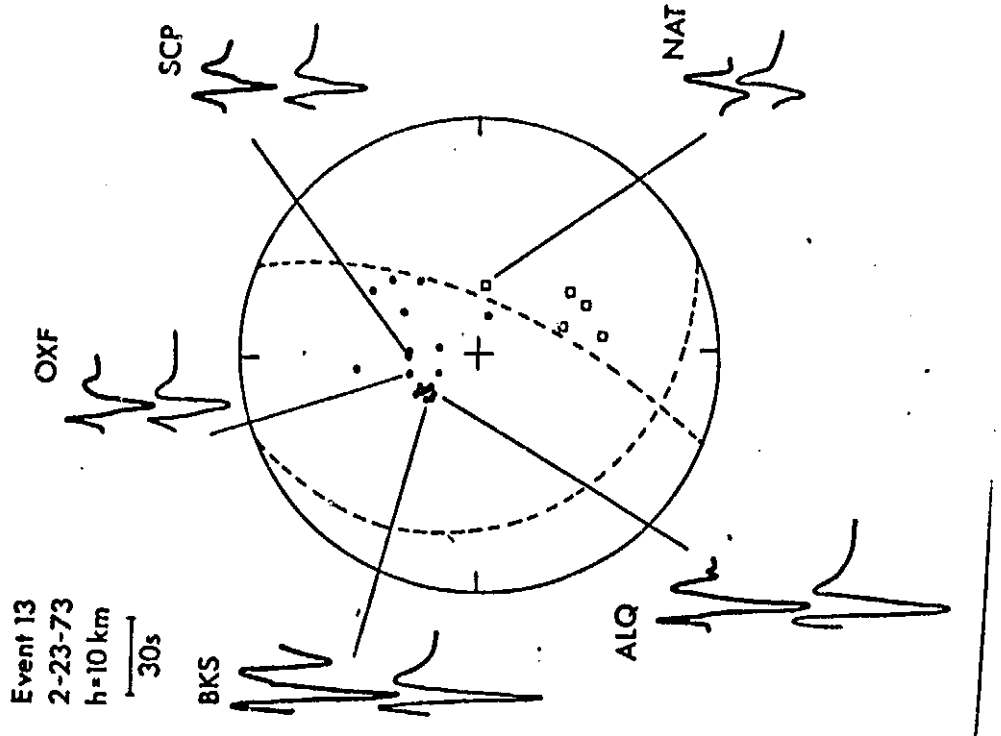

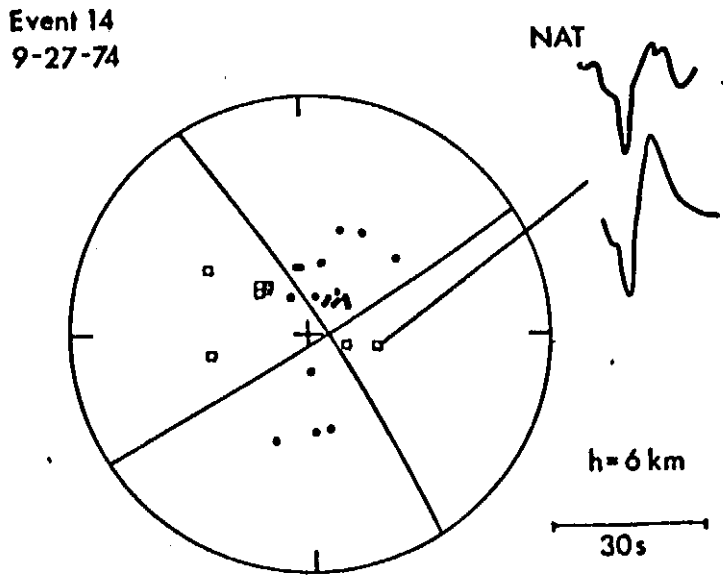

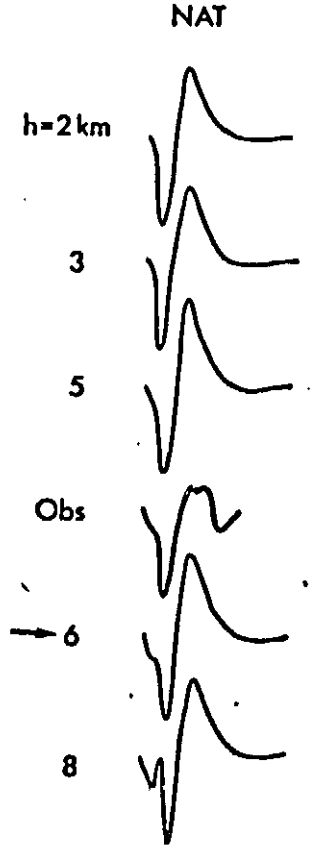

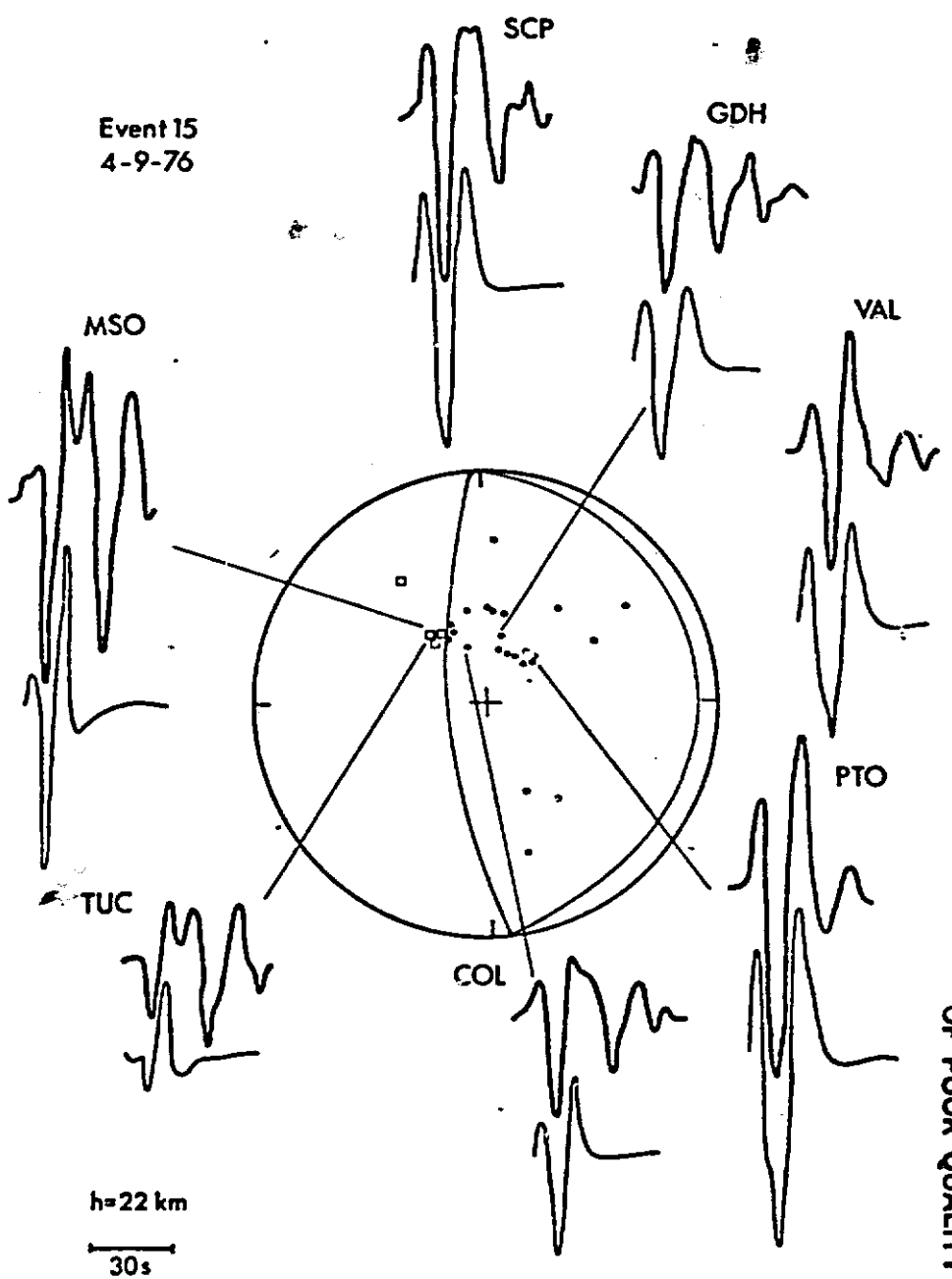

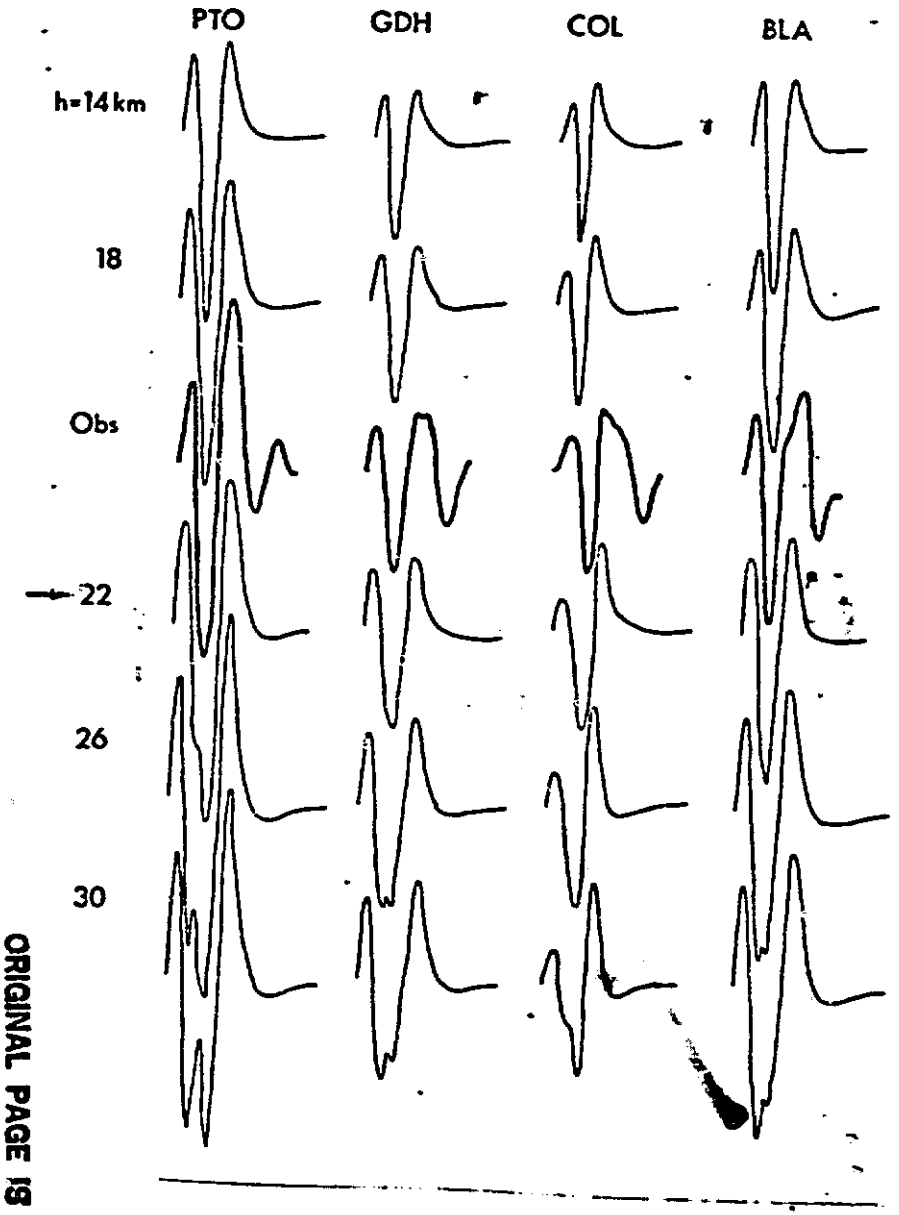

ORIGINAL PAGE IS
OF POOR QUALITY

ORIGINAL PAGE IS
OF POOR QUALITY

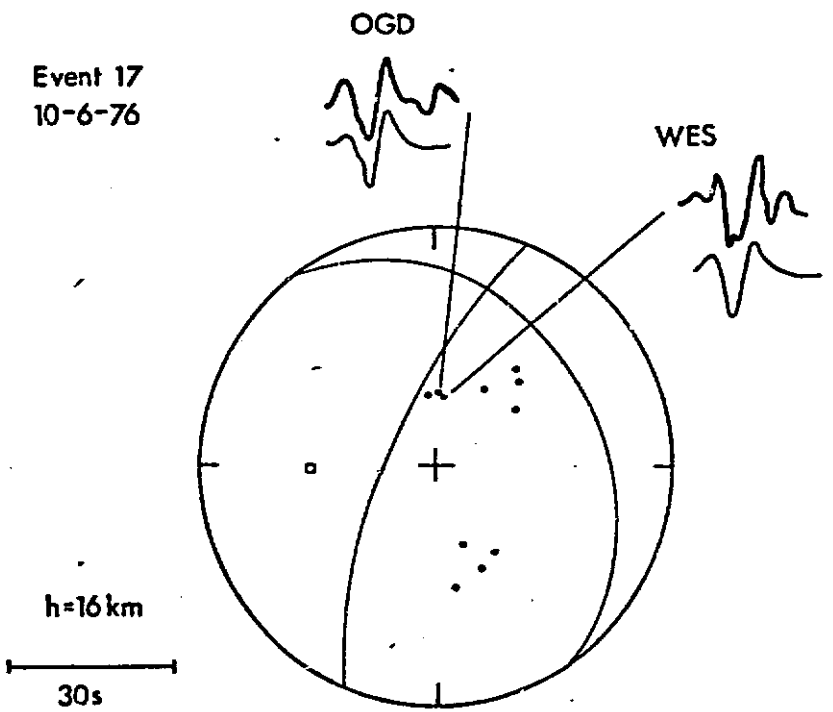
OGD
Event 17
10-6-76
WES
h=16km
30s

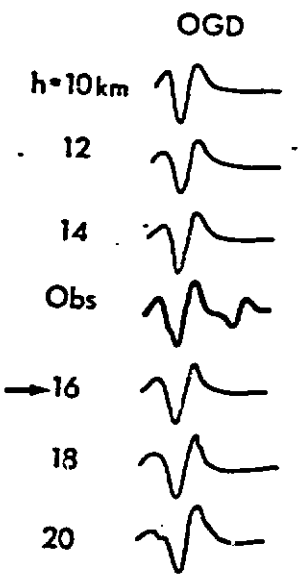
OGD
h=10km
12
14
Obs
16
18
20